

MOTOR IMAGERY EEG SIGNAL CLASSIFICATION USING DEEP
LEARNING FOR BRAIN COMPUTER INTERFACES

A THESIS SUBMITTED TO
THE GRADUATE SCHOOL OF NATURAL AND APPLIED SCIENCES
OF
MIDDLE EAST TECHNICAL UNIVERSITY

BY
YOUSEF REZAEI TABAR

IN PARTIAL FULFILLMENT OF THE REQUIREMENTS
FOR
THE DEGREE OF DOCTOR OF PHILOSOPHY
IN
BIOMEDICAL ENGINEERING

SEPTEMBER 2017

Approval of the thesis:

**MOTOR IMAGERY EEG SIGNAL CLASSIFICATION USING DEEP
LEARNING FOR BCI**

submitted by **YOUSEF REZAEI TABAR** in partial fulfillment of the requirements
for the degree of **Doctor of Philosophy in Biomedical Engineering Department,
Middle East Technical University** by,

Prof. Dr. Gülbin Dural Ünver
Dean, Graduate School of **Natural and Applied Sciences**

Prof. Dr. Hakan I. Tarman
Head of Department, **Biomedical Engineering**

Prof. Dr. Uğur Halıcı
Supervisor, **Electrical and Electronics Eng. Dept., METU**

Examining Committee Members:

Prof. Dr. Nevzat Güneri Gençer
Electrical and Electronics Engineering Department, METU

Prof. Dr. Uğur Halıcı
Electrical and Electronics Engineering Department, METU

Prof. Dr. Bilge Yılmaz
Physical Medicine and Rehabilitation, Health Sciences University

Assoc. Prof. Dr. İlkey Ulusoy
Computer Engineering Department, Hacettepe University

Assist. Prof. Dr. Fikret Arı
Electrical and Electronics Engineering Department,
Ankara University

Date:

I hereby declare that all information in this document has been obtained and presented in accordance with academic rules and ethical conduct. I also declare that, as required by these rules and conduct, I have fully cited and referenced all material and results that are not original to this work.

Name, Last Name: YOUSEF REZAEI TABAR

Signature :

ABSTRACT

MOTOR IMAGERY EEG SIGNAL CLASSIFICATION USING DEEP LEARNING FOR BRAIN COMPUTER INTERFACES

Rezaaei Tabar, Yousef
Ph.D., Department of Biomedical Engineering
Supervisor : Prof. Dr. Uğur Halıcı
Co-Supervisor: Prof. Dr. Canan Kalaycıoğlu

September 2017, 133 pages

In this thesis we proposed a novel method for classification of Motor Imagery (MI) EEG signals based on deep learning. Convolutional Neural Networks (CNN) and Stacked Autoencoders (SAE) networks were investigated for MI EEG classification. A new form of input is introduced to combine time, frequency and location information extracted from EEG signal and also a new deep network combining CNN and SAE is proposed in this thesis. In the proposed network, the features that are extracted by CNN are classified through the deep SAE network. The results obtained on public datasets revealed that the proposed method provides better classification performance compared to other state of art approaches.

Furthermore, four different experiments were conducted on totally 16 subjects to collect MI EEG signals in addition to public datasets. Two of these experiments were used to record motor imagery data and perform offline classification. Online feedback was provided in the other two sets of experiments, where EEG signal was classified

in real time and appropriate visual feedback was presented to the subject during the experiment. Our proposed signal processing method was applied to the recorded data as well as public datasets and compared with present state of art methods.

Keywords: Brain Computer Interface (BCI), Electroencephalography (EEG), Motor Imagery, Signal processing, Classification, Deep Learning, Convolutional Neural Network, Stacked Autoencoders

ÖZ

BEYİN BILGISAYAR ARAYÜZÜ İÇİN DERİN ÖĞRENME KULLANARAK MOTOR İMGELEME EEG SINYALI SINIFLANDIRMA

Rezaaei Tabar, Yousef
Doktora, Biyomedikal Mühendisliği Bölümü
Tez Yöneticisi : Prof. Dr. Uğur Halıcı
Ortak Tez Yöneticisi : Prof. Dr. Canan Kalaycıoğlu

Eylül 2017, 133 sayfa

Bu tezde derin öğrenme tabanlı Motor İmgeleme (MI) EEG sinyallerinin sınıflandırılması için yeni bir yöntem önerilmiştir. Çalışmada EEG Motor imgeleme sınıflandırılması için Konvolüsyonel Sinir Ağları (CNN) ve Yığılanmış Otokodlayıcı (SAE) ağları araştırılmıştır. EEG sinyalinden çıkarılan zaman, frekans ve konum bilgilerini birleştirmek için yeni bir girdi şekli tanıtılmış ve ayrıca CNN ve SAE yapılarını birleştiren yeni bir derin ağ yapısı da önerilmiştir. Bu derin ağda, CNN'de çıkarılan öznitelikler derin SAE ağları vasıtasıyla sınıflandırılmaktadır. Açık veri setlerinde elde edilen sonuçlar, önerdiğimiz yöntemin literatürdeki mevcut yaklaşımlara kıyasla daha iyi sınıflandırma performansı sağladığını ortaya koymuştur.

Açık veri setlerine ek olarak, Motor İmgeleme EEG verisi toplamak üzere ayrıca toplam 16 denek üzerinde dört değişik MI EEG deneyi gerçekleştirilmiştir. Bu deneylerin ikisinde MI EEG verileri çevrim-dışı sınıflandırma yapmak üzere kaydedilmiştir. EEG sinyallerinin gerçek zamanlı olarak sınıflandırıldığı ve deney

sırasında uygun görsel geri bildirimlerin deneğe sunulduğu diğer iki deneyde ise gerçek zamanlı geribildirim sağlanmıştır. Önerilen sinyal işleme yöntemi kaydedilen verilere ve açık data setlerine uygulanmış ve son teknoloji yöntemleriyle karşılaştırılmıştır.

Anahtar Kelimeler: Beyin Bilgisayar Arayüzü (BBA), Elektroensefalografi (EEG), Motor İmgeleme, Sinyal İşleme, Sınıflandırma, Derin öğrenme, Konvolüsyonel Sinir Ağları, Otokodlayıcı, Yığınlanmış Otokodlayıcı

To my dear wife Gülçin and

my parents

ACKNOWLEDGMENTS

First and foremost, I am deeply indebted to my advisor, Prof. Dr. Uğur Halıcı for her precious guidance, consistent support and numerous opportunities that she has provided me over the years. Her deep insights helped me at various stages of my research. This thesis would not be possible without her endless patience and encouragement.

I owe a great debt of gratitude to my co-advisor Prof. Dr. Canan Kalaycıoğlu not only for kindly opening her laboratory to me, but for patiently advising me on my experiments and giving substantive feedbacks whenever I need.

I express my gratitude to thesis monitoring committee members Prof. Dr. Nevzat Güneri Gençer and Assist. Prof. Dr. Fikret Arı. They have closely monitored the progress of the study and the quality of the thesis has been remarkably improved with their valuable comments and discussions.

I would like to thank to Ankara University Brain Research Center which provided me a great opportunity to perform my experiments and also to all people who participated in my experiments as subject. I would also like to thank my friend Ahmad Hekmat Kashtiban for his enormous help in performing my experiments.

I would like to heartfully thank my family, especially to my dearest parents Eshrat Hafezi and Yaghoub Rezaei Tabar, for their constant love, encouragement, moral support and blessings. Finally, and most importantly, I would like to thank my dear wife Gülçin who provided me endless love, support and encouragement during this thesis. She also had a large contribution to this study not only by participating patiently in my long exhausting experiments but more importantly by providing brilliant ideas and comments to improve this study.

I acknowledge that this study was partially supported by projects METU BAP-03-01-2015-001 and METU BAP-03-01-2016-003.

TABLE OF CONTENTS

| | |
|--|-------|
| ABSTRACT..... | v |
| ÖZ | vii |
| ACKNOWLEDGMENTS..... | x |
| TABLE OF CONTENTS..... | xii |
| LIST OF TABLES..... | xvi |
| LIST OF FIGURES..... | xviii |
| LIST OF ABBREVIATIONS..... | xxi |
| CHAPTERS | |
| 1. INTRODUCTION..... | 1 |
| 1.1 Motivation of the Thesis..... | 1 |
| 1.2 Scope of the Thesis..... | 2 |
| 1.3 Literature Survey..... | 3 |
| 1.4. Contribution of the Thesis..... | 7 |
| 1.5 Organization of the Thesis..... | 9 |
| 2. OVERVIEW OF BRAIN COMPUTER INTERFACE SYSTEMS..... | 11 |
| 2.1 Measuring Brain Activity..... | 13 |
| 2.2 Brain Activities Used In EEG Based BCI..... | 15 |
| 2.2.1 P300..... | 16 |

| | |
|---|----|
| 2.2.2 SSVEP..... | 18 |
| 2.2.3 SCP..... | 19 |
| 2.2.4 Sensory-Motor Rhythms and Motor Imagery..... | 19 |
| 2.3 EEG Signal Preprocessing..... | 22 |
| 2.3.1 Referencing..... | 22 |
| 2.3.2 Temporal Filtering..... | 23 |
| 2.3.3 Signal Enhancement..... | 23 |
| 2.3.4 EEG Artifacts..... | 23 |
| 2.4 EEG Signal Processing..... | 24 |
| 2.5 Feedback and Control..... | 25 |
| 2.6 BCI Applications..... | 26 |
| 3. SIGNAL PROCESSING BACKGROUND..... | 27 |
| 3.1 Feature Extraction..... | 27 |
| 3.1.1 Time and Frequency Domain Features..... | 28 |
| 3.1.2 Common Spatial Pattern (CSP)..... | 28 |
| 3.2 Classification..... | 30 |
| 3.2.1 Linear Discriminant Analysis (LDA)..... | 30 |
| 3.2.2 Support Vector Machine (SVM)..... | 31 |
| 3.2.3 Filter-Bank Common Spatial Pattern..... | 33 |
| 3.3 Artificial Neural Networks and Deep Learning..... | 35 |
| 3.3.1 Artificial Neural Networks (ANN)..... | 35 |
| 3.3.2 Multi-Layer Perceptron (MLP)..... | 37 |
| 3.3.3 Convolutional Neural Networks..... | 39 |
| 3.3.4 Autoencoders and Stacked Autoencoders..... | 41 |

| | |
|--|----|
| 3.3.5 Deep Neural Networks..... | 44 |
| 4. DATA COLLECTION EXPERIMENTS..... | 47 |
| 4.1 Public Datasets..... | 48 |
| 4.2 EEG Recording Devices and environments | 50 |
| 4.2.1 Brainamp EEG recording device and recording environment..... | 50 |
| 4.2.2 G.Nautiulus EEG recording device and environment..... | 51 |
| 4.3 Data Recording Electrodes..... | 53 |
| 4.4 Preparation Procedures | 55 |
| 4.5 Tools and Softwares..... | 57 |
| 4.6 Experiment I..... | 58 |
| 4.7 Experiment II..... | 61 |
| 4.8 Experiment III..... | 63 |
| 4.9 Experiment IV..... | 68 |
| 5. METHOD PROPOSED FOR MOTOR IMAGERY CLASSIFICATION..... | 73 |
| 5.1 Input Image Form..... | 74 |
| 5.2 Convolutional Neural Network | 76 |
| 5.3 Stacked Autoencoder | 78 |
| 5.4 Combined CNN-SAE..... | 79 |
| 6. RESULTS | 81 |
| 6.1 Classification Results on Public Datasets..... | 82 |
| 6.1.1 Results of BCI Competition IV Dataset 2b..... | 82 |
| 6.1.2 Results of BCI Competition II Dataset III..... | 87 |
| 6.1.3 Discussion of Proposed Network for Public Datasets..... | 88 |
| 6.2 Results on Data Collection Experiments | 94 |
| 6.2.1 Experiment I | 95 |

| | |
|-----------------------------|-----|
| 6.2.2 Experiment II | 102 |
| 6.2.3 Experiments III | 107 |
| 6.2.4 Experiments IV | 108 |
| 7. CONCLUSION..... | 111 |
| APPENDIX A..... | 117 |
| REFERENCES..... | 121 |
| CURRICULUM VITAE..... | 131 |

LIST OF TABLES

TABLES

| | |
|--|----|
| Table 1.1 Summary of deep learning methods for EEG signal classification..... | 4 |
| Table 2.1 Properties of different signal acquisition methods..... | 14 |
| Table 4.1 Overview of experiment specifications..... | 48 |
| Table 4.2 Specifications of commonly available datasets..... | 48 |
| Table 4.3 Subject information for experiment I..... | 59 |
| Table 4.4 MI tasks related to each visual stimulus..... | 61 |
| Table 4.5 Subject information for experiment II..... | 62 |
| Table 4.6 Experiment II details..... | 63 |
| Table 4.7 The flow of each recording session..... | 71 |
| Table 6.1 BCI Competition IV dataset 2B Accuracy (%) results for CNN, SAE and CNN-SAE methods..... | 84 |
| Table 6.2 Kappa value results of CNN and CNN-SAE methods compared with FBCSP [72], Twin SVM [87], DDFBS [86], Bi-spectrum [61] And RQNN [103] Methods..... | 85 |
| Table 6.3 Accuracy results of session to session classification for BCI Competition IV dataset 2B..... | 87 |
| Table 6.4 BCI competition II dataset III. accuracy (%) results for CNN, SAE, CNN-SAE , the winner algorithm [133] and convolutional DBN [23] methods..... | 88 |

| | |
|--|-----|
| Table 6.5 Effect of filter size on CNN performance. Nh=93..... | 93 |
| Table 6.6 Accuracy results for experiment I dataset using proposed method..... | 96 |
| Table 6.7 Kappa results for experiment I dataset using proposed method..... | 96 |
| Table 6.8 Accuracy results for experiment I dataset using FBCSP method..... | 97 |
| Table 6.9 Kappa results for experiment I dataset using FBCSP method..... | 97 |
| Table 6.10 Comparison between accuracy results of methods for experiment I..... | 98 |
| Table 6.11. Accuracy results of CNN and CNN-SAE methods for experiment I after artifact removal..... | 99 |
| Table 6.12 Accuracy results of FBCSP method for experiment I after artifact removal..... | 99 |
| Table 6.13 Accuracy results of CNN-SAE method for experiment II..... | 103 |
| Table 6.14 Kappa results CNN-SAE method for experiment II..... | 103 |
| Table 6.15 Accuracy results of FBCSP method for experiment II..... | 104 |
| Table 6.16 Kappa results of FBCSP method for experiment II..... | 104 |
| Table 6.17 Comparison between accuracy results of methods for experiment II.... | 105 |
| Table 6.18 Accuracy results of experiment III, Graz sessions..... | 107 |
| Table 6.19 Accuracy results of experiment III, CNN sessions..... | 107 |
| Table 6.20 Results of experiment IV for 15 recording sessions..... | 109 |

LIST OF FIGURES

FIGURES

| | |
|--|----|
| Figure 2.1 Overview of a BCI system..... | 12 |
| Figure 2.2 An example electrode placement according to the international 10–20 system..... | 16 |
| Figure 2.3 P300 spelling paradigm character matrix [35]..... | 17 |
| Figure 2.4 A sample of character sets based on SSVEP [39]..... | 19 |
| Figure 2.5 MI based speller with six hexagons chosen by two MI tasks [50]..... | 21 |
| Figure 2.6 MI based speller with four boxes each chosen by one of four MI tasks [51]..... | 21 |
| Figure 3.1 SVM example for 2D case..... | 32 |
| Figure 3.2 Architecture of the applied FBCSP method..... | 34 |
| Figure 3.3 A single neuron unit..... | 36 |
| Figure 3.4 A sample 3 layer MLP network..... | 37 |
| Figure 3.5 Lenet network taken from [131]..... | 40 |
| Figure 3.6 Autoencoder network example..... | 42 |
| Figure 4.1 Timing of BCI Competition II dataset III [134]..... | 49 |
| Figure 4.2 Timing of BCI Competition IV dataset 2b [135]..... | 50 |

| | |
|---|----|
| Figure 4.3 a. Recording room, b. Amplifier and power bank, c. Electrode input box..... | 51 |
| Figure 4.4 a. METU-Vision recording room. b. G.Nautiulus cap. c. G.Nautiulus base station | 52 |
| Figure 4.5 Electrode locations for experiments I and II..... | 53 |
| Figure 4.6 Electrode locations for experiment III..... | 54 |
| Figure 4.7 Electrode placement of G.Nautiulus cap, channels used for difference computation are connected with red line..... | 55 |
| Figure 4.8 Example of Clench teeth, eye blink and alpha waves..... | 57 |
| Figure 4.9 Timing of the experiment I..... | 60 |
| Figure 4.10 4 different visual stimuli used in the experiments..... | 60 |
| Figure 4.11 Timing of data acquisition part of experiment III..... | 64 |
| Figure 4.12 The timing of Graz experiment with online feedback..... | 65 |
| Figure 4.13 Simplified flowchart of CSP-LDA online classification part..... | 66 |
| Figure 4.14 Simplified flowchart of CNN online classification part..... | 67 |
| Figure 4.15 Timing of experiment IV..... | 69 |
| Figure 4.16 Simplified flowchart of experiment IV..... | 70 |
| Figure 5.1 a) A Right hand sample input image including 2 frequency bands for each electrode C3, Cz and C4. b) The same image as a 3D tensor..... | 75 |
| Figure 5.2 Proposed convolutional neural network model, NF=30..... | 77 |
| Figure 5.3. Proposed SAE model with 6 hidden layers..... | 79 |
| Figure 5.4. The proposed CNN-SAE network. Number of neurons in each layer is shown at top of the layer and the type of each layer is shown at the bottom..... | 80 |
| Figure 6.1 Average of input images for right and left hand classes and subjects 2 and 4..... | 89 |

| | |
|--|-----|
| Figure 6.2. Weight values W_k $k=1, 2, \dots, NF=30$, of filters of size $N_h \times 3$ learned by CNN for subject 4. For each filter there are $N_h=93$ components along vertical axis while there are 3 components along horizontal axis..... | 91 |
| Figure 6.3. Effect of number of epoch on kappa value and training time..... | 92 |
| Figure 6.4. Average of input images for right and left hand classes and subjects 4 and 6..... | 101 |
| Figure 6.5 Confusion matrix for subject S7..... | 106 |
| Figure 6.6 Accuracy results of experiment IV for 15 sessions..... | 110 |
| Figure A.1. Impedance measurement of data electrodes..... | 118 |
| Figure A.2. Impedance measurement of reference electrodes..... | 119 |
| Figure A.3. Impedance measurement of ground electrodes..... | 120 |

LIST OF ABBREVIATIONS

| | |
|-------|---------------------------------------|
| AE | Autoencoder |
| ANN | Artificial Neural Network |
| BCI | Brain Computer Interface |
| BHS | Squeeze ball with both hands fingers |
| BLDA | Bayesian Linear Discriminant Analysis |
| CAE | Convolutional Autoencoder |
| CAR | Common Average Reference |
| CLIS | Completely Locked-In State |
| CNN | Convolutional Neural Network |
| CSD | Current Source Density |
| CSP | Common Spatial Pattern |
| DBN | Deep Belief Network |
| ECOG | Electrocorticographic |
| EEG | Electroencephalography |
| EM | Expectation Maximization |
| ERD | Event-Related Desynchronization |
| ERS | Event-Related Synchronization |
| FBCSP | Filter-Bank Common Spatial Pattern |
| FEM | Foot Movement |

| | |
|--------|---|
| FES | Squeeze right foot fingers |
| FFT | Fast Fourier Transform |
| FLDA | Fisher Linear Discriminant Analysis |
| fMRI | Functional Magnetic Resonance Imaging |
| FRFS | Fuzzy-Rough set-based Feature Selection |
| GA | Genetic Algorithm |
| HMM | Hidden Markov Model |
| ICA | Independent Component Analysis |
| K-NNC | K-Nearest Neighbor Classifier |
| LDA | Linear Discriminant Analysis |
| LHM | Left Hand Movement |
| LHS | Squeeze ball with right hand fingers |
| MeA | Micro-electrode arrays |
| MEG | Magnetoencephalography |
| MIBIF | Mutual Information based Best Individual Feature |
| MIFS | Mutual Information based feature selection |
| MINBPW | Mutual Information-based Naïve Bayesian Parzen Window |
| MIRSR | Mutual Information-based Rough Set Reduction |
| MLP | Multilayer Perceptron |
| NBPW | Naïve Bayesian Parzen Window |
| NIRS | Near-Infrared Spectroscopy |
| PCA | Principal Component Analysis |
| PSD | Power Spectral Density |
| PSH | Push |

| | |
|---------|---------------------------------------|
| Pull | Pull |
| RBM | Restricted Boltzmann Machine |
| ReLU | Rectified Linear Unit |
| RHM | Right Hand Movement |
| RHS | Squeeze ball with right hand fingers |
| SAE | Stacked Autoencoder |
| SCP | Slow Cortical Potentials |
| SMR | Sensory-Motor Rhythms |
| SNR | Signal to Noise Ratio |
| SSVEP | Steady State Visual Evoked Potentials |
| std dev | Standard Deviation |
| STFT | Short Time Fourier Transform |
| SVM | Support Vector Machine |
| TOM | Tongue Movement |

CHAPTER 1

INTRODUCTION

1.1 Motivation of the Thesis

A Brain Computer Interface (BCI) system provides an alternative pathway between human brain and external devices. This process starts by recording the brain activity and continues through the signal processing part to detect the user's intent. Then an appropriate signal is sent to the external device to control the device according to the detected signal. BCI is now a flourishing field where many research groups all over the world are studying this topic. BCI systems have been studied for variety of applications for healthy and unhealthy people. However, designing a complete BCI system suitable for commercial use is still a challenge.

A BCI is a system that can recognize a certain set of patterns in brain signals. Electroencephalography (EEG) is the most convenient approach for collecting these brain signals considering its time and space resolution and non-invasive application. Motor Imagery (MI) signals are one of the well-known brain patterns commonly used in BCI applications. The term motor imagery refers to imagination of moving a body part without actually moving it. It is known that, the brain patterns during MI are similar to those of actual body movement. The recognition of these brain patterns are performed in the signal processing part of the BCI system. Therefore, signal processing methods play a critical role on the performance of the BCI. By the time

this thesis study was started, conventional machine learning approaches were being used in the signal processing part of BCI systems. These approaches were investigated in many studies and performed satisfactory under certain conditions. On the other hand deep learning methods have been applied successfully on many machine learning problems especially in computer vision field. Convolutional Neural Networks (CNN) for example are very successful in detecting complex features and patterns for image classification. Complex features and non-linear relationships between these features can be modeled inherently by the deep network through several layers of neurons. Since the nature of brain patterns in EEG is complex and highly non-linear, deep learning methods can provide higher success rate in the classification of these patterns. Furthermore, continuous data recording in BCI systems provide a large amount of data that is an important factor in the training of deep networks. These facts motivated us to use deep learning methods for classification part of BCI in this thesis study.

1.2 Scope of the Thesis

Brain Computer interface systems are investigated in this study where EEG is used as the signal acquisition method. The main objective of this thesis is to study the signal processing part of BCI. In order to control the BCI system, motor imagery signals are used in this study. Deep learning methods are investigated for the classification of MI related brain patterns. EEG signal acquisition, processing and feedback steps in BCI are studied in this thesis by performing different experiments where MI is used to control BCI and deep learning methods are used for signal processing.

1.3 Literature Survey

In this part, an overview of deep learning methods for EEG signal classification including, also the methods developed in this thesis study, is presented. These methods are summarized in Table 1.1. In this table, the method presented in [1] is the method developed in this thesis. This method is applied for MI classification where Short Time Fourier Transform (STFT) is used to construct the input images. Utilized deep learning methods are Convolutional Neural Networks (CNN) for feature extraction and Stacked Auto encoder (SAE) for classification. EEG signals are collected from three channels and in CNN, the convolution is applied to one dimension which is time.

The methods in Table 1.1 are sorted according to their publication years. The article which presents the method developed in this thesis [1] and also the methods which use MI, STFT or CNN are bolded in this table since they are more related to the scope and contribution of this thesis. Different input data forms and network configurations used in these studies are discussed briefly in the following.

Table 1.1. Summary of deep learning methods for EEG signal classification

| Study | Year | Application Area | Input Domain | Deep Learning Method | Number of Channels | Convolution Dimension |
|-----------------------------|-------------|----------------------------------|---|----------------------|--------------------|---------------------------------|
| Mirowski et al. [2] | 2009 | Epilepsy | Bivariate features, time | CNN | 6 | 2D features and time |
| Wulsin et al. [3] | 2011 | Anomaly detection | Time, frequency features | DBN | 10-17 | - |
| Cecotti and Graser [4] | 2011 | P300 | Channel, time series | CNN | 64 | 1D channel; 1D time |
| Langkvist et al. [5] | 2012 | Sleep stage detection | Channel, time series | DBN | 8 | - |
| Ahmed et al. [6] | 2013 | Rapid serial visual presentation | Time, frequency features | DBN | 256 | - |
| Stober et al. [7] | 2014 | Auditory music retrieval | Time, frequency (STFT) | CNN | 12-13 | 2D frequency and time |
| Cecotti et al. [8] | 2014 | ERP detection | Channel, time series, spatial filter | CNN | 32 | 1D time |
| Xiu et al. [9] | 2014 | MI | Frequency (FFT) | DBN | 3 | - |
| Ren and Wu [10] | 2014 | MI | Channel, frequency | Convolutional DBN | 3,60,118 | 1D frequency |
| Bashivan et al. [11] | 2015 | Mental load detection | Location, time, frequency | Recurrent CNN | 64 | 2D location |
| Stober et al. [12] | 2015 | Auditory music retrieval | Channel, time series, PCA | CNN, CAE | 64 | 2D channel and time |
| Manor and Geva [13] | 2015 | Rapid serial visual presentation | Channel, time series | CNN | 64 | 1D channel; 1D time |
| Sakhavi et al. [14] | 2015 | MI | Time, frequency (Hilbert transform) | CNN, MLP | 22 | 1D time |
| Yang et al. [15] | 2015 | MI | ACSP features | CNN | 22 | 2D frequency and time |
| Tabar and Halici [1] | 2016 | MI | Channels, time, frequency (STFT) | CNN-SAE | 3 | 1D time |
| Antoniades et al. [16] | 2016 | Epilepsy | Channel, time series | CNN | 12 | 1D time |
| Liang et al. [17] | 2016 | Epilepsy | Channel, time, frequency (FFT) | CNN | 15-24 | 2D frequency and time |
| Page et al. [18] | 2016 | Epilepsy | Channel, time series | CNN | 20-23 | 2D channel and time |
| Thodoroff et al. [19] | 2016 | Epilepsy | Location, time, frequency (FFT) | Recurrent CNN | 23 | 2D location |
| Shamwell et al. [20] | 2016 | Rapid serial visual presentation | Channel, time series | CNN | 64 | 1D channel; 1D time |
| Lawhern et al. [21] | 2016 | P300, MI | Channel, time series | CNN | 50,22 | 1D channel; 2D time and channel |
| Kwak et al. [22] | 2017 | SSVEP | Channel, frequency (FFT) | CNN | 8 | 1D channel |
| Tang et al. [23] | 2017 | MI | Channel, time series | CNN | 28 | 1D channel |

Several EEG studies employ Deep Belief Network (DBN) in order to perform tasks like anomaly measurement of EEG signals [3], classification of image RSVP events [6], Sleep stage detection [5], feature extraction [10] and motor imagery classification [9]. In a study by Xiu et. al [9], a DBN model was applied for two class MI classification and was shown to be more successful than the SVM method.

Convolutional neural networks are used in several EEG studies for epilepsy prediction and monitoring [2, 16-19], detection of visual-evoked responses [8, 13, 20, 22], auditory music retrieval [7, 12], mental workload classification [11], P300 classification [21, 24] and motor imagery classification [9, 14, 15, 23].

In [2], bivariate features are computed for any two EEG channels as a measure of a certain relationship between two signals. These features are computed for different time windows and the 2D input image is constructed. The input images are then used in a 2D CNN.

The time series of EEG channels are used to construct the input image in [4, 13, 20] and used in a CNN where 1D convolution is applied separately on time and space domains. Similar to these studies, raw EEG signals (channel, time series) are used in [8, 16, 18] where convolution is applied either on time [8, 16] or time and channel domains [18].

In [14], Hilbert transform was used to extract the energy of each channel. The extracted energies are summed over channels and used in a network where CNN and Multi-Layer Perception (MLP) models are used. Fast Fourier Transform (FFT) was used in [17] in order to construct 3D input data (channel, frequency, time). 2D Convolution was applied in frequency and time domains in this study. In [22], FFT was used to extract 120 frequency samples for each channel and use them in a CNN where 1D convolution is applied in channel domain. In [12], principle component analysis (PCA) features are extracted from EEG signals and CNN and Convolutional Autoencoder (CAE) networks were used to learn most distinguishable features.

A five layer CNN is applied to raw EEG data in [23], in order to classify left and right hand motor imagery tasks from two subjects. In [21], several CNN's are studied in order to construct a compact fully convolutional network for different EEG-based

BCIs. They show that their proposed network compares favorably to the current state-of-the-art approaches for many different BCI modalities. In a recent study [11], a new form of multi-dimensional features was proposed and employed in a recurrent-convolutional neural network architecture in order to model cognitive events from EEG data. The input data in this study includes location, time and frequency information. In [10], a convolutional deep belief network is used to classify frequency features of motor imagery EEG signals.

Studies above are generally using CNN to learn the features in EEG signal and also to classify them. However in our proposed network [1], the features are learned in the CNN, but they are classified through a deep SAE network. This way more complex relationships between the features can be modeled.

EEG signals are usually fed to the CNN as raw signals in the studies above. However, there are some studies that convert EEG signals to 2D images differently. EEG signals are converted to 2D images and used in CNN network in [7] for auditory music retrieval purpose. Short Time Fourier Transform (STFT) is used in this study to extract frequency-time distribution of each channel. The extracted 2D images are then classified separately by a CNN and the final decision is made by using majority voting method. Our proposed input form [1] is different from this study by combining STFT outputs of different channels and using them in BCI application. This way the network also learns the spatial relationship between the activation patterns. In [11], the authors proposed a new form of features that preserve the spatial, spectral, and temporal structure of EEG. In this method, power spectrum of the signal from each electrode is estimated and sum of squared absolute values are computed for three selected frequency bands. Then polar projection method is used to map the electrode locations from 3D to 2D and construct the input images. The classification is performed by a recurrent convolutional network in this study. . The same method was used in [19] for automatic seizure detection. Unlike [11] where spectral measurements are aggregated for each band, in our proposed method [1], spectral content of mu and beta frequency bands are used explicitly. This way we preserve activation patterns among different frequencies as well as time and location.

1.4. Contribution of the Thesis

A new method for classification of EEG MI signals is proposed in this thesis. Besides, a new form of input that combines time, frequency and location information extracted from MI EEG signal is introduced in this study. Short Time Fourier Transform (STFT) method was used to convert EEG time series into 2D images. Input data is used in a 1D Convolutional Neural Network (CNN) to learn the activation patterns of different MI signals. 1D convolution is applied only in time axis, rather than frequency and location. Therefore, the shape of activation patterns (i.e. power values from different frequencies) and their location (i.e. EEG channel) are being learned in the convolutional layer. Max-pooling is applied after convolution in time axis, which makes CNN partially invariant to the time location of activation patterns. Then a Stacked Autoencoder (SAE) with 6 hidden layers is used to improve the classification through a deep network.

The proposed approach is analyzed and evaluated by using BCI Competition IV dataset 2b and BCI Competition II dataset III. The results of methods used in this study are compared with the results of current state of art algorithms in this field.

In order to investigate the performance of our proposed classification method in a BCI system, we performed several motor imagery experiments in this thesis. In experiments I, a motor imagery experiment was designed to record EEG signals related to brain activities during motor imagery tasks. The experiment was applied to 9 subjects where four different motor imagery tasks were performed. The recorded data was classified using proposed methods and compared to Filter-Bank Common Spatial Pattern (FBCSP) method which is widely used in this field.

By investigating the results of experiment I, several problems were determined. The recording time for each session was so long which caused the subjects to loose concentration. The MI tasks were also not evident. Therefore experiment II was designed with shorter recording times and 10 evident MI tasks. This experiment was

applied to 7 subjects. The recorded data was classified similar to experiment I and successful subjects and most distinguishable tasks were determined. Improvement in the overall MI performance was observed at the end of this experiment.

In order to investigate the proposed classification method on a real time system, experiment III was designed and performed on one subject. This experiment was designed similar to Graz experiment [25]. Two MI tasks were used in this experiment where the performed tasks were classified in real time and the results were provided to the subject via visual feedback. Two sessions of this experiment was performed by using a classification method based on Common Spatial Pattern and Linear Discriminant Analysis (CSP-LDA) similar to Graz experiment. Another two sessions were performed by using the proposed CNN method for classification. The experiment was applied successfully and the performance was observed to improve with subject training.

The effect of subject training was further investigated in experiment IV where 15 recording sessions with real time feedback were applied during 45 days on one subject. The proposed classification method was used to classify the recorded data in this experiment. The changes in motor imagery performance were monitored during 15 sessions.

By performing these experiments we had the opportunity to test our classification method in different BCI related conditions. Furthermore we were able to investigate different aspects of BCI experiments.

By the time this thesis study was started, deep learning methods were used only in few BCI studies [4, 8, 9] and CNN was not used for MI based BCI yet. STFT method employed in this thesis was used previously in only one EEG study [7] to converted EEG signals to 2D images for auditory music retrieval purpose. Different from this study, STFT is used for MI classification in this thesis study. Moreover, different from [7], in our proposed method the STFT outputs of different channels are combined to preserve time, frequency and location information in one 2D image.

During the paper review and publication period of this study, the interest on using deep learning methods in EEG studies started growing and several other studies published by different groups [11-15]. The amount of studies in this field started growing rapidly after the publication of our study [16-23]. Deep learning methods are shown in these studies to provide fast classification with higher performance comparing to the conventional methods.

1.5 Organization of the Thesis

The rest of this thesis is organized as follows: In chapter 2, a brief overview of a BCI system is presented. Different aspects of a BCI system are discussed in this chapter. In Chapter 3, theoretical background of signal processing methods used in this study is presented. In chapter 4, data collection experiments performed during this thesis are discussed. The details of public datasets used in this thesis are also explained in this chapter. Our proposed method for MI classification is explained in details in chapter 5.

In chapter 6, first the performance results of our proposed method are investigated on public datasets. The results are compared to current state of art methods and different factors of the proposed method are discussed. Then the results of proposed classification methods are discussed on data recorded during data collection experiments.

Finally the conclusion of this thesis is presented in chapter 7.

CHAPTER 2

OVERVIEW OF BRAIN COMPUTER INTERFACE SYSTEMS

Human brain controls the body by passing signals through peripheral nervous system. This process is started with the human's intent and continues through peripheral nerves until the destination body part is reached. Recent advances in electrophysiological recording technology offer alternative ways to bypass the peripheral nervous system and control of a device directly by brain. Such a system that is responsible for translating brain activity to device control command is called Brain Computer Interface (BCI) [26].

A BCI measures the brain activity patterns produced by user's intent and uses it for applications like communication or control. This can be very helpful for patients with motor disabilities. However the application of BCI is not limited to people with disabilities. BCI can be used in variety of applications from communication tools for Completely Locked-In State (CLIS) patients to video gaming for healthy people.

An overview of a BCI system is given in Figure 2.1. The device to be controlled may be a wheelchair, a neuroprosthesis, a computer, a game console or any other device. In a BCI system, the user represents his/her intention by a mental activity. The resulting brain signals are transmitted to a computer and processed to generate a control signal for the device to be manipulated. The control signal is used to change the state of the device controlled and a feedback about the new state of the device is provided to the user. The loop continues as the user changes its mental activity according to the new state of the device.

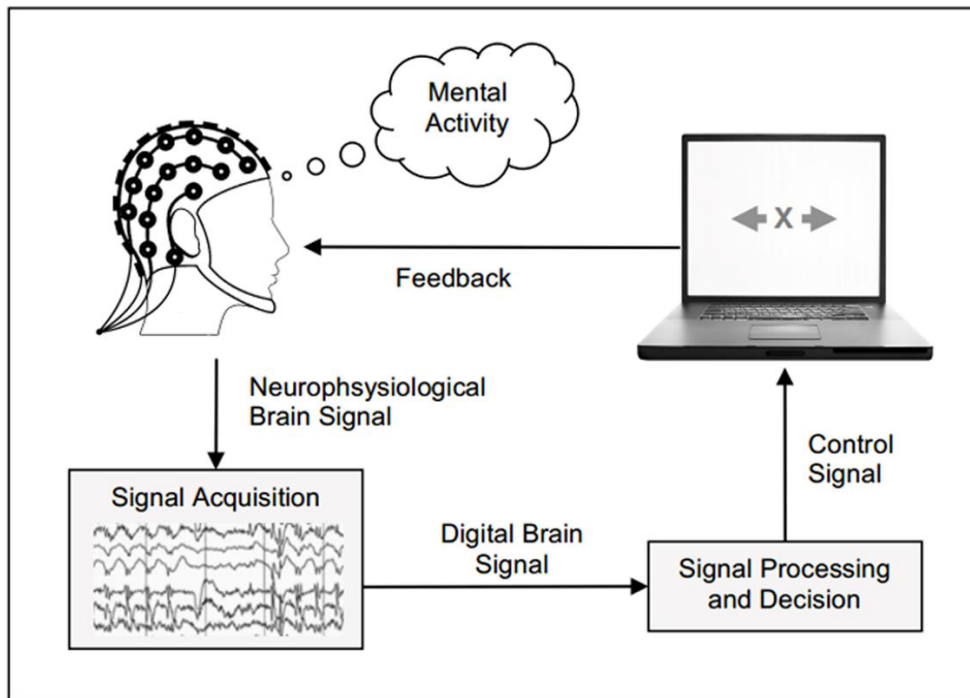


Figure 2.1. Overview of a BCI system

Any BCI system interacts with the user by using different types of feedback signals. Using these feedbacks provides the adaptation of the user to the system and also the system to the user. Subjects learn to regulate their brain activities by using the online feedback signals sent by the BCI system. The information collected may also be used to train the BCI system through machine learning algorithms.

There are different control paradigms that define how the user interacts with the BCI system. In asynchronous control, users can interact with a BCI anytime without worrying about timing. However, in a synchronous control system there are specific time intervals that user should respond to only in these periods. This is the easiest and probably the most common paradigm in BCI applications.

People with motor disabilities can use BCI to control their environment. Controlling the TV, lights or room temperature can improve the quality of life for these people [27]. Locomotion is another BCI application that helps disabled people to transport.

This way, people with physical impairments can control their wheelchairs autonomously [28]. Improvements in BCI technology have opened a new way to extend BCI use by non-disabled people. BCI provides a new interaction modality to play video games or use computers. In some recent studies, simple video games like Pacman are being controlled by motor imagery [29, 30].

Speech communication, which is also called silent speech, is one of the main applications of the BCI for people who have communication disabilities. There have been a lot of studies in the field. In these studies, variety of brain activities have been used to select the target letter from an on-screen display. One of the most popular paradigms for BCI control in communication applications is to use P300 event-related brain potentials. These signals are used in many speech communication studies in BCI [31-35]. Steady State Visual Evoked Potentials (SSVEP) are other types of control signals that have been used frequently for speech communication [36-40]. Motor imagery signals are also popular in speech communication [41-43].

The aim of this chapter is to discuss different parts of a BCI systems. In part 2.1, how to measure brain activity in general is explained. Different brain activity patterns used in BCI are explained in part 2.2. An overview of signal preprocessing methods deployed in BCI systems is presented in part 2.3. The signal processing part of BCI systems is briefly explained in part 2.4. Feedback and control part of a BCI system is explained in part 2.5. Finally, the applications of BCI systems are explained briefly in part 2.6.

2.1 Measuring Brain Activity

Brain activity produces electrophysiological and hemodynamic activities. There are different sensors that can detect different types of activities in the brain. Signal acquisition methods can be categorized in to two main groups: invasive and non-invasive techniques. Table 2.1, which is an extended version of the table provided in [44], summarizes different signal acquisition methods.

Table 2.1. Properties of different signal acquisition methods.

| Imaging Technique | Activity measured | Direct/Indirect Measurement | Temporal Resolution | Spatial Resolution | Risk | Portability |
|-------------------|-------------------|-----------------------------|---------------------|--------------------|-----------------|--------------|
| MeA | Electrical | Direct | ~ 0.03 s | ~2.8 mm | Highly invasive | Portable |
| ECoG | Electrical | Direct | ~0.005 s | ~10 mm | Invasive | Portable |
| EEG | Electrical | Direct | ~ 0.05 s | ~10 mm | Non-Invasive | Portable |
| MEG | Magnetic | Indirect | ~ 0.05 s | ~5 mm | Non-Invasive | Non-Portable |
| fMRI | Metabolic | Indirect | ~1 s | ~1 mm | Non-Invasive | Non-Portable |
| NIRS | Metabolic | Indirect | ~1 s | ~5mm | Non-Invasive | Portable |

Invasive methods record the brain signals using sensors implanted inside the body. Micro-electrode arrays (MeA) are highly invasive since they are implanted inside the brain [45]. Electrographic (ECoG) activity recording is another invasive approach in which the sensors are placed not inside but on the surface of the brain [46]. Despite the accurate signal recording ability of the invasive methods, surgery risks and implant related problems make these methods less preferable for BCI applications. However, there are some studies that used EcoG [47] and MeA [48] for BCI applications.

Non-invasive techniques involve all the methods that record brain activity from outside of the body boundaries. These methods can measure two groups of signals: signals from hemodynamic (blood oxygenation levels) activities and signals from electrophysiological (neuronal) activities [49]. The first group of signals can be detected with Functional Magnetic Resonance Imaging (fMRI) or Near-Infrared Spectroscopy (NIRS) methods. In fMRI, blood oxygenation level-dependent (BOLD) signals associated with cortical activation are being measured. Different oxygen levels of the blood can also be measured by NIRS which is a portable device with a higher temporal resolution but lower spatial resolution compared to fMRI [50]. There are few studies that use fMRI for BCI applications [51, 52]. This is according to the difficulty in real time measurement of the brain activity. On the other hand, fNIRS is

being used in several BCI studies in the recent years, although it has lower spatial resolution [53-55].

Magnetoencephalography (MEG) and Electroencephalography (EEG) methods are two basic modalities for measuring brain electrophysiological activities. MEG measures the brain activity with high resolution by measuring the magnetic fields induced by the neuron's electric current. Although MEG equipment is large and expensive that makes it a poor choice for BCI applications [44], some studies have used MEG for BCI applications [56-58].

EEG also records brain activity by measuring the electrical fields produced by firing neurons. EEG signals have comparatively low spatial resolution but, high temporal resolution with cheap and easy to use equipment [44]. These features make the EEG a proper choice for BCI applications. EEG is used as the signal acquisition method in a plenty of BCI studies and therefore, it is explained in detail in the following part.

2.2 Brain Activities Used In EEG Based BCI

In EEG, sensor electrodes are placed over the head to measure the brain activity. The number of electrodes can change from 1 to more than hundred electrodes. To place the electrodes in accurate places over head and measure the activities in different parts of the brain, the international 10–20 system is being used. In this system, the distances between the electrodes are 10% or 20% of the front–back or right–left distance of the skull. Each region has a letter corresponding to the brain lobe (F frontal, T temporal, C central, P parietal, and O occipital) and a number specifying the hemisphere location. An example placement of 19 electrodes according to the international 10–20 system is shown in Figure 2.2.

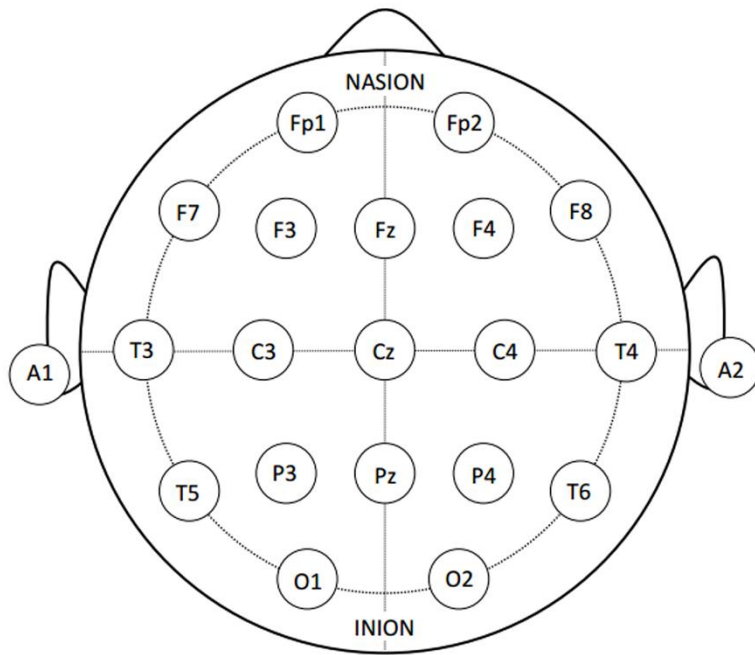


Figure 2.2 An example electrode placement according to the international 10–20 system

The brain as a result of conscious or unconscious mechanisms may generate different brain activity signals. The function of most of these signals is not clear yet. However, the physiological phenomena of some of these signals are understood and being used in BCI applications. These signals are P300 evoked potentials, Steady State Visual Evoked Potentials (SSVEP), Slow Cortical Potentials (SCPs) and Sensory-Motor Rhythms and Motor Imagery.

2.2.1 P300

P300 evoked potentials are positive peaks in the EEG because of infrequent task related stimuli. These potentials appear in the EEG signal, approximately 300 ms

after the stimulus. To evoke P300, user is given series of random stimulus. Whenever the target (infrequent) stimulus is observed, P300 appears in the EEG [31]. Visual stimuli is used in most of P300 based BCI systems. However there are few studies that employ auditory stimuli [59]. Visual P300 evoked potentials are widely used in BCI applications specially for speech communication [31-35, 60]. In such applications, a matrix of characters is displayed to the subject. The rows and columns of the matrix are intensified sequentially and the subject attends to the target character. The attention of the subject to an intensified character evokes an enhanced P300 component. A classifier can be trained to detect the target character by using the combination of intensified rows and columns. A sample character matrix used in P300 spelling paradigm of [60] is shown in Figure 2.3.

| TYPE | | | | | |
|------|---|---|---|---|---|
| A | B | C | D | E | F |
| G | H | I | J | K | L |
| M | N | O | P | Q | R |
| S | T | U | V | W | X |
| Y | Z | 1 | 2 | 3 | 4 |
| 5 | 6 | 7 | 8 | 9 | - |

Figure 2.3. P300 spelling paradigm character matrix [60]

It is difficult to detect the target character from a single P300 trial. Therefore each row and column is usually flashed for several times. This decreases the information

transmission rate that is an important factor in BCI systems. The accuracy of P300 signal classification is also too low in current applications.

P300 signals have also been used for other BCI applications like controlling cursor on the screen [61] and robot control [62].

2.2.2 SSVEP

SSVEP signals are oscillations observable at the occipital lobe, because of visual stimulation. Frequencies of the oscillations are the same as the frequencies of the stimulation [63]. When the subject focuses on a stimulus, the amplitude in the corresponding frequency bands is increased. By using this fact, it is possible to detect if the subject is looking at the display part with frequency f or $2f$, $3f$, etc. Several graphical interfaces have been proposed for this purpose. Figure 2.4 shows a simple form of SSVEP speller. In this example, symbol v is selected in three stages. Each stage is composed of four boxes in the display with different flickering frequencies [64]. In each stage, subject focuses on the box containing the symbol v .

Different forms of SSVEP based spellers are introduced for speech communication [36, 38, 39]. SSVEP signals are also used in the literature for other applications like cursor control [37]. Since the SSVEP is embedded in other ongoing brain activity and also noise, the recording interval should be long. Another limitation is that only flickering frequencies within a particular frequency range evoke a reasonable SSVEP response [65]. Further studies are needed to provide a SSVEP based speller for commercial uses.

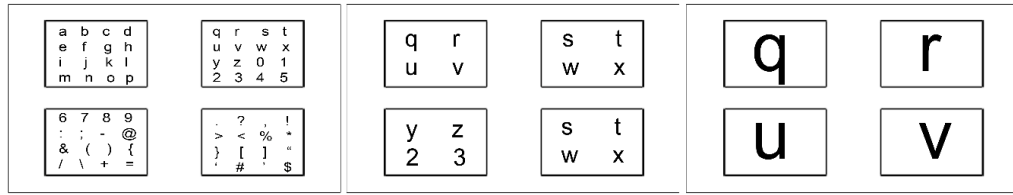


Figure 2.4. A sample of character sets based on SSVEP [64]

2.2.3 SCP

SCP appears as slow voltage shift in the EEG in the frequency range 1-2 Hz. Decrease in cortical excitability causes negative SCPs and increase in cortical excitability causes positive SCPs. It is shown that users can be trained to control their SCPs by using visual or auditory feedback signals [66]. SCP signals are used in different studies in order to provide communication for ALS patients [67]. Currently the classification accuracies of different methods for SCP signal classification are in acceptable rates. However the information transfer rate is so low comparing to other BCI systems. Besides the time needed to train subjects before successful application is about several months.

2.2.4 Sensory-Motor Rhythms and Motor Imagery

According to the state of the brain, different oscillations happen in brain activity. These oscillations are categorized into 4 different groups based on their frequency band in EEG: delta (1-4 Hz), theta (4-8 Hz), mu (8-13 Hz), beta (13-25 Hz), and gamma (25-40 Hz). Sensory-Motor Rhythms (SMR) refers to oscillatory activities observed in somatosensory and motor areas. The activations in different parts of the body are mapped to different regions in the sensorimotor cortex of the brain. An activity in a particular part of body causes a decrease in SMR activity in the related

brain area. This decrease is called Event-Related Desynchronization (ERD) [68]. Correspondingly, Event-Related Synchronization (ERS) is the increase in SMR activity during the relaxation period after the body movements. These ERD and ERS activities also happen when the subject is imagining the body movement and not actually moving the body. ERS/ERD oscillations can be observed in EEG in beta and mu frequency bands.

The term motor imagery refers to imagination of moving a body part without actually moving it. As it is discussed above, this imagination causes ERD activities in brain that can be observed in EEG. However, ERD/ERS patterns of all body parts cannot be discriminated in EEG. The produced patterns should be large enough to be distinguished from the background EEG. Currently, there are four types of motor imagery actions that can be detected via EEG. These actions are movement of left hand, right hand, feet and tongue. These four motor imagery signals can be used to control BCI after attending sufficient training sections [69].

MI related signals are usually recorded by using C3, C4 and Cz electrodes according to international 10-20 system. Activity invoked by imagining the movement of right hand can be observed mostly in electrode location C3 in the left part of the sensorimotor cortex of the brain. Left hand movement imagery can be observed mostly in C4 location in the right part of sensorimotor cortex of the brain.

Movement imageries of left and right feet are not distinguishable since the corresponding motor rhythm origination areas take part in a sulcus (groove in the cerebral cortex). Therefore, the measured potential on the scalp are so close spatially. They both invoke activity mostly over Cz area [70]. Motor imagery is used in wide range of BCI applications in order to send the desired command. In [71] motor imagery is used for cursor movement. It is also used for controlling wheelchair [72] and robot arm [73]. Speech communication is another popular application of motor imagery [41, 42, 74]. Different spelling interfaces have been proposed in literature for MI based communication.

A speller is presented in [75] by using only two commands: left hand and both feet. In this study, 30 different characters are divided into 6 hexagons around a circle

(figure 2.5). By left hand command the arrow rotates in clockwise manner showing the selected box and by feet command the box is selected. A character can be selected in two stages.

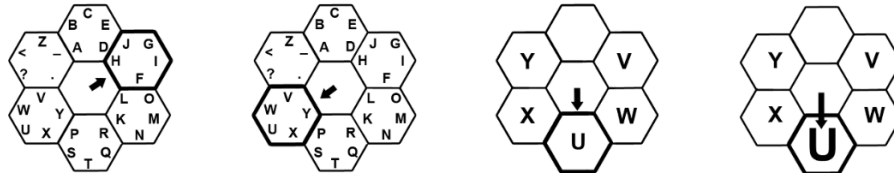


Figure 2.5. MI based speller with six hexagons chosen by two MI tasks [75].

Another speller system based on MI system, which is proposed in [76] shown in Figure 2.6. This system is composed of four boxes. 26 English characters and a space symbol are grouped in three boxes. The fourth box is used for undo command. The subject selects one of the boxes by imagining the movement of the corresponding body part. They have used left hand, right hand, both hands and both feet movement for command. The desired symbol can be selected in three stages.

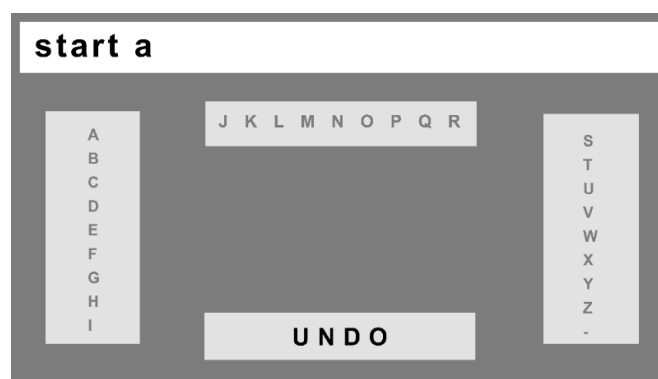


Figure 2.6. MI based speller with four boxes each chosen by one of four MI tasks [76].

The classification method plays a critical role in the performance of a MI based BCI system. Current state of art signal processing methods for BCI systems are discussed in part 2.3. Although the classification performance for different MI tasks is high for some subjects, other subjects may face difficulties in performing MI task. This causes a large difference between classification performances of subjects [77]. Despite the large amount of studies that investigate MI based BCI's, there is no usable commercial BCI in current state.

2.3 EEG Signal Preprocessing

The goal of preprocessing step is to improve the quality of the desired patterns in EEG and enhance the Signal to Noise Ratio (SNR). There are three main steps in EEG signal preprocessing: Referencing, temporal filtering and signal enhancement. Preprocessing also involves removal of undesired EEG artifacts.

2.3.1 Referencing

The choice of referencing in EEG based BCI applications can change the results dramatically. There are three main referencing strategies in EEG.

Common reference: In this approach an electrode far from other electrodes is selected as reference. This method is widely used in BCI applications.

Average reference: In this method, the average of the activity of all electrodes is subtracted from the measurements.

Current Source Density (CSD): It is "the rate of change of current flowing into and through the scalp" [78]. This quantity can be derived from EEG data, and it may be interpreted as the potential difference between an electrode and a weighted average of their surrounding electrodes.

2.3.2 Temporal Filtering

Informative brain signals for BCIs are found in the frequencies below 30 Hz. Therefore, all other content with higher frequencies can be removed using a low pass filter. Depending on the EEG application, specific frequency bands may also be selected using band-pass filters.

2.3.3 Signal Enhancement

Due to the volume conduction effects, potentials from a large area affect the measured potential in one electrode. To estimate contribution of each electrode, a linear transformation may be applied to EEG signal. Methods like Common Average Reference (CAR) and Laplacian filter preserve the original values of electrodes. Some other methods like Principal Component Analysis (PCA) [79] and Independent Component Analysis (ICA) [80] try to find independent sources without a direct reference to original channels. Some of these methods are explained in further parts of the thesis.

2.3.4 EEG Artifacts

EEG signal includes undesired potentials that corrupt the brain signals. These signals are called artifacts and should be cleaned before the processing step. Artifacts may originate from outside the human body (non-physiological) or inside human body (physiological). The first type artifacts may originate due to recording equipment. There are also some activities inside human body that may cause artifact. Ocular, caused by eye blinking and pupil movement, and muscular, caused by movement of body parts, are two main groups of physiological artifacts.

Artifacts can be handled by using three different strategies: avoiding, rejecting and removing. Artifacts may be avoided by asking the subjects to avoid moving and eye blinking. Artifacts can also be identified and rejected by an expert in offline applications. Artifact removal approach attends to detect and remove the artifacts automatically during the signal processing step. Because of the online application of BCI, this approach is the preferred method for BCI studies. There are several methods for artifact removal in the literature like linear filtering, linear combination and regression and Principle Component Analysis (PCA). Some of these methods are explained in the further parts of this thesis.

2.4 EEG Signal Processing

Once the brain activity patterns are measured, the next step is to process these signals in order to translate them into the appropriate control commands. Similar to other machine learning and pattern recognition problems, signal processing is usually applied in feature extraction and classification steps for BCI systems.

There are many feature extraction and classification methods employed in different studies for signal processing part of BCI systems. Time and frequency domain features and CSP method are used in this thesis for feature extraction and explained in details in parts 3.1.1 and 3.1.2. Principal Component Analysis (PCA) [79], Independent Component Analysis (ICA) [81], Genetic Algorithm (GA) [82] and AdaBoost [83] are other feature extraction methods which are used widely in BCI studies.

PCA is used to reduce the dimension of the feature space before classification in many studies [84-87]. It is also used in [88] to remove the EEG artifacts and reduce noise. ICA is also a well-known method in BCI studies usually used to remove artifacts from the EEG signal before the classification [89]. However it can also be used as a classification method [90]. In BCI studies, GA method is used to select features from Power Spectral Density (PSD) of each EEG channel during motor imagery task [91] and to select features for P300 classification [92]. AdaBoost

method is used for feature selection and also for classification purposes in some BCI studies [86, 93].

Conventional classification methods in machine learning are employed for signal classification in BCI studies. Linear Discriminant Analysis (LDA), Support Vector Machine (SVM) and Filter-Bank Common Spatial Pattern methods are used in this thesis and discussed in parts 3.2.1-3. Artificial Neural Networks and Deep Learning methods are also explained in details in part 3.3.

Other classification methods like K-Nearest Neighbor Classifier (K-NNC) [94], Bayesian Statistical Classifier [95] and Hidden Markov Models (HMM) [96] has also been used in BCI studies. K-NNC is proven to be efficient when the dimension of the feature vector is low that makes it not very popular in BCI research [44]. Bayesian classifiers have been used in some motor imagery and P300 evoked potentials studies [44, 91]. HMM has also been employed in some BCI studies [97, 98].

A new method for signal processing of EEG signals in BCI systems is proposed in this thesis which is described in details in chapter 5.

2.5 Feedback and Control

Any BCI system should interact with the user by using different types of feedback signals. The adaptation of the user to the system and also system to the user is provided by using these feedbacks. Subjects learn to regulate their brain activities by using the online feedback signals sent by the BCI system. System also uses the information provided the subject to train the machine learning algorithms in the processing step.

There are different control paradigms that define how the user interacts with the BCI system. In asynchronous control, users can interact with a BCI anytime they want without worrying about predefined time windows. However in a synchronous control system there are specific time windows that user should respond only in those

periods. This is the easiest and probably the most common paradigm in BCI applications.

2.6 BCI Applications

BCI provides new communication and control channels without using peripheral nerves and muscles. Therefore, it can be very helpful for patients with motor disabilities. One major application of BCI is for people who have severe communication disabilities. People with motor disabilities can also use BCI to control their environment. Controlling the TV, lights or room temperature can improve the quality of life for these people. Locomotion is another BCI application which helps disabled people to transport. This way, people with physical impairments can control their wheelchairs autonomously.

Improvements in BCI technology have opened a new way to extending BCI use to non-disabled people. BCI provides a new interaction modality to play video games or use computers. In some recent studies, simple video games like Pacman are being controlled by motor imagery [53].

CHAPTER 3

SIGNAL PROCESSING BACKGROUND

BCI can be seen as a pattern recognition system that classifies each brain activity pattern into a class according to its features. Therefore signal processing plays an important role in the performance of the BCI systems. In this chapter, signal processing methods which are used in this study are discussed. An overview of feature extraction and classification methods employed in this study are presented in parts 3.1 and 3.2 respectively. Then, artificial neural networks and deep learning methods are discussed in more details in part 3.3.

3.1 Feature Extraction

The goal of signal processing stage of a BCI system is to separate brain patterns related to subject's intention from the other patterns. Therefore, we deal with a pattern recognition problem where different patterns should be classified according to their features. Selecting suitable features is a challenging issue. The values recorded from one electrode may contain overlapped signals from different sources. In this section, we briefly discuss most common feature extraction methods for BCI applications.

3.1.1 Time and Frequency Domain Features

Time domain features can be used when event related potentials are present in the signal. The relevant information can be separated based on the EEG signal amplitude by using methods like windowing and down sampling. Frequency domain features are derived from oscillations in the EEG signal. These features are mostly used in BCI systems based on SSVEP and motor imagery tasks. Different types of time [9, 23] and frequency [84, 99] domain features have been used in BCI studies. In [100], a fourth order Butterworth band-pass filter is used to select the frequency bands between 6–30 Hz, including mu and beta bands that correspond to limb movements. Then, different frequency bins and time segments are selected as features. In [101], bispectrum of motor imagery EEG signal is extracted from frequency component and classified by using LDA method.

Event related desynchronization (ERD) and event-related synchronization (ERS) can also be used as features. ERD and ERS are defined as the percentage of power decrease (ERD) or power increase (ERS) in a defined frequency band in relation to the reference interval with second duration before the verification of an event [99]. The band powers can be used as features in the classification algorithms.

3.1.2 Common Spatial Pattern (CSP)

Common Spatial Pattern (CSP) method [102] tries to map EEG channels into a subspace where the differences between channels are maximized and the similarities are reduced. The variances of the signals filtered by CSP can be directly used as features for classification [103]. This method has been used in many BCI applications especially for motor imagery tasks [84-88, 102-105].

CSP is originally designed to help classification of two classes of motor imagery tasks. The goal of CSP is to design a spatial filter that map EEG data into a subspace where the variances are optimal for discrimination of two classes. Suppose

$E \in R^{ch \times time}$ is our input EEG signal where ch is the number of channels and $time$ is the number of samples per channel. Then the output signal can be computed as:

$$S = W^T E \quad (3.1)$$

where $W^T \in R^{d \times ch}$ is the projection matrix and $S \in R^{d \times time}$ is the filtered output signal. Here d is the number of channels after projection. The normalized spatial covariance matrices of EEG data for classes 1 and 2 can be obtained as:

$$R_1 = \frac{E_1 E_1^T}{tr(E_1 E_1^T)} \quad (3.2)$$

$$R_2 = \frac{E_2 E_2^T}{tr(E_2 E_2^T)} \quad (3.3)$$

Where $tr(x)$ is the sum of diagonal elements of x . The average normalized covariances \overline{R}_1 and \overline{R}_2 can be obtained by averaging over all trails in classes 1 and 2. The composite spatial covariance R can be factorized as

$$R = \overline{R}_1 + \overline{R}_2 = U_0 \Sigma U_0^T \quad (3.4)$$

where U_0 is the matrix of eigenvectors and Σ is the diagonal matrix of eigenvalues. In order to equalize the variances spanned by U_0 , the whitening transformation P is used.

$$P = \sqrt{\Sigma^{-1}} U_0^T \quad (3.5)$$

$$S_1 = P \overline{R}_1 P^T, S_2 = P \overline{R}_2 P^T \quad (3.6)$$

This way S_1 and S_2 share common eigenvectors and the sum of two corresponding eigenvalues is one.

$$S_1 = U \Sigma_1 U^T, S_2 = U \Sigma_2 U^T, \Sigma_1 + \Sigma_2 = I \quad (3.7)$$

Therefore, the eigenvector with the largest value for S_1 has the smallest eigenvalue for S_2 and vice versa. So when we project whitened EEG onto first and last eigenvectors in U (i.e., the eigenvectors corresponding to the largest Σ_1 and Σ_2),

optimal separating variance is achieved. The projection matrix W can be computed as

$$W = U^T P. \quad (3.8)$$

CSP can be generalized for multiclass problems by performing the same two class method on different combination of classes. In this thesis, CSP method was used together with LDA in experiment III described in part 5.7.

3.2 Classification

The classification step aims to determine the subject's intention by using the features provided in the previous stage. These features are used to construct boundaries between classes in the training stage of the classifier and then they are used to discover the intention in the recognition stage. Some of the most popular classification methods used in BCI studies are discussed in the followings.

3.2.1 Linear Discriminant Analysis (LDA)

LDA is a simple classifier with acceptable accuracy and low computational requirements [106]. LDA is designed for classification of two classes but can be extended for multi classes. For a two-class problem, LDA tries to define a hyperplane in the feature space that distinguishes the classes. This hyperplane is defined by a linear discrimination function. The plane can be defined as:

$$g(x) = w^T x + w_0 \quad (3.9)$$

where w is the weight vector, x is the feature vector of the test sample and w_0 is a threshold. The input sample is assigned to one class based of the sign of $g(x)$ function. One common way to compute w is:

$$w = \Sigma_C^{-1}(\mu_2 - \mu_1) \quad (3.10)$$

where μ is the mean value and the common covariance matrix is defined as:

$$\Sigma_C = \frac{1}{2}(\Sigma_1 + \Sigma_2) \quad (3.11)$$

LDA has some drawbacks like failing in the presence of strong noise and not being stable. LDA can be used also for dimension reduction for feature extraction before classification. There are some improved algorithms based on LDA like Fisher LDA (FLDA) [107] and Bayesian LDA (BLDA) [108]. Due to the ability of online computation, this method has been applied in many BCI studies [42, 67, 84, 109].

3.2.2 Support Vector Machine (SVM)

The main idea in SVM is to select the hyperplanes separating the classes in a way that the distance from the nearest training points of different classes is maximized [110]. Figure 3.1 shows a separating hyperplane for a simple 2D case. Filled circle and squares are the nearest training points from different classes and the optimum hyperplane is selected in a way that the margin is maximized.

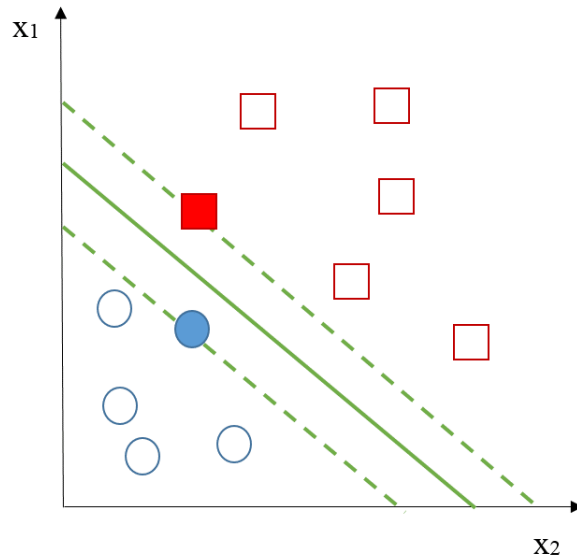


Figure 3.1. SVM example for 2D case.

SVM was proposed originally for classification of two classes but it can be extended to multi classes. It provides simple, robust and fast classification without needing a large training set. This method has been used in many BCI applications especially to classify P300 evoked potentials [69, 86, 109, 111, 112]. In [113], specific frequency bands are selected by performing time-frequency map analysis and CSP method is applied for feature extraction. The extracted features are then classified using SVM. In [114], the features are extracted by using CSP method similar to [113] and the frequency bands that lead to most successful classification are selected for each subject. Then twin SVM method [115] is used to classify features extracted from EEG motor imagery signals. Twin SVM is a modified version of SVM where two nonparallel planes are determined by SVM in order to classify the data.

3.2.3 Filter-Bank Common Spatial Pattern

Filter-Bank Common Spatial Pattern (FBCSP) method is developed based on CSP for motor imagery signal classification. This method has been designed for motor imagery classification and achieved best results in BCI competition IV for datasets 2a and 2b [105]. FBCSP is capable of performing two or multi-class classification and applied successfully in several motor imagery studies [116-118]. Therefore we applied FBCSP method as a baseline for MI classification and we compare the results of our proposed method with this method.

FBCSP method is composed of four stages. In the first stage 9 zero-phase band pass filters based on Chebyshev type 2 filters are applied to the data to cover the frequency bands between 8-40Hz. The frequency bands are 4-8, 8-12, 12-16, 16-20, 20-24, 24-28, 28-32, 32-36 and 36-40 Hz. In the second stage a CSP filter is applied to the output of each filter. CSP filter is constructed by using training data in order to perform a transformation that the variance of the output is optimized for discriminating two classes.

In the third stage a feature selection method is applied to select the most informative features. Several feature selection methods have been tested in the original study. These methods are Mutual Information based Best Individual Feature (MIBIF), Mutual Information-based Naïve Bayesian Parzen Window (MINBPW), Mutual Information based feature selection (MIFS), Fuzzy-Rough set-based Feature Selection (FRFS) and Mutual Information-based Rough Set Reduction (MIRSR). In our application, MIBIF algorithm was used for feature selection. This method leads to slightly better classification in the main study [104].

The features are then classified in the fourth stage by using classification methods. There are also several classification methods tested in the original study and Support Vector Machine (SVM) and Naïve Bayesian Parzen Window (NBPW) classifier methods are proposed to use for classification [104]. SVM method is used as classifier in our application.

The architecture of the FBCSP method applied in this thesis is shown in Figure 3.2. Four different stages of the method can be observed in the picture. Stage 1 and 2 were applied like the original study. In stages 2 and 3, MIBIF and SVM methods were used as proposed in the study. The details of MIBIF is presented in the next paragraph.

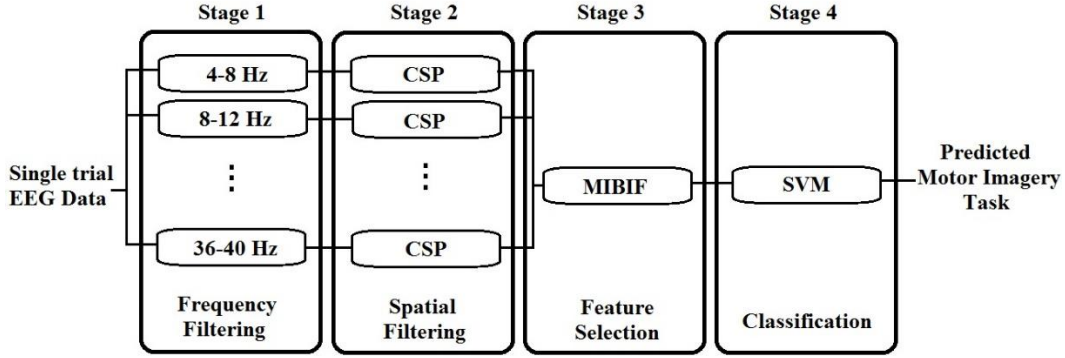


Figure 3.2. Architecture of the applied FBCSP method

In the feature selection part, the problem is to find a set of features S with k features that maximizes the mutual information $I(S, \Omega)$ where Ω is the class number. The mutual information between class number Ω and features X is defined as

$$I(X; \Omega) = H(\Omega) - H(\Omega | X). \quad (3.13)$$

With class number $\omega \in \Omega = \{1, \dots, N_w\}$, the conditional entropy is defined as

$$H(\Omega | X) = - \int_X \sum_{\omega=1}^{N_w} p(\omega | x) \log_2 p(\omega | x) dx \quad (3.14)$$

$H(\Omega | X)$ can be estimated by using the train data and applying classifier. MIBIF algorithm used for feature selection is described as follows:

Step 1. Initialize set of n features F where the set of selected features (S) is empty.

Step 2. Compute the mutual information $I(f_i; \Omega)$ for all features $f_i \in F$.

Step 3 Select best k features that maximize $I(f_i; \Omega)$ by a repetitive method.

The number of selected features k was selected as 4 in our application as proposed in [104]. The selected features are used in the SVM classifier for classification of the input signal.

3.3 Artificial Neural Networks and Deep Learning

In this part, theoretical background of artificial neural networks and deep learning methods will be discussed. Basic information about neural networks is provided in part 3.3.1. Multi-layer perception (MLP) and Convolutional Neural Network (CNN) methods are discussed in details in parts 3.3.2 and 3.3.3. Autoencoders and Stacked Autoencoders (SAE) are explained in part 3.3.4. Finally a general overview of deep neural networks is presented in part 3.3.5.

3.3.1 Artificial Neural Networks (ANN)

Artificial neural networks are non-linear classifiers that have been used in a wide variety of pattern recognition applications. ANNs are inspired by biological neurons where each neuron receives several input signals and produces an output if a threshold is reached. An ANN is composed of neurons and the connections between them. Each neuron has several inputs and one output. A single neuron is shown in Figure 3.3. In this figure, x_1-x_n are the inputs of the neuron and $h_{w,b}(x)$ is the output. There is also one bias input that settles the activation threshold of the neuron. Each connection has a weight value that describes the significance of the connection. These weight values are stored in the weight vector W .

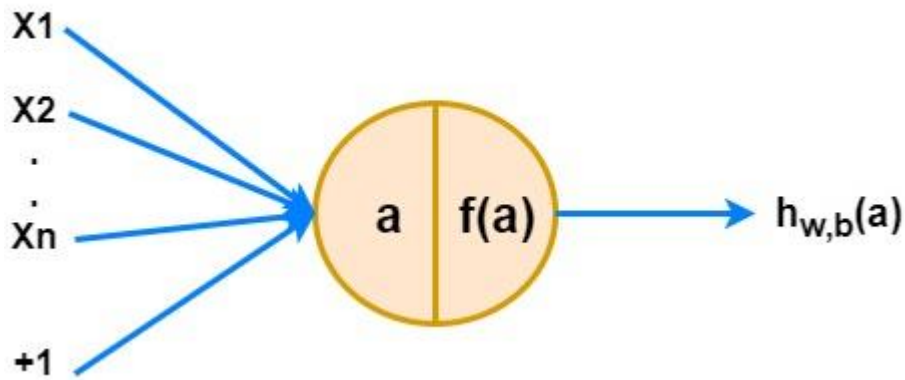


Figure 3.3. A single neuron unit

The output of the neuron can be defined as

$$h_{w,b}(x) = f(a) \quad (3.15)$$

where

$$a = \sum_{i=1}^n W_i x_i + b. \quad (3.16)$$

Here $f(a)$ is called the activation function of the neuron and a is the potential of the neuron. The activation function describes the switching status of the neuron and is dependent to neuron inputs and the threshold b . The most common form of output function used in ANN studies is the sigmoid function defined as:

$$f(a) = \frac{1}{1 + \exp(-a)} \quad (3.17)$$

Artificial neural networks are used in many BCI applications to classify two or more tasks [119-125]. In [125], a recurrent quantum neural network is designed to extract features from motor imagery signals by performing unsupervised learning. Afterwards, these features are classified by LDA classifier. ANNs have also been used in the preprocessing step of EEG studies to improve the classification accuracy [44].

3.3.2 Multi-Layer Perceptron (MLP)

A set of neurons with the same activation function f , construct one layer. In feedforward networks, the output of each neuron in layer l is only connected to the neurons of layer $l+1$. Hence, connections between the neurons do not form a directed cycle in this topology. The Multi-Layer Perceptron (MLP) is a form of feedforward network which is composed of one input layer, one or more hidden layers and one output layer. Each neuron in layer l of MLP is connected to all neurons in layer $l+1$. The output of the network is computed layer by layer and the final output is produced in the output layer. The number of layers in the network is called the depth of the network while the number of neurons in each layer is called the width of that layer. A sample MLP network is shown in figure 3.4. The depth of this network is 3 and the width of the hidden layer is 4.

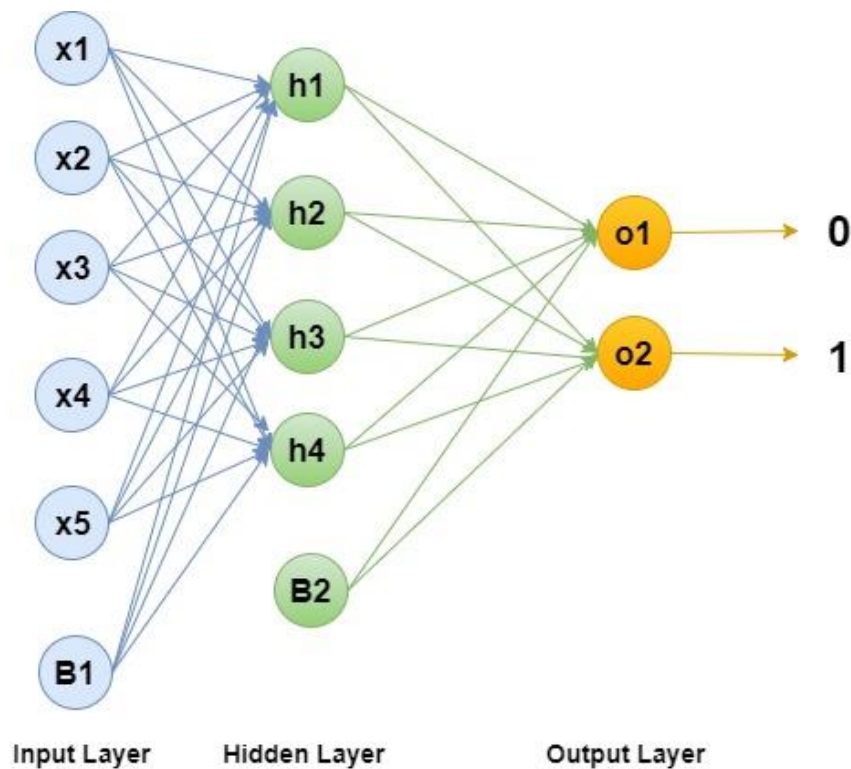


Figure 3.4 A sample 3 layer MLP network

MLP networks are commonly used for supervised learning where there is a labeled dataset. In supervised learning, the parameters of MLP network (i.e. weight W and bias b) are changed in order to fit to the data. Hence when a trial data x is fed to the input layer of the network, the produced value at the output layer should be the same as label of trial x . The learning problem can be solved by using back-propagation algorithm [126]. In this algorithm, a labeled training set is fed to the network and the difference between the computed output and the expected output is minimized.

Assume we have a training set of paired signal and related label as $\{(x_1, y_1), (x_2, y_2), \dots, (x_m, y_m)\}$. The error between the computed output and the expected output is called cost function and generally defined as mean squared error (equation 3.18).

$$J(W, b) = \left[\frac{1}{m} \sum_{i=1}^m (h_{w,b}(x) - y)^2 \right] \quad (3.18)$$

In order to minimize cost function J , gradient descent method can be used. In this method, gradient of the cost function is computed with respect to network parameters and the parameters are updated. In one iteration of gradient descent algorithm, the weight and bias values of the network are updated as

$$W_{ij}^l = W_{ij}^l - \alpha \frac{\partial}{\partial W_{ij}^l} J(W, b) \quad (3.19)$$

$$b_i^l = b_i^l - \alpha \frac{\partial}{\partial b_i^l} J(W, b). \quad (3.20)$$

Here, α is the learning rate, W_{ij}^l is the weight value of the connection between the neuron i in layer $l+1$ and neuron j in layer l and b_i^l is the bias value of layer $l+1$. In

order to compute $\frac{\partial}{\partial W_{ij}^l} J(W, b; x, y)$ and $\frac{\partial}{\partial b_i^l} J(W, b; x, y)$, backpropagation

algorithm can be used as follows [126]:

1. Compute all the activations for all hidden layers L_l and output layer L_{nl} . This step is called the forward pass.

2. Compute the error term $\delta_i^{n_l}$ for each neuron in the output layer as

$$\delta_i^{n_l} = -(y_i - h_{w,b}(x)_i) \cdot f'(a_i^l) \quad (3.21)$$

where a_i^l is the potential of the neuron i in layer l as defined in equation 3.16 and f is the activation function.

3. Compute the error term δ_i^l for each node i in hidden layer l as

$$\delta_i^l = \left(\sum_{j=1}^{s_{l+1}} W_{ji}^l \delta_j^{l+1} \right) \cdot f'(a_i^l) \quad (3.22)$$

where s_{l+1} is the number of neurons in layer $l+1$.

4. Finally compute the desired partial derivatives as

$$\frac{\partial}{\partial W_{ij}^{l+1}} J(W, b; x, y) = f'(a_j^{l+1}) \delta_i^{l+1} \quad (3.23)$$

$$\frac{\partial}{\partial b_i^{l+1}} J(W, b; x, y) = \delta_i^{l+1} \quad (3.24)$$

Steps 2-4 are considered as backward pass, where the derivatives of the cost function are propagated back through the network.

3.3.3 Convolutional Neural Networks

Convolutional Neural Networks (CNN) are multi-layer feed forward neural networks with several convolution-pooling layer pairs and a fully connected layer at the output. Standard CNN [127, 128] is designed to recognize shapes in images and is partially invariant to the location of the shapes. Input image is convolved with several 2D filters in the convolutional layer and subsampled to a smaller size in the pooling layer. Network weights and filters in the convolution layer are learned through back-propagation algorithm in order to decrease the classification error. A well-known CNN network(Lenet) [128] for image recognition is shown in Figure 3.5.

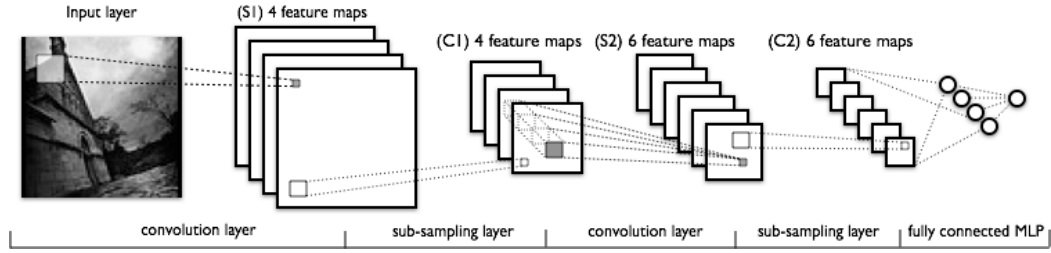


Figure 3.5 Lenet network taken from [129]

The input to the CNN is a $M \times M \times D$ image where M is the width and height of the image and D is the depth of the image. The depth of image is usually 3 for color images. The convolutional layers have k filters of size $N \times N \times Q$ where the size of filters are smaller than the input image. The image can have different width and height sizes. Here, these values are kept equal for simplicity.

The output of each convolutional layer is a set of K , $(M-N-1) \times (M-N-1)$ feature maps. One feature map h^k is determined by convolving input image X with weight filter W^k and adding the bias b_k as

$$h_{ij}^k = f((W^k * x)_{ij} + b_k) \quad (3.25)$$

where f is the activation function and $*$ is the convolution operator defined as

$$f(m, n) * g(m, n) = \sum_{u=-\infty}^{\infty} \sum_{v=-\infty}^{\infty} f(u, v) g(m-u, n-v). \quad (3.26)$$

A pooling layer is applied to the output of convolutional layer in order to reduce the dimension. Different types of pooling methods like max-pooling and average-pooling can be used in this layer. These methods operate on sub-regions of the feature map and deliver the maximum or average of that sub-region.

After convolutional-pooling layers, several fully connected layers may be applied. These layers are identical to standard feed forward networks. CNN's can be trained by using backpropagation algorithm similar to MLP.

Convolutional neural networks are used in several studies for classification of P300 [24] and motor imagery[14, 15, 23] EEG signals. In [23], a five layer CNN is applied to raw EEG data in order to classify left and right hand motor imagery tasks from two subjects. In [21], several CNN's are studied in order to construct a compact fully convolutional network for different EEG-based BCIs. They show that their proposed network compares favorably to the current state-of-the-art approaches for many different BCI modalities. In a recent study [11], a new form of multi-dimensional features was proposed and employed in a recurrent-convolutional neural network architecture in order to model cognitive events from EEG data.

3.3.4 Autoencoders and Stacked Autoencoders

Autoencoders [130] are simple neural networks that can be used for unsupervised learning. Autoencoder tries to set the output values equal to input values. A sample autoencoder is shown in Figure 3.6.

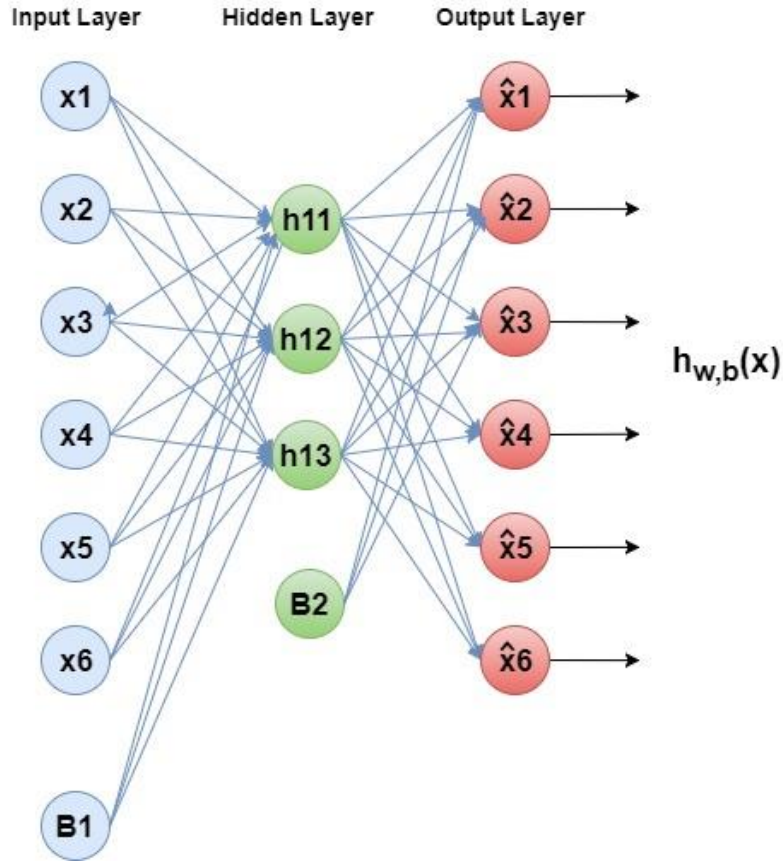


Figure 3.6. Autoencoder network example.

The number of output neurons is the same as inputs but the number of hidden neurons is different. So the input data is expressed with different (in most of the cases less) number of units. The weight values of these hidden neurons can be determined by using backpropagation algorithm. During training, the input x is first mapped to the hidden layer to produce hidden output y . Then, y is mapped to the output layer to produce z values. These two steps can be formulated as

$$y = f(W_y x + b_y) \quad (3.27)$$

$$z = f(W_z y + b_z) \quad (3.28)$$

where f is the activation function and W_y and W_z are the weights from input to hidden and hidden to output layers. b_y and b_z are bias values of hidden and output layers. If

we set $W_y = W_z^T$ where W_z^T is the transpose of W_z and denote it as W , the weights are said to be tied. This helps to obtain the model parameters by minimizing the cost function E . A sample cost function is presented in equation 3.18.

$$\arg \min_{W, b_y, b_z} [E(x, z)] \quad (3.29)$$

Here $E(x, z)$ is the reconstruction error when the network is trained to reconstruct the output values equal to the applied input values. Then the model parameters can be updated using equations 3.30-32 [131].

$$W = W - \alpha \frac{\partial E(x, z)}{\partial W} \quad (3.30)$$

$$b_y = b_y - \alpha \frac{\partial E(x, z)}{\partial b_y} \quad (3.31)$$

$$b_z = b_z - \alpha \frac{\partial E(x, z)}{\partial b_z} \quad (3.32)$$

Here α denotes the learning rate of the algorithm. After an AE is trained, the learned features in the hidden layer can be passed to any classifier like SVM in order to perform classification. They can also be used as input of the higher layer in a deep AE network, which is called Stacked Auto Encoder (SAE).

SAE is a neural network composed of an input layer, several AEs and an output layer. SAE's are generally trained by greedy layer-wise training method. In this method, each AE layer is trained separately in an unsupervised manner and the output of the hidden layer in the previous AE is used as input of the next layer in the deep network. After this unsupervised pre-training step, supervised fine-tuning step is applied to learn the whole network parameters by using back-propagation algorithm. In this step, all the layers of SAE are treated as a multilayer neural network and the weight and bias parameters are improved.

3.3.5 Deep Neural Networks

Deep neural network is a recent approach in neural networks allowing the network to extract much more complex features of the input by using several hidden layers. Each layer has a nonlinear activation function. This way, deep networks can represent much more functions in a compact form. The algorithms used to train the deep neural networks are called Deep Learning in general. The learned network can then be used for new test sets. Different deep learning architectures like CNN, SAE and Deep Belief Networks (DBN) [132] have been applied with great success in various scientific areas.

DBNs are multilayer deep networks formed by stacking Restricted Boltzmann Machine (RBM) [133] units. Similar to Autoencoders, each RBM unit has a single layer for hidden feature detection which extracts the patterns from the previous layer in a supervised way. Unlike AE, RBM's try to find stochastic representation of the previous layer. DBN is used in several EEG studies in order to perform tasks like anomaly measurement of EEG signals [3], classification of image RSVP events [6] and feature extraction [10]. In a study by An et. al [9], a Deep Belief Network (DBN) model was applied for two class MI classification and DBN was shown more successful than the SVM method. In [10], a convolutional deep belief network is used for classification of motor imagery EEG signals.

Due to the larger set of parameters, training a deep network is a difficult work. Computation time of deep networks is high comparing to simple neural networks. The computation time can be decreased by using some techniques like mini batching where training set is divided to several mini batches.

Overfitting is another problematic issue which appears while training deep networks. In this case, the network is trained to learn noises inside the training data and isn't successful in the classification of test data. Overfitting can be avoided by using larger train sets and also using dropout. Dropout refers to dropping out some neurons in the network. This way, complex fitting of the network to the data is prevented. Greedy

layer-wise training is another method for training deep networks which results in more successful learning in some machine learning problems.

CHAPTER 4

DATA COLLECTION EXPERIMENTS

In order to evaluate our proposed signal processing algorithm, two commonly available datasets were used in this study. These datasets are explained in part 4.1. Further investigation of the proposed method was also performed by performing different motor imagery and BCI experiments. Experiments I and II included only data acquisition step. However the signal processing methods were applied to data afterwards. In experiments III and IV, EEG data was processed in real time and online feedback was provided.

Different EEG recording devices, environments, tools and experiment designs were used in these experiments. The specifications of each experiment are summarized in Table 4.1. The content of this table is explained in details in the following parts. EEG recording devices and experiment environments are discussed in part 4.2. Data recording electrodes and experiment preparation procedures are presented in parts 4.3 and 4.4. In part 4.5, tools and softwares used in each experiment are explained. Experiment procedures are explained separately for each experiment in parts 4.6-9.

Table 4.1. Overview of experiment specifications

| Experiment | Location | Recording Device | Recording Software | Online Feedback | Experiment Design | Signal processing |
|------------|-------------|------------------|--------------------|-----------------|-------------------|-------------------|
| I | BAUM | Brainamp | BrainVision | --- | Psychtoolbox | Matlab |
| II | BAUM | Brainamp | BrainVision | --- | Psychtoolbox | Matlab |
| III | BAUM | Brainamp | OpenVibe | OpenVibe | OpenVibe | OpenVibe, Matlab |
| IV | METU-Vision | G.Nautiulus | OpenVibe | OpenVibe | OpenVibe | OpenVibe, Matlab |

4.1 Public Datasets

Two different datasets from BCI competition II and IV have been used for testing the developed methods in this thesis. Both datasets include left and right hand motor imagery data. These datasets are very well known in this field and have been used in many similar studies [10, 101, 105, 113, 114, 125, 134]. The specifications of each dataset are shown in Table 4.2.

Table 4.2 Specifications of commonly available datasets

| Dataset | Year | Subjects | Trials | Sample rate | Channels | Motor imagery tasks |
|----------------------------|------|----------|----------------------|-------------|------------|------------------------|
| Competition II dataset III | 2003 | 1 | 140 right + 140 left | 128 Hz | C3, Cz, C4 | Left hand , Right hand |
| Competition IV dataset 2b | 2008 | 9 | 200 right + 200 left | 250 Hz | C3, Cz, C4 | Left hand , Right hand |

The experiment timing of BCI Competition II dataset III [135] is shown in Figure 4.1. Two seconds after the trial starts, an acoustic stimulus indicates the beginning of the trial and a cross is displayed on the screen for 1s. Then, an arrow (left or right) is displayed on the screen. In this period, the subject is asked to move a bar into the direction of the arrow by performing right/left hand motor imagery.

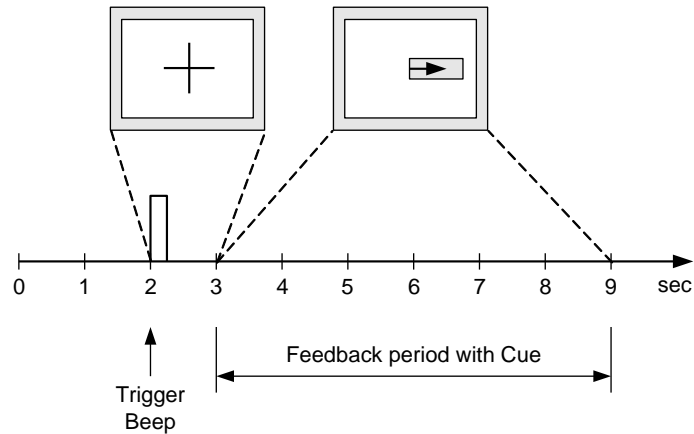


Figure 4.1. Timing of BCI Competition II dataset III [135]

The training set of BCI Competition IV dataset 2b [136] was used in this thesis. The experiment timing of this dataset is shown in Figure 4.2. At the start of each trial, a fixation cross is shown in the screen and an additional short acoustic warning tone is sent. 3 seconds later, an arrow is displayed for 1.25 seconds as a cue pointing to the side of the requested motor imagery task. After that there is a period of 4 seconds in which the subjects have to imagine the corresponding hand movement.

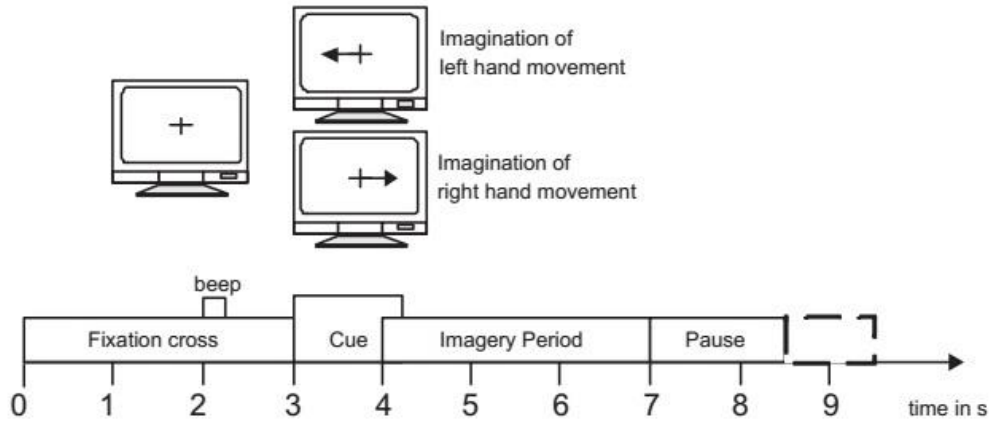


Figure 4.2. Timing of BCI Competition IV dataset 2b [136]

4.2 EEG Recording Devices and environments

Data acquisition experiments were performed by using two different EEG recording devices. Experiments I-III were performed using Brainamp EEG recording device in Ankara University brain research center (BAUM). Experiment IV was performed in METU-Vision lab by using G.Nautiulus EEG recording device. These devices and related recording environments are discussed in parts 5.1.1 and 5.1.2.

4.2.1 Brainamp EEG recording device and recording environment

In experiments I-III, Brainamp DC 32 channel EEG device (Brain Products GmbH, Munich, Germany) was used for signal recording. EasyCap [137] was used to position electrodes on the brain according to international 10-20 system. The electrodes were connected to the amplifier through an electrode input box. The recording device contained an amplifier, a power pack and a USB adapter. The amplifier was connected to the recording PC through an optical fiber connected to the USB adapter.

The recordings were performed in a sound proof room and the subject was seated in front of a 22” screen. The recording device was connected to a PC outside the room where EEG signals were monitored by an observer in real time. The data was recorded with 500 Hz sample rate. Another PC was used in order to provide visual stimuli to the subject and also send stimuli signals to the recording PC. The recording room is shown in Figure 4.3.a together with the amplifier and power bank (4.3.b) and electrode input box (4.3.c).

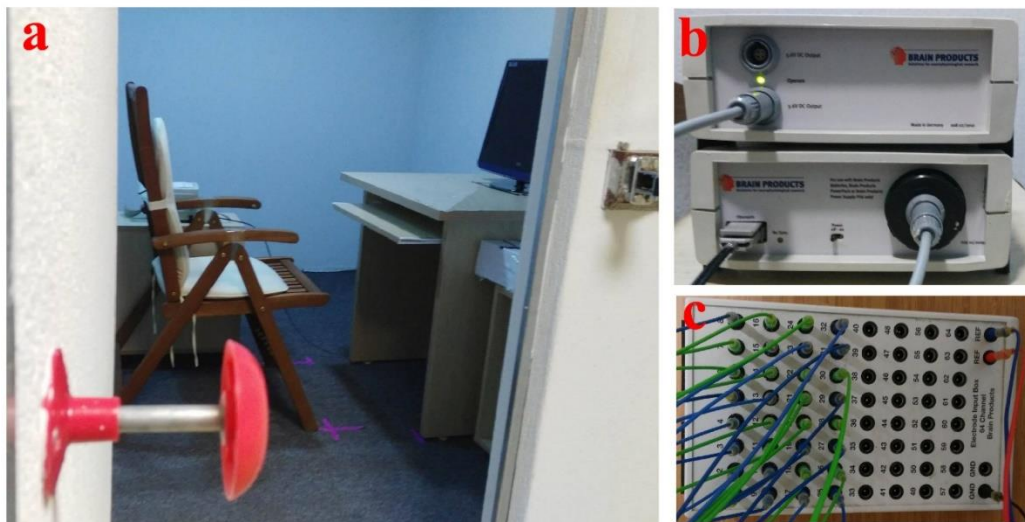


Figure 4.3. a. Recording room, b. Amplifier and power bank, c. Electrode input box

4.2.2 G.Nautilus EEG recording device and environment

G.Nautilus (gTEC, Austria) 16 channels wireless EEG device was used for data recording in experiment IV. Different studies have compared this device with current research-grade systems and show that G.Nautilus device is almost as good as current research-grade systems [138, 139]. This device has been used in some recent studies in P300 [140] and motor imagery [141] based BCI systems.

This device is composed of a 16 channels cap and a base station that is connected to the PC. The electrodes on the cap are connected to the amplifier placed on the cap. The amplifier is connected wirelessly to the base station. The data is transmitted via the 2.4 GHz band and the indoor operating range is about 10 m. Data recording, stimuli and visual commands were handled in the same computer for this device.

A specific gel provided by the manufacture, was used to decrease the impedance between electrodes and the skin. The device is capable of 250 Hz and 500 Hz recording. The recordings were performed in METU-Vision laboratory where other people were present in the room. The subject was seated on a chair in front of a 14'' screen. Different parts of the G.Nautilus device and the recording room are shown in Figure 4.4.



Figure 4.4. a. METU-Vision recording room. b. G.Nautilus cap. c. G.Nautilus base station

4.3 Data Recording Electrodes

Total 28 data electrodes were used to record EEG data in experiments I and II. The position of electrodes on the head are shown in Figure 4.5 according to international 10-20 system. Common reference method with linked-ear referencing was used in these experiments. There was also a ground (G) electrode placed in forehead and two reference electrodes connected to both ears. The ground electrode acts like a baseline for electrode voltage measurement. It is important to mention that this electrode is a signal ground not a true earth ground. The voltage values of each electrodes is measured as a differential between the electrode and the reference. Two electrodes (VEOG and HEOG) were placed near left ear to detect eye movements.

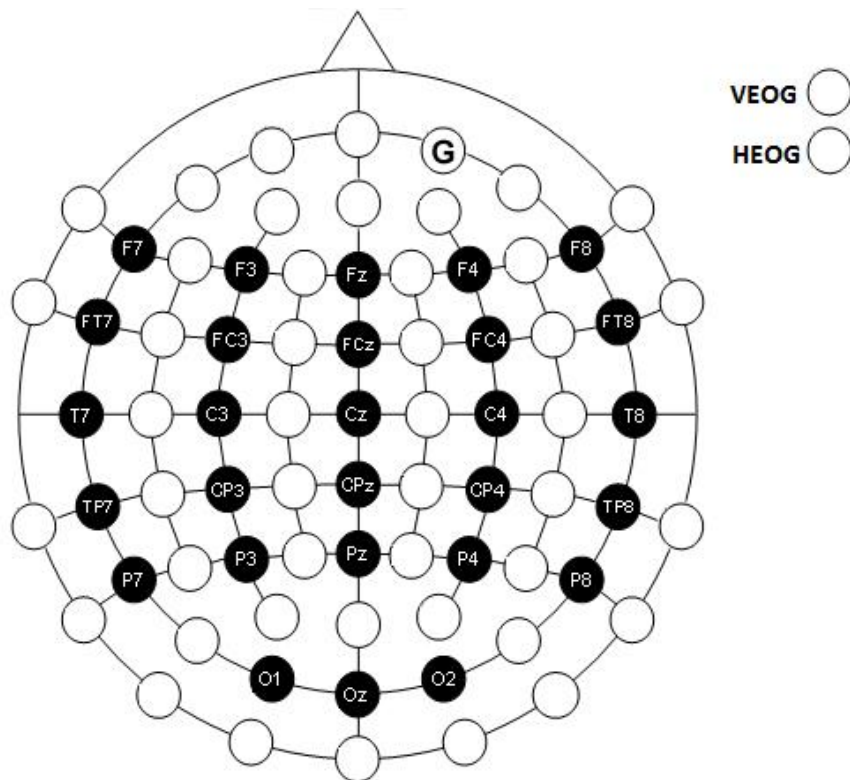


Figure 4.5 Electrode locations for experiments I and II

In experiment III, 5 data electrodes were used to record EEG data. The position of electrodes on the head are shown in Figure 4.6. These electrode positions were selected in order to cover the motor cortex area where motor imagery related oscillatory activities are observed the most [68]. The reference and ground electrodes were positioned similar to experiments I and II.

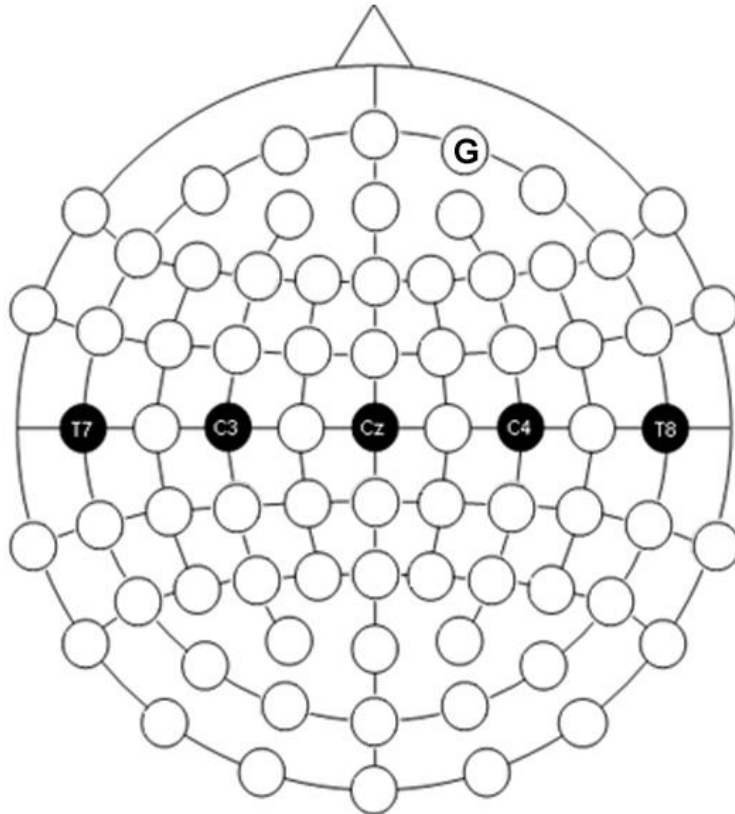


Figure 4.6 Electrode locations for experiment III

The placement of electrodes on G.Nautilus cap used in experiment IV is shown in Figure 4.7. In this experiment, data was recorded from 6 electrodes (F3, Fz, F4, C3, Cz, C4). Several studies in the literature suggest that using bipolar recording can remove the common noise of both electrodes [136, 142]. This method is used for EEG recording of BCI competition IV dataset 2b [136] in order to record motor

imagery signals from C3, Cz and C4 channels. In experiment IV, all the channels were measured by referencing to right earlobe. However the differences between C3-F3, Cz-Fz and C4-F4 were evaluated computationally and used as C3, Cz and C4 channel values in signal processing step. The channels which were used for difference computation are connected by red line in Figure 4.7.

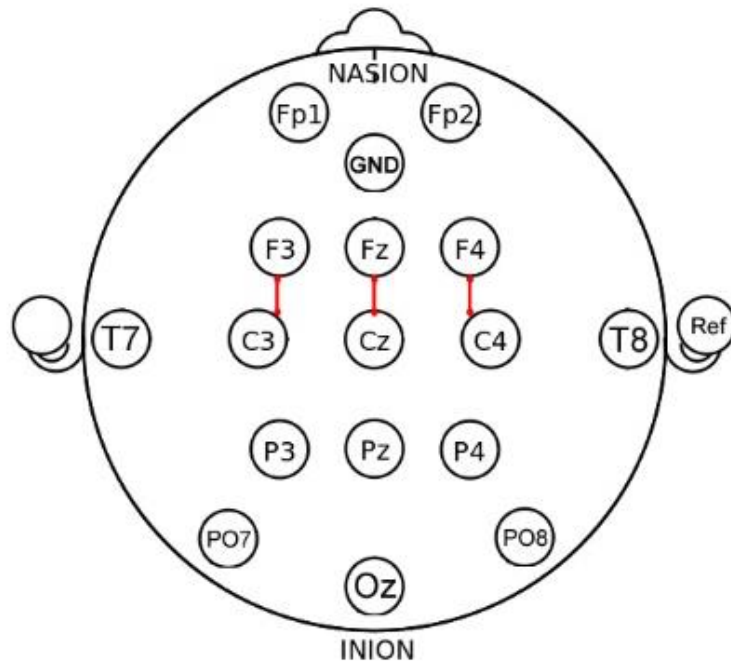


Figure 4.7. Electrode placement of G.Nautilus cap, channels used for difference computation are connected with red line

4.4 Preparation Procedures

Before starting each experiment a preparation procedure was applied to each subject. The goal of this step was to place electrodes in their specific locations, decrease the impedance between electrodes and head skin and prepare the subjects for the

experiment. This procedure was applied differently for Brainamp and G.Nautilus devices.

In Brainamp experiments, first a brief information about the study was presented to the subject. Then the circumference of the subject's head and the distance between the nasion and the inion was measured. An appropriate cap was selected and placed on the subject's head in a way that Cz is halfway between the ears and also nasion and inion. Then a cotton swab dipped in alcohol was used to push the hair aside in each electrode position and clean the skin. Afterwards, electrodes were placed in their positions and a syringe was used to fill the electrodes with high-chloride, abrasive electrolyte gel (Abralylt HiCl, EASY CAP).

The gap between electrode and skin was filled with conductive gel and the electrode impedance was reduced. At this step, the subject was moved to the recording room and the electrodes were connected to the amplifier. The impedance value of each electrode should be measured and kept under a threshold before the experiment starts. BrainVision software provided by the device manufacture, was used to observe the impedance values. The impedance value of each electrode was decreased by applying extra gel and spreading it by a cotton swab. The impedance values of data electrodes were kept below 5 k Ω for experiments I-III. The impedance values of ground and reference electrodes were kept near 0 k Ω . The details of impedance measurement by the device are provided in appendix A. This preparation procedure takes about 30 to 60 minutes for each recording session.

In G.Nautilus experiment, first the cap was placed on the subjects head and the electrodes were filled with a specific gel provided by the manufacture. Then the impedance values of electrodes were measured by using official software of the device. The impedance values were kept under 30 k Ω . Unfortunately the impedance measurement software does not provide lower values.

Since impedance values below 30 k Ω were not provided, we performed a signal monitoring session before starting each session. This way we could observe the quality of the signal and add extra gel to electrodes that have poor quality. In this session, we tried to observe Clench teeth and eye blink artifacts. We also tried to see

alpha waves (~ 8-12 Hz) while the eyes are closed. An example of these control signals are shown in Figure 4.8. After the desired signals were observed, motor imagery experiments were started. This preparation procedure takes about 10 minutes for each recording session.

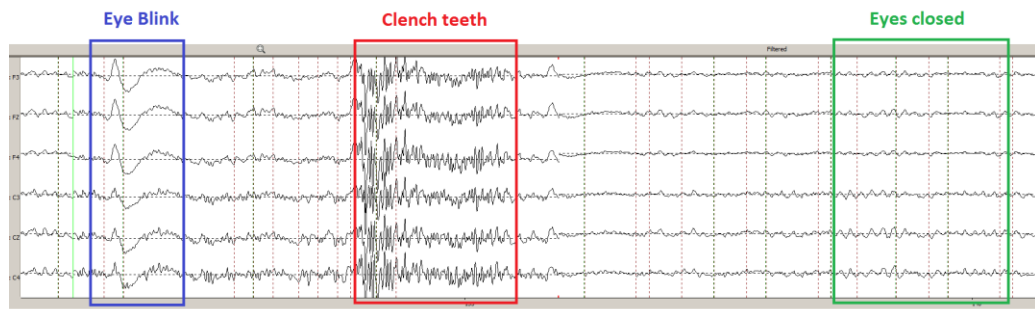


Figure 4.8. Example of Clench teeth, eye blink and alpha waves.

4.5 Tools and Softwares

Several tools and softwares were used in this study in order to design the experiments and record and process the signal.

Psychophysics toolbox [143] in Matlab was used to design experiments I and II. The stimulus timings and visual commands were handled by using this toolbox. In these experiments, EEG data was monitored and recorded by another PC using BrainVision Recorder software provided by the manufacture. Afterwards Matlab was used to apply the signal processing algorithms to the recorded data.

OpenVibe[144] tool was used in the experiments III and IV for experiment design, signal processing and data recording and monitoring. This tool was able to connect successfully to both Brainamp and G.Nautilus devices and monitor and record the data.

OpenVibe is an open source software platform designed for performing real time neuroscience experiments. BCI systems can be designed and tested by using the graphical user interface provided by OpenVibe. It provides several algorithms and tools for processing data in real time. These tools are introduced in the form of boxes that can be added to the project. The experiments can be designed by connecting these boxes via the graphical interface of the tool. Data passes through the boxes in form of signal, matrix and stimulation.

In order to perform online MI experiments, recorded EEG signals should be packed into data packets and passed to the processor. Then, the signal should be processed and the appropriate feedback signal should be sent. Our proposed deep learning based signal processing method was developed in Matlab environment. Therefore, the connection between the recorder device and Matlab should be ensured during these experiments. In our experiments, OpenVibe provided a successful and fast connection between the recorder device and the signal processing boxes. The online experiments in this thesis was performed using OpenVibe tool.

The synchronization between recorder and processor is an important issue in real time EEG experiments. The size of data packets, recording frequency and the frequency of calling the processor are critical parameters for synchronization. These values were optimized in OpenVibe tool during several preliminary experiments before performing experiments III and IV.

4.6 Experiment I

In this experiment, our aim was to record EEG signals related to different motor imagery tasks. Visual stimuli was used to guide the subjects to perform the desired task. There was no online feedback in this experiment and signal processing methods was applied to the data after the recording in order to classify different tasks. Right hand movement, left hand movement, feet movement and both hand movement imagery tasks were used in this experiment.

This experiment was designed similar to Graz motor imagery experiment [25] which is a very well-known experiment in this field. The subjects were asked to perform 4 different motor imagery tasks. These tasks were right hand movement, left hand movement, feet movement and both hand movement. The experiment was performed by using visual stimuli as commands.

Each subject attended to four recording sessions. Each session consisted of 20 trials for each MI task. Each recording session lasted about 13 minutes and the subjects had 3-5 minutes for resting between the sessions. The experiment was performed on 9 healthy subjects with ages between 19 and 37 years old. The detail information about the subjects is presented in Table 4.3.

Table 4.3. Subject information for experiment I

| Subject | Gender | Age | Educational Level | Hand Preference |
|---------|--------|-----|-------------------|-----------------|
| 1 | Male | 33 | M.S. | Right |
| 2 | Female | 29 | B.S. | Right |
| 3 | Female | 37 | B.S. | Right |
| 4 | Female | 21 | Student | Left |
| 5 | Female | 22 | Student | Right |
| 6 | Female | 19 | Student | Right |
| 7 | Female | 21 | Student | Right |
| 8 | Male | 34 | M.S. | Right |
| 9 | Male | 29 | B.S. | Left |

The timing of the experiment is shown in Figure 4.9. First a diamond shape appears in the screen for 1.25 seconds. The subject focuses on the screen in this time period. Then the command is shown for 5 seconds. During this time, the subject performs the

motor imagery task continuously. Then the command is cleared to provide resting time for a period selected randomly between 2.5 and 3.5 seconds.

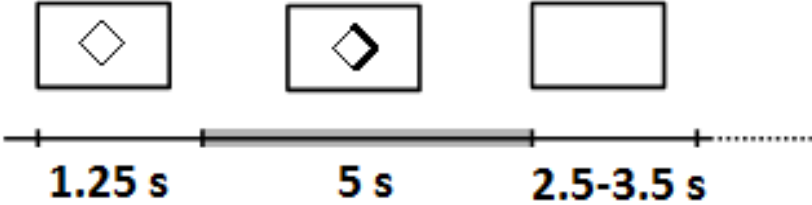


Figure 4.9. Timing of the experiment I

The stimuli were selected in a way that minimum visual evoked potential would be observed. Therefore the color of the screen was selected as grey and the change in the shape was kept minimum for different task commands. Four different visual commands related to four MI acts are shown in Figure 4.10. The related motor imagery tasks for each stimulus are listed in Table 4.4.

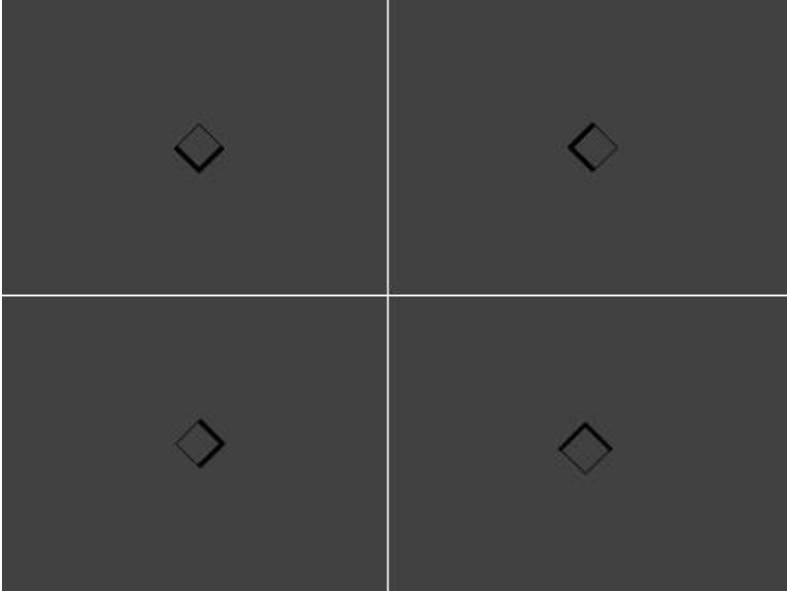






Figure 4.10. 4 different visual stimuli used in the experiments

Table 4.4. MI tasks related to each visual stimulus

| Visual stimulus | Related MI task |
|---|---------------------------|
|  | Right hand movement (RHM) |
|  | Left hand movement (LHM) |
|  | Feet movement (FEM) |
|  | Both hands movement (BHM) |

The experiment was performed by using Brainamp DC 32 channel EEG device with 500 Hz sample rate. Data was recorded from 28 electrodes in this experiment.

4.7 Experiment II

By investigating the results of experiment I, several issues with the experiment were determined. The recording sessions in experiment I were too long that caused subjects to loose concentration. The MI tasks were also not evident. Therefore experiment II was designed in order to improve motor imagery performance by using these experiences. The length of the recording sessions were decreased in this experiment in order to prevent subjects from getting tired and loosing concentration. We introduced 10 different motor imagery tasks in this experiment. Our goal in this experiment was to detect motor imagery tasks that are most distinguishable and also detect subjects with high motor imagery performance. The experiment was applied

to 7 subjects. All subjects were healthy and their ages were between 20 and 34 years. The detailed information about subjects is presented in Table 4.5.

Table 4.5. Subject information for experiment II

| Subject | Gender | Age | Educational Level | Hand Preference |
|---------|--------|-----|-------------------|-----------------|
| 1 | Male | 21 | Student | Right |
| 2 | Male | 19 | Student | Right |
| 3 | Female | 29 | M.S. | Right |
| 4 | Male | 21 | Student | Left |
| 5 | Male | 19 | Student | Right |
| 6 | Male | 34 | M.S. | Right |
| 7 | Female | 30 | M.S. | Right |

Each subject attended 3 sessions performing totally 10 different motor imagery tasks. The details of each session are presented in Table 4.6. In session 1, four motor imagery tasks were performed in four runs where the number of trials for each task was 10. Session 2 was also performed with four motor imagery tasks in four runs. Similarly the number of trials for each task was 10 in session 2. In session 3 we asked the subjects to perform 2 complex imagery tasks: pushing and pulling. This session was done in 2 runs with 20 trials for each task.

Table 4.6. Experiment II details

| Sessions | Number of runs | Task | Number of tasks per session |
|----------|----------------|--|-----------------------------|
| 1 | 4 | 1.Right hand movement (RHM) | 10 |
| | | 2.Left hand movement (LHM) | 10 |
| | | 3.Right foot movement (FEM) | 10 |
| | | 4.Tongue movement (TOM) | 10 |
| 2 | 4 | 1.Squeeze ball with right hand fingers (RHS) | 10 |
| | | 2.Squeeze ball with right hand fingers (LHS) | 10 |
| | | 3.Squeeze right foot fingers (FES) | 10 |
| | | 4.Squeeze ball with both hands fingers (BHS) | 10 |
| 3 | 2 | 1.Push (PSH) | 20 |
| | | 2.Pull (PLL) | 20 |

There was 2-3 minutes resting period between the sessions and the subjects were allowed to walk in the lab after 5th section for 5 minutes. The recorded data was analyzed by the signal processing methods and most successful subject was selected for further experiments. Motor imagery tasks were also analyzed and the most distinguishable tasks for the selected subject was determined.

Similar to experiment I, experiment II was also performed by using Brainamp DC 32 channel EEG device with 500 Hz sample rate. Data was recorded from 28 electrodes in this experiment.

4.8 Experiment III

In experiments I and II we were able to record MI data and perform offline classification. So in order to go further and investigate the proposed method in a real time BCI system, experiment III was designed. Our aim in this experiment was to design a system that determines the motor imagery task performed by the subject and deliver the appropriate feedback in real time. Accordingly, a motor imagery experiment with online visual feedback was designed and performed on one subject. The subject was 30 years old healthy female and she was selected according to the performance of experiment II (subject 7). Due to our problems in arranging

appropriate subjects for long time experiments, we were not able to perform this experiment on a group of subjects. However, we were able to successfully design and apply a real time BCI experiment.

Right and left hand movement motor imagery tasks were used in this experiment. A cue was shown to the subject and she was asked to perform the related motor imagery task for a period of time. An arrow was presented to the subject during this period either heading left or right and its size changing to indicate the performance of the subject on the corresponding task.

This experiment was performed in two steps which were data acquisition and online classification steps. First the data was recorded for left hand and right hand motor imagery tasks in the data acquisition part. The aim of this part was to provide data for the training of the classifier so there wasn't any online feedback in this part. The timing of this experiment is shown in Figure 4.11. Each trial starts with the presentation of a cross at the center of the monitor. At 3000 ms, an arrow is shown for 1250 ms, indicating either left or right hand task. The subject performs the expected motor imagery task for 3000 ms after the arrow is disappeared. Then a black screen is presented to the subject for 1500 ms and the trial is ended. Three sessions of recording with 20 right and 20 left hand motor imagery tasks were performed in this part.

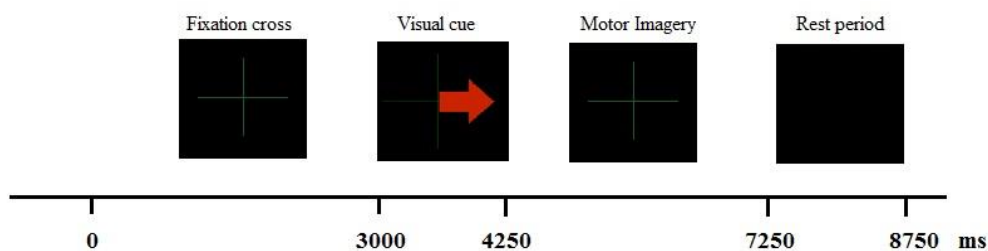


Figure 4.11. Timing of data acquisition part of experiment III

Then the recorded data was used to train the classifier. Two different classification methods were applied separately in this experiment. First method is based on CSP spatial filter and LDA classifier. This method was used originally in Graz experiment [25]. In the second method, our proposed CNN network was used for classification. The computation time for CNN-SAE method was so long that we were not able to perform online experiments using CNN-SAE. The computation time was about 90 ms for CNN and 360 ms for CNN-SAE. The long computation time for CNN-SAE was due to the large size of saved SAE network that takes a long time to load.

The trained classifiers was then used to proceed online classification step. The timing of the online classification part is similar to the data acquisition part except in the motor imagery period, a bar indicating the performance of motor imagery task is displayed to the subject. The timing is presented in Figure 4.12.

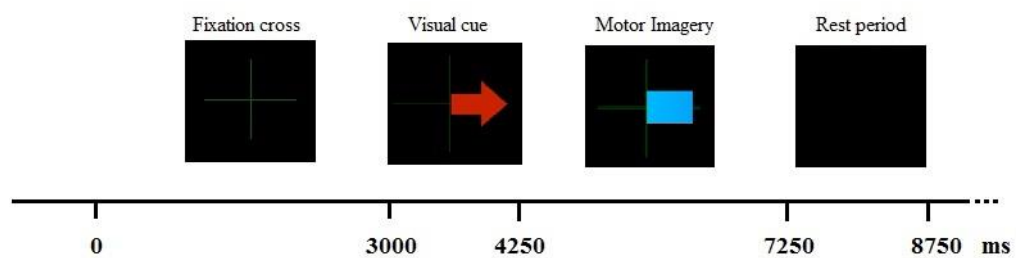


Figure 4.12. The timing of Graz experiment with online feedback

Online classification part was designed separately in OpenVibe for CSP-LDA and CNN methods. These experiment designs are explained in the following parts.

A simplified flowchart of CSP-LDA online classification part is presented in Figure 4.13. The data is received in the “Acquisition client” box and passed to the “Identity” buffer. The stimuli needed for the experiment are produced in “Graz Motor Imagery BCI Stimulator”. Each stimulus is produced according to the experiment timing and passed to the “Graz visualization” box to show the appropriate cue.

The signal is passed from the buffer to the “Channel Selector” box to select the channels and the previously trained CSP filter is applied to the selected channels in the “CSP Spatial Filter box”. Then a Butterworth filter with low-cut frequency equal to 8 Hz and high-cut frequency equal to 24 Hz is applied to the signal in the “Temporal filter” box. At the “Time based epoching” box, a 1000 ms long slice of signal is extracted and passed to the next box each 60 ms. Then the feature vectors are extracted in the “Feature aggregator” box and the signal is classified in the “Classifier processor” box.

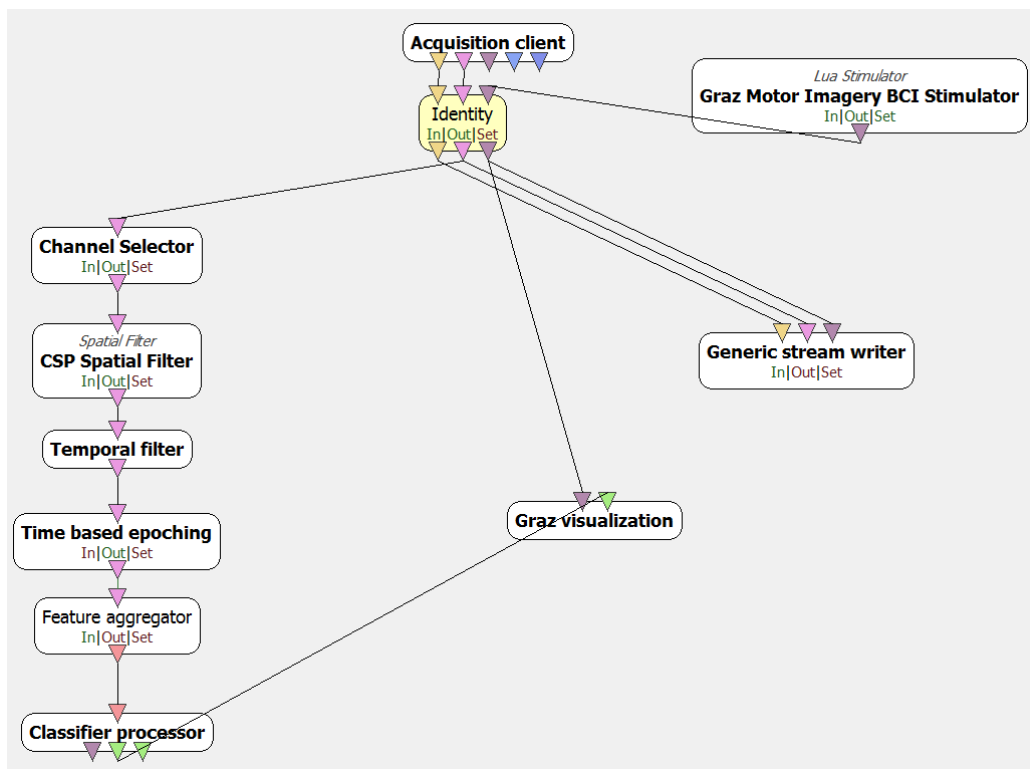


Figure 4.13. Simplified flowchart of CSP-LDA online classification part

The output of the classifier box is a 1x2 vector that includes the probabilities of each class. The output is sent to the “Graz Visualization” box to provide the result of classification to the subject via visual feedback. Visual feedback is in the form of bars spreading to the left or right according to the result of classification. The EEG signal

of the whole experiment together with the stimuli are saved in the “Generic stream writer” box.

The flowchart of the CNN online classification part is shown in Figure 4.14. Here, the “Switch director” box receives the stimuli from the stimulator and commands the “Stream Switch” box to connect or disconnect data to the next box. The “Switch director” box is set to connect signal during the feedback time so the signal would be processed. Then in the “Time based epoching” box, a 400 ms long slice of data is extracted and passed to the “Matlab Scripting” box each 400 ms (no overlap). Matlab box is triggered when there is a new input signal packet in the input. So the Matlab box is called each 400 ms. This value is the optimized value for the system in order to perform in real time without delay. The rest of the boxes are the same as CSP-LDA online classification part.

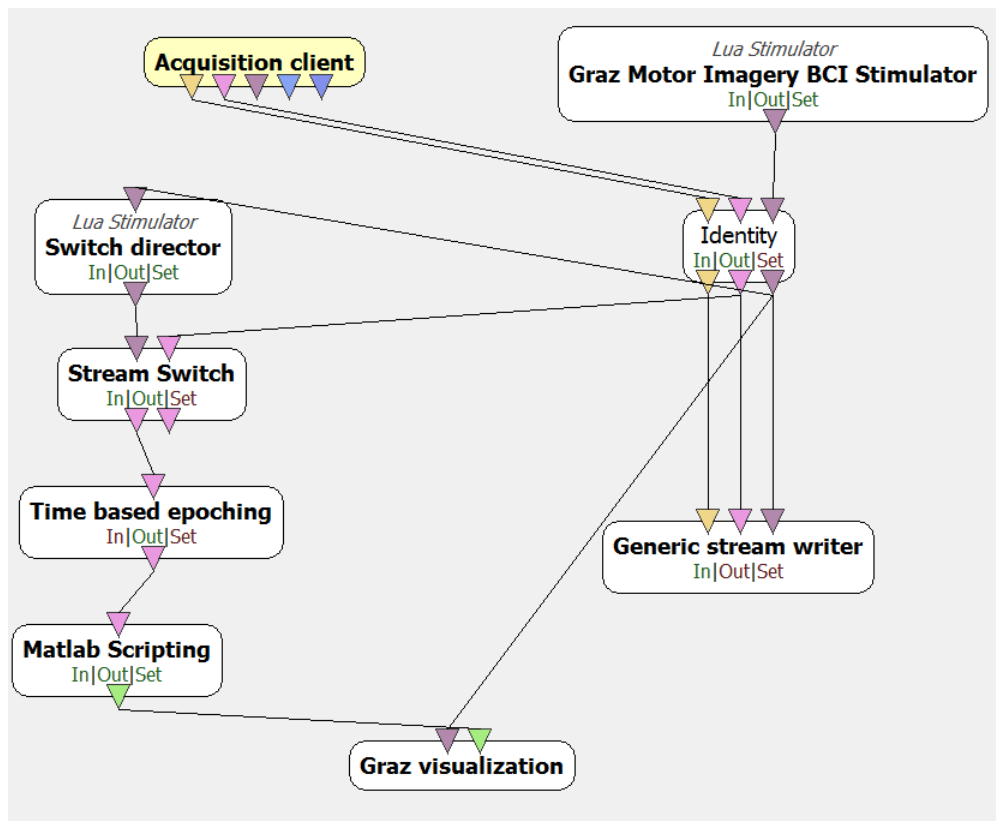


Figure 4.14. Simplified flowchart of CNN online classification part

The online classification step was applied to one subject in two sessions for CSP-LDA and two sessions for CNN methods. Each session was composed of 20 left hand and 20 right hand trials. Data acquisition, training and online classification steps were performed for each session separately.

The experiment was performed by using Brainamp DC 32 channel EEG device with 500 Hz sample rate. Data was recorded from 5 electrodes in this experiment.

There was a 7 days period between two sessions. Before each session, a subject training session was performed where there was no cues presented and the subject could freely perform motor imagery task and see the classification results via bars. This way, the subject was able to improve her skills by using the online feedback. We observed that the performance of motor imagery is improved after the subject training sessions.

4.9 Experiment IV

The positive effect of subject training on MI performance was observed in experiment III. However the amount of data sessions in this experiment were not enough to come to a conclusion. Therefore, experiment IV was designed in order to perform further investigation on the effect of subject training on MI performance. A new wireless EEG recording device was used in this experiment. The preparation period and experiment setup was much simpler with the new device. Therefore we were able to perform experiments faster. We were also able to perform experiments in METU-Vision lab where the environmental conditions were more likely to day life conditions.

In this experiment we tried to improve the motor imagery performance by performing several subject training sessions. Training subjects by providing online feedback is known to improve the motor imagery quality [136, 145]. Therefore we designed

subject training sessions in this experiment where visual feedback was presented to the subject after each trial.

The timing of this experiment is shown in Figure 4.15. First a cross is shown on the screen for 2 seconds. The subject focuses on the screen in this time period. Then the motor imagery command is shown on the screen in the shape of an arrow turning left or right. The arrow is shown for 1.3 seconds and the subject performs related right hand/left hand motor imagery in this period. Then an image which shows the activity patterns of the brain during cue period is shown to the subject for 7 seconds. This image is constructed by applying short time Fourier transform on the signals recorded from channels C3, Cz and C4 and extracting the frequency bands between 6-13 Hz and 17-30 Hz. The image has three rows which corresponds to C3, Cz and C4 channels from up to bottom. So when the subject performs a left hand motor imagery task, the activation in C4 is decreased and C3 (upper side) becomes brighter. This image is being used as an input in our deep learning network for signal classification and discussed in details in part 4.1. The activation image is displayed to the subject for 7 seconds and the experiment continues to the next trial.

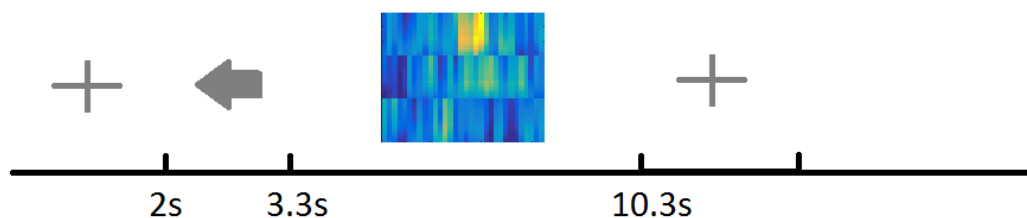


Figure 4.15 Timing of experiment IV

The experiment design in OpenVibe is shown in Figure 4.16. The data is received in the “Acquisition client” box and passed to the “Identity” buffer. The stimuli needed for the experiment are produced in “Graz Motor Imagery BCI Stimulator”. Each stimulus is produced according to the experiment timing and passed to the “Matlab scripting” box to show the appropriate cue. The signal is passed to the “Stimulation

based epoching” box to extract 1 second period starting 300 ms after the cue appears. Then, F3, Fz, F4, C3, Cz and C4 channels are being selected in the “Channel selector” box. A 4. Order Chebychev bandpass filter is applied to the selected channels in “Temporal filter” box in order to extract frequency bands between 5 and 35 Hz. Bipolar computation is performed in “Matlab scripting” box and the feedback image is constructed. Command cues and visual feedback display is being handled in Matlab. It is also important to mention that a notch filter (48-52 Hz) is applied to the signal by recording device in order to remove power line noise.

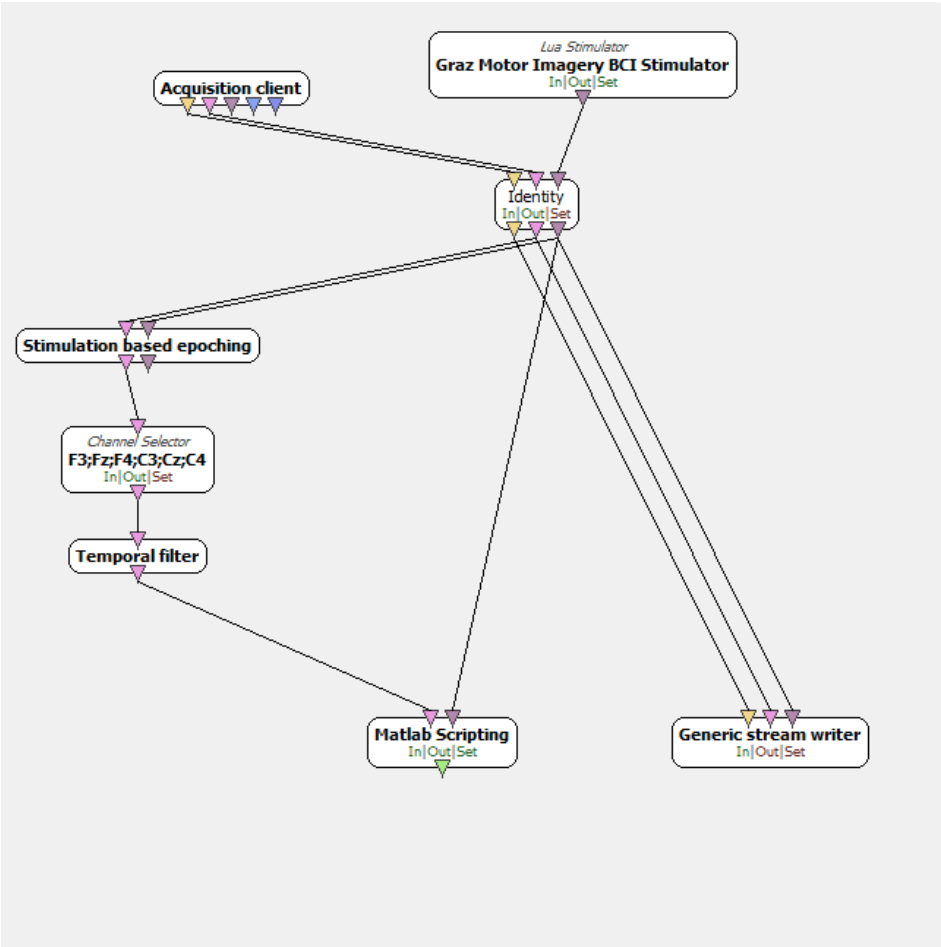


Figure 4.16. Simplified flowchart of experiment IV

Each recording session in this experiment was composed of 9 runs. The flow of each session is described in Table 4.7. After signal monitoring, a test recording run was performed in order to get subject ready for the experiment. Then 2 right hand only, 2 left hand only and 4 both hands runs were performed as shown in Table 4.7. The subject was guided to perform only right hand motor imagery in right hand only and left hand motor imagery in left hand only runs. Commands for left and right hand motor imagery were displayed randomly in both hands runs. Three last both hands experiments were used to train the classification network and evaluate the accuracy. Each run was composed of 30 trials.

15 sessions of experiments were performed on one subject in a 45 days period. The subject was the author of the thesis which was 34 years old healthy male and fully aware of all aspects of this study. The changes in motor imagery performance and the effect of subject training were investigated in this period.

G.Nautilus (gTEC, Austria) 16 channels wireless EEG device was used for data recording in this experiment where the recording sample rate was 250 Hz. Data was recorded from F3, Fz, F4, C3, Cz and C4 electrodes. The differences between C3-F3, Cz-Fz and C4-F4 electrodes were evaluated computationally and used as C3, Cz and C4 channel values in the signal processing step.

Table 4.7. The flow of each recording session.

| 0 | 1 | 2 | 3 | 4 | 5 | 6 | 7 | 8 | 9 |
|-------------------|----------------|-----------------|----------------|------------|-----------------|----------------|------------|------------|------------|
| Signal Monitoring | Test Recording | Right Hand only | Left Hand only | Both Hands | Right Hand only | Left Hand only | Both Hands | Both Hands | Both Hands |

CHAPTER 5

METHOD PROPOSED FOR MOTOR IMAGERY CLASSIFICATION

In this chapter our proposed method for MI signal classification based on deep learning[1] is explained. In this method, a new form of input that combines time, frequency and location information extracted from MI EEG signal is introduced. Short Time Fourier Transform (STFT) method was used to convert EEG time series into 2D images. Unlike [11] where spectral measurements are aggregated for each band, in this study, spectral content of mu and beta frequency bands are used explicitly. This way we preserve activation patterns among different frequencies as well as time and location.

In our approach, input data is used in a 1D Convolutional Neural Network to learn the activation patterns of different MI signals. 1D convolution is applied only in time axis, rather than frequency and location. Therefore, the shape of activation patterns (i.e. power values from different frequencies) and their location (i.e. EEG channel) are being learned in the convolutional layer. Max-pooling is applied after convolution in time axis, which makes CNN partially invariant to the time location of activation patterns. Then a Stacked Autoencoder with 6 hidden layers is used to improve the classification through a deep network. The input image form, CNN and CNN-SAE networks are discussed in details in parts 5.1-3.

5.1 Input Image Form

As we discussed before in part 2.2.4, the energy in mu band (8-13 Hz) observed in motor cortex of the brain decreases by performing an MI task (ERD) [68] that. An MI task also causes an energy increase in the beta band (13-30 Hz) (ERS). Left and right hand movement MI tasks are said to cause ERD and ERS respectively in the right and left sides of the motor cortex affecting EEG signals at C4 and C3 electrodes according to 10-20 international system. Cz is also affected MI tasks. Considering these facts, we designed our network input in order to take advantage of time and frequency properties of the data in these locations.

In order to convert EEG signals to 2D matrices, first a Short Time Fourier Transform (STFT) was applied on the time series. If we consider each trial to be 2 seconds long and the sample rate to be 250 Hz (BCI Competition IV dataset 2b data), each trial includes 500 samples. STFT was performed with window size equal to 64 and time lapses equal to 14. Starting from sample 1 toward sample 500, STFT is computed for 32 windows over 498 samples and the last 2 samples, remaining at the end, are simply ignored. This leads to a 257x32 image where 257 and 32 are the number of samples along the frequency and time axes respectively.

Then we extracted mu and beta frequency bands from the output spectrum. The frequency bands between 6-13 and 17-30 were considered to represent mu and beta bands. The frequency bands are slightly different than literature but they were resulted in a better data representation in our experiments. The size of extracted image for mu band was 16x32 where the size of extracted image for beta band was 23x32. In order to keep the effect of both bands similar, beta band was resized to 15x32 by using cubic interpolation method. Then these images were combined to make a $N_{fr} \times N_t$ image where $N_{fr}=31$ and $N_t=32$.

This process was repeated for $N_c=3$ electrodes which are C4, Cz and C3. The results were combined in a way that the electrode neighboring information was preserved. The size of the resulting input image is $N_h \times N_t$ where $N_h=N_c \times N_{fr}=93$. A sample input image constructed for a right hand MI task trial is illustrated in Figure 5.1. By using

the proposed method, brain activations in right and left sides of the motor cortex of the brain, cause different activation patterns along the vertical cortex of the brain.

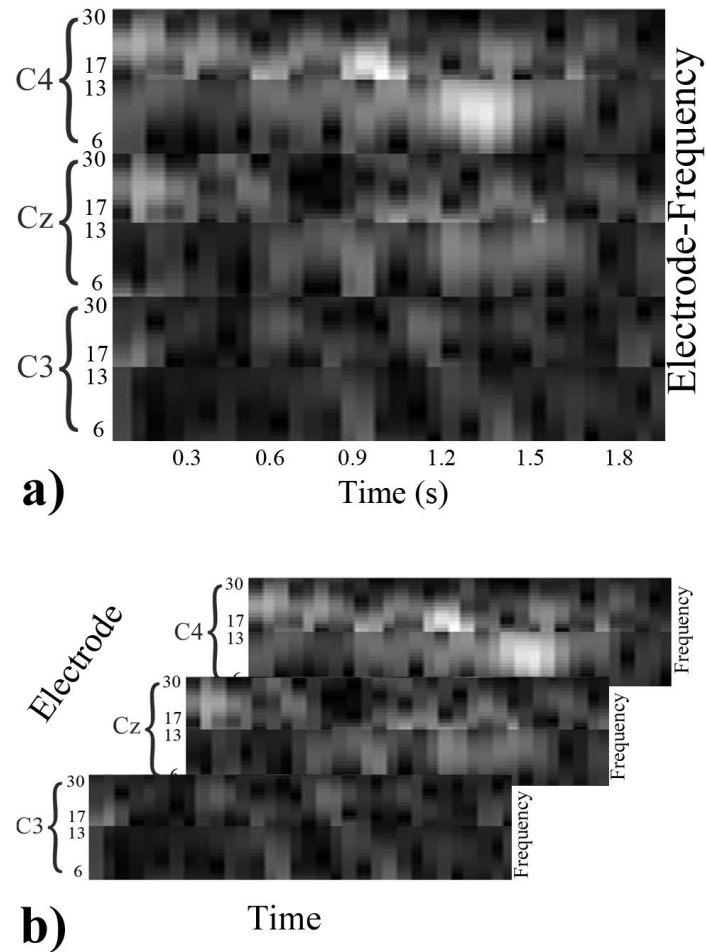


Figure 5.1. a) A Right hand sample input image including 2 frequency bands for each electrode C3, Cz and C4. b) The same image as a 3D tensor

The ERD effect in C3 channel is clear in Figure 5.1 for a sample that corresponds to a right hand MI task (darker 6-13 Hz band in C3 compared to C4). However the ERS effect in C3 electrode is not strong for this sample. Similar to right hand, for a sample collected for left hand MI task, such activation is expected to occur at the electrodes

taking place at the opposite side. These images are constructed for each trial sample and used as the input of CNN and SAE networks in the next stage.

5.2 Convolutional Neural Network

Convolutional Neural Networks (CNN) are originally designed to recognize different shapes and patterns inside an image. In order to take advantage of CNN, EEG data was converted to 2D images in the previous part. In this new data form, frequency, time and electrode location information are used together. Vertical location of the activation on the input image plays an important role in the classification performance while its horizontal location is not that critic. Therefore, instead of 2D filtering that is commonly used in literature, we introduced filters having the same height as the input and 1D filtering is applied only along the horizontal axis.

Notice that, instead of giving the input to CNN as a 2D image, it is also possible to give it as a 3D tensor as shown in Figure 5.1.b, where the dimensions are time, frequency and electrodes. Since we are using 1D convolution only in time axis, this is not necessary in our case. For the studies considering the two dimensional locations of electrodes, 4D tensors may be used as input requiring adjustment of the filters and convolutions accordingly. Consequently we used a CNN that has only one convolutional layer with 1D filtering and one pooling layer. By using this network, we are able to train filters to respond differently to different activation patterns along the vertical axis. We also take advantage of tolerance of MI data to localization in time by sweeping filters along the time axis.

Totally $N_F=30$ filters with size $N_h \times 3$ are trained via this network. The proposed CNN structure is presented in Figure 5.2. At the convolution layer, the input image is convolved with trainable filters and put through the output function f to form the output map. The k th feature map at a given layer is obtained similar to equation 3.25 as

$$h_{ij}^k = f(a) = f((W^k * x)_{ij} + b_k) \quad (5.1)$$

In our case with 1D filtering with filter size $N_h \times 3$, j is equal to 1 and $i=1, 2, \dots, N_t-2$. The activation function f is selected as Rectified Linear Unit (ReLU) function. ReLU is approximated by softplus function defined as

$$f(a) = \text{ReLU}(a) = \ln(1 + e^a) \quad (5.2)$$

where a is the potential of the neuron defined in equation 3.16.

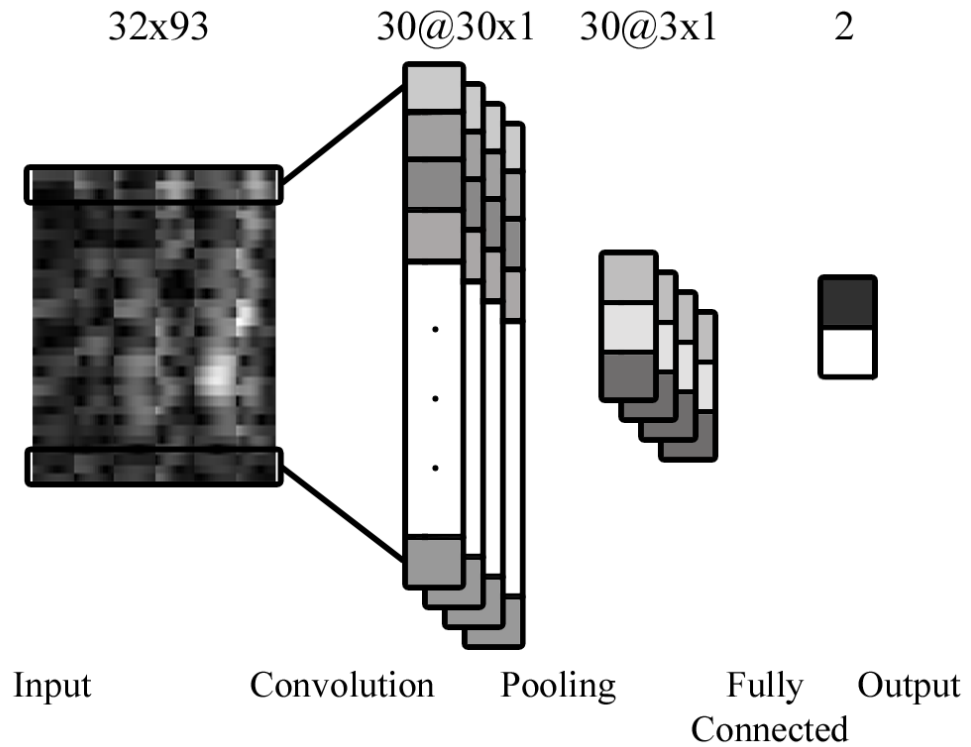


Figure 5.2. Proposed convolutional neural network model, $N_F=30$.

The output of convolutional layer has N_F vectors with $(N_t-2) \times 1$ dimension. At the max-pooling layer, sampling factor 10 and zero padding is applied. Therefore, the output maps from the previous layer are subsampled into N_F vectors with 3×1 dimension. The max-pooling layer is followed by a fully connected layer having two outputs representing left and right hand MI. Parameters of the CNN are learned by

using back-propagation algorithm. In this method, the labeled training set is fed to the network and the error E is computed considering the difference between the network output and the desired output. Then, gradient descent method is used to minimize this error E by changing network parameters similar to MLP. Weight matrix W^k and bias value b_k for filter k can be computed as follows

$$W^k = W^k - \alpha \frac{\partial E}{\partial W^k} \quad (5.3)$$

$$b_k = b_k - \alpha \frac{\partial E}{\partial b_k} \quad (5.4)$$

Finally, the trained network is used for classification of the new samples in the test set.

5.3 Stacked Autoencoder

In this step, a Stacked Autoencoder (SAE) was used as described in part 3.3.4. Our proposed SAE network used in this study is shown in Figure 5.3. This model is composed of 1 input layer, 6 hidden layers and one output layer. The number of nodes at each layer is indicated at the top of the figure. This model provides a deep network in order to classify EEG features.

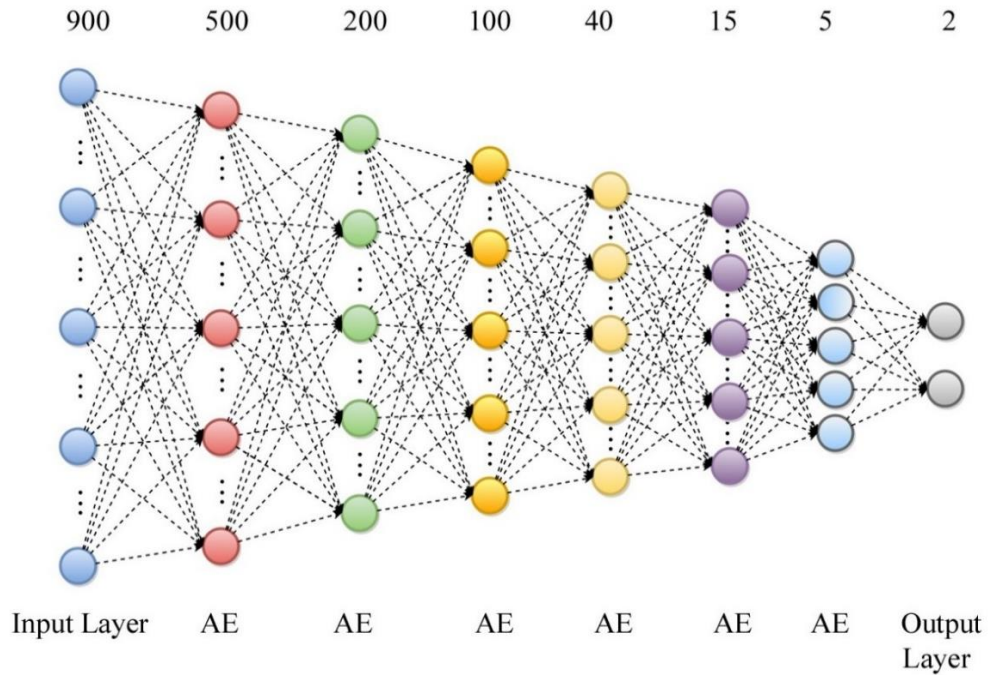


Figure 5.3. Proposed SAE model with 6 hidden layers

5.4 Combined CNN-SAE

The amplitude of recorded EEG signal is very low. Therefore, the signal is very sensitive to external and internal noises [44]. Artifacts like eye blinking and muscle movement are another source of disturbance that cause irrelevant effects that corrupts the desired brain pattern. Furthermore, some subjects are unable to perform successful MI tasks in some trials. These issues cause the input data to vary slightly among the trials. In order to overcome these problems, we propose a new deep structure, which includes a CNN followed by a SAE. The proposed model is shown in Figure 5.4.

In this deep structure, firstly the CNN structure explained in part 3.3.3 is employed over the input data and the filters and network parameters are learned. Then the output of the convolutional layer of CNN is used as input to the SAE network. Input layer

of SAE has 900 neurons that is the output of 30 neurons in the convolutional layer for each of 30 filters trained in CNN. By using this model, we aim to take advantage of extracting features considering time, frequency and location information of EEG data by using a CNN. We also try to improve the classification accuracy through the deep network in SAE part.

Once training is completed, the computational complexity of CNN-SAE for testing is

$$O(N_h \times N_t \times N_F \times N_{F_s}) + O((N_t \times N_F)^2 \times N_L). \quad (5.5)$$

The first term is the computational complexity of CNN part of the network, where $N_h \times N_t$ is the input image size, N_f is the number of convolutional filters and N_{F_s} is the filter size. The second term is the computational complexity of SAE part, where N_L is the number of layers; there is a square term in the complexity since SAE layers are fully connected.

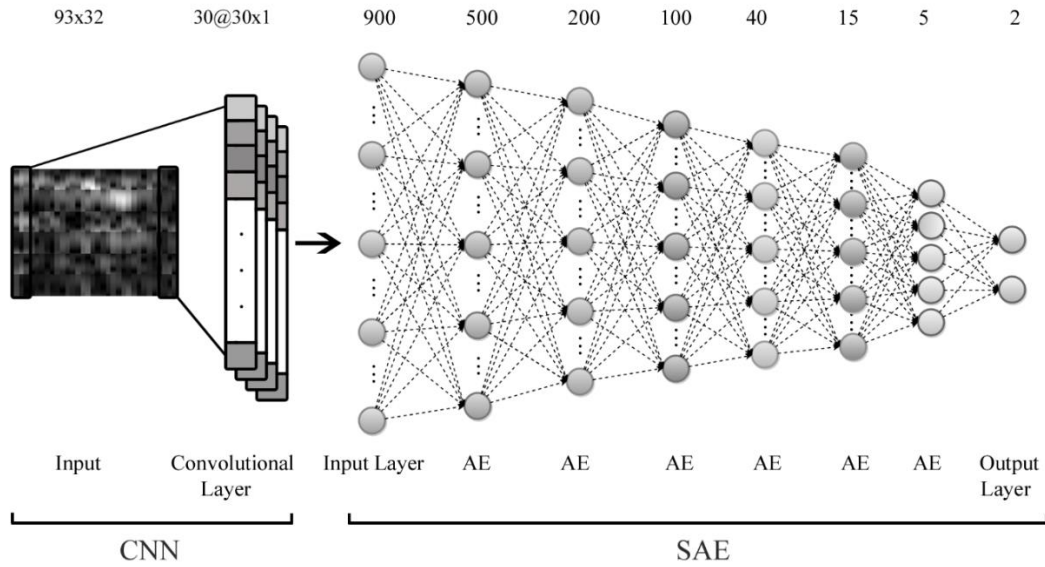


Figure 5.4. The proposed CNN-SAE network. Number of neurons in each layer is shown at top of the layer and the type of each layer is shown at the bottom.

CHAPTER 6

RESULTS

In this chapter, the performance results of our proposed classification methods and MI experiments are presented. In part 6.1, the results of our proposed CNN, SAE and combined CNN_SAE methods are discussed on two public datasets. The results are compared to FBCSP method and other current state of art methods in this field and presented in parts 6.1.1 and 6.1.2. Different aspects of the networks proposed in this thesis are discussed in part 6.1.3.

The proposed method was used to classify MI signals recorded in experiment I. The results are compared to FBCSP method and presented in part 6.2.1. Experiment II was performed to improve MI performance by using 10 different MI tasks. The proposed method and FBCSP were applied to the data recorded during this experiment. These results are presented and discussed in part 6.2.2.

Real time MI experiments with online feedback were performed in experiment III. CNN and CSP-LDA methods were used in the signal processing step of these experiment. The experiments were performed separately for each signal processing method and the results are presented in part 6.2.3. The MI performance was observed to improve by subject training in experiment III. Therefore 15 recording sessions were performed in experiment IV in order to investigate the effect of subject training. The proposed CNN-SAE method was used to classify the MI tasks in this experiment. The results of experiment IV are presented in part 6.2.4 for 15 sessions.

6.1 Classification Results on Public Datasets

In this part, the performance of our proposed method is evaluated by comparing to current state of art methods in this field. Dataset III from BCI Competition II and training set of dataset 2b from BCI Competition IV were used for performance evaluation in this part. In this study, the experiments were conducted in Matlab environment on an Intel 4.00 GHz Core i7 PC with 16 GB of RAM. Matlab deep learning toolbox [146] was used for designing and testing the proposed networks. The toolbox was slightly changed in order to perform 1D convolution and max-pooling in CNN network.

The results comparison for these datasets are provided in parts 6.1.1 and 6.1.2. The results of the proposed method are discussed in part 6.1.3. The detailed information about the effect of different parameters of the network and training can be found in this part.

6.1.1 Results of BCI Competition IV Dataset 2b

In BCI Competition IV dataset 2b, the classifiers were trained and tested separately for each subject. The performance of the proposed method was evaluated by mean accuracy and kappa value [147] metrics using 10x10 fold cross-validation. In this way, in each session, 90% of 400 trials were selected randomly as the training set and the remaining 10% were selected as the test set. The classification accuracy was computed as the number of successfully classified trials divided by the total number of trials in the test set. This process was repeated for 10 times and average accuracy was computed.

Similar to [105], for each EEG trial, we extracted the time interval between 0.5 and 2.5 seconds after the cue was displayed. Then STFT was applied to the extracted signal and the input was constructed as explained in part 4.1.

Our proposed combined CNN-SAE network was used to evaluate the final classification results. CNN and SAE methods were also applied separately in order to compare the effect of each network on classification performance.

In CNN method, we used the network described in part 4.2, which has one convolutional and one max-pooling layers. The network was trained by using batch training method with batch size equal to 50 for 300 epochs.

In SAE method, the input image was down-sampled and turned to a 900x1 vector in order to be used as input to the SAE network. A network with 6 hidden layers was used for classification as described in section 3.3.3. Each Autoencoder in SAE was trained for 200 epochs with batch size 20. Then fine tuning was applied for 200 epochs with batch size 40.

In combined CNN-SAE method, filters and other network parameters (i.e. neuron bias values) learned by CNN method were used to compute the output values of the convolutional layer of the CNN network. Computed output values were then converted to vectors as explained in Section 3.3.4 and used as the input of SAE network. The structure of the SAE part of the network and the training configuration for this method were the same as SAE method.

The accuracy results of CNN, SAE and CNN-SAE methods are presented in Table 6.1. We also applied SVM classifier to the same input images in order to investigate the role of SAE deep network in classification performance. As you can see in Table 6.1, the average accuracy results of CNN and CNN-SAE methods are higher than SVM with the same input data. Inter subject standard deviation of CNN-SAE method is also higher than SVM. The average accuracy of CNN-SAE is also higher than SAE method which emphasizes the role of CNN in extracting features. We can also observe that SAE network performs unsuccessful classification by using EEG input images without any feature extraction.

Table 6.1. BCI Competition IV dataset 2B Accuracy (%) results for CNN, SAE and CNN-SAE methods

| Subjects | Accuracy % (mean \pm std. dev.) | | | |
|-------------------------|-----------------------------------|------|-------------|------|
| | CNN | SAE | CNN-SAE | SVM |
| 1 | 74.5 | 61.0 | 76.0 | 71.8 |
| 2 | 64.3 | 47.5 | 65.8 | 64.5 |
| 3 | 71.8 | 45.0 | 75.3 | 69.3 |
| 4 | 94.5 | 81.3 | 95.3 | 93.0 |
| 5 | 79.5 | 62.8 | 83.0 | 77.5 |
| 6 | 75.0 | 47.8 | 79.5 | 72.5 |
| 7 | 70.5 | 53.8 | 74.5 | 68.0 |
| 8 | 71.8 | 63.8 | 75.3 | 69.8 |
| 9 | 71.0 | 56.5 | 73.3 | 65.0 |
| Average | 74.8 | 57.7 | 77.6 | 72.4 |
| Inter subject std. dev. | 8.4 | 11.2 | 8.1 | 8.7 |

Most of motor imagery studies in the literature use kappa metric for performance evaluation. The kappa value is a measure for classification performance removing the effect of accuracy of random classification [147]. Kappa is calculated as

$$kappa = \frac{acc - rand}{1 - rand} \quad (6.1)$$

Here *acc* is the classification accuracy and *rand* is the result of random classification which is 0.5 for two class classification in this dataset. Kappa results of our method is compared to current state of art studies in Table 6.2. The performance results of these state of art methods are taken from the values provided in the original papers.

Table 6.2. Kappa value results of CNN and CNN-SAE methods compared with FBCSP [105], Twin SVM [114], DDFBS [113], Bi-spectrum [101] And RQNN [125] Methods

| Subject | Mean kappa value (mean \pm std. dev.) | | | | Best kappa value | | | |
|-----------|---|--------------|--------------|--------------|------------------|-------|--------------|--------------|
| | CNN | CNN-SAE | FBCSP | Twin SVM | CNN-SAE | DDFBS | Bi-spectrum | RQNN |
| 1 | 0.488 | 0.517 | 0.546 | 0.494 | 0.738 | 0.710 | 0.600 | 0.640 |
| 2 | 0.289 | 0.324 | 0.208 | 0.416 | 0.458 | 0.310 | 0.310 | 0.590 |
| 3 | 0.427 | 0.494 | 0.244 | 0.322 | 0.845 | 0.750 | 0.300 | 0.650 |
| 4 | 0.888 | 0.905 | 0.888 | 0.897 | 1.000 | 0.470 | 0.980 | 0.990 |
| 5 | 0.593 | 0.655 | 0.692 | 0.722 | 0.750 | 0.190 | 0.660 | 0.460 |
| 6 | 0.495 | 0.579 | 0.534 | 0.405 | 0.796 | 0.200 | 0.610 | 0.510 |
| 7 | 0.409 | 0.488 | 0.409 | 0.466 | 0.699 | 0.780 | 0.750 | 0.810 |
| 8 | 0.443 | 0.494 | 0.413 | 0.477 | 0.751 | 0.770 | 0.800 | 0.800 |
| 9 | 0.415 | 0.463 | 0.583 | 0.503 | 0.550 | 0.730 | 0.760 | 0.770 |
| Average | 0.494 | 0.547 | 0.502 | 0.526 | 0.732 | 0.546 | 0.641 | 0.691 |
| std. dev. | 0.169 | 0.161 | 0.213 | 0.177 | | | | |

Mean kappa value of CNN and CNN-SAE methods are compared to FBCSP [105] (winner algorithm of the competition) and Twin SVM [114] methods in the left side of Table 6.2. On the average, the FBCSP and Twin SVM approaches obtain Kappa values of 0.502 and 0.526 respectively whereas the average Kappa value is 0.547 for our CNN-SAE approach. This indicates that our method provides 9.0% improvement with respect to FBCSP and 4.0% improvement with respect to Twin SVM in terms of average Kappa value.

CNN-SAE method has the best kappa values for 5 out of 9 subjects. Our approach outperforms FBCSP and Twin SVM methods both for 6 out of 9 subjects. Inter subject standard deviation values for CNN, CNN-SAE, FBCSP and twin SVM methods are presented in Table 6.2. Our proposed CNN-SAE method has the lowest inter subject standard deviation value among these methods. The corresponding standard deviation values are 0.0213 for FCSP and 0.177 for Twin SVM, whereas it

is 0.0161 for CNN-SAE, which demonstrates 24.4% improvement with respect to FBCSP and 9.0% improvement with respect to Twin SVM on the standard deviation of Kappa values across subjects. This is showing that CNN-SAE method is more robust to subject dependent differences than other methods. All these results show that CNN-SAE method provides more reliable classification with higher accuracy.

Some other studies only provide best case kappa values for dataset 2b. To compare our approach with these studies we also provide best case kappa values for CNN-SAE method. As it is presented in the right side of Table 6.2, the average of best kappa value of our approach is higher than DDFBS [113], Bi-Spectrum [101] and RQNN [125] approaches. Our approach outperforms DDFBS and Bi-spectrum methods both for 6 out of 9 and RQNN for 5 out of 9 subjects.

EEG signals are known to vary from one session to another [44]. This makes it difficult to make a reliable BCI system where the signal processing algorithm is trained once and used for classification afterwards. In order to investigate this issue, session to session classification was performed on BCI Competition IV dataset 2b. Sessions 1 and 2 with 240 trials were used to train the network and session 3 with 160 trials was used to test the network. Results of the session to session classification are presented in Table 6.3.

Table 6.3 Accuracy results of session to session classification for BCI Competition IV dataset 2B

| Subjects | Accuracy % | | |
|----------|------------|------|---------|
| | CNN | SAE | CNN-SAE |
| 1 | 76.3 | 57.5 | 78.1 |
| 2 | 60.0 | 58.1 | 63.1 |
| 3 | 56.3 | 50.6 | 60.6 |
| 4 | 95.6 | 94.4 | 95.6 |
| 5 | 79.4 | 75.0 | 78.1 |
| 6 | 65.6 | 67.5 | 73.8 |
| 7 | 65.6 | 76.2 | 70.0 |
| 8 | 70.6 | 75.6 | 71.3 |
| 9 | 82.5 | 78.1 | 85.0 |
| Average | 72.4 | 70.3 | 75.1 |

The average accuracy value for all subjects was 72.4% for CNN and 75.1% for CNN-SAE methods respectively. The average result of session to session classification is %2.3 lower for CNN and %2.5 lower for CNN-SAE than those given in Table 6.1. Since the experimental protocol was different between first two sessions and session 3, reduction in the accuracy was expected. However, the results of session to session classification is not necessarily lower for all subjects. As you can see in Table 6.3, the accuracy of CNN-SAE method for subject 9 is higher when using session to session classification. This may be due to large session-to-session variation in performance of subject 9. It is well known that, beside across subjects, BCI performance is also inconsistent within subjects and fluctuates greatly over time, which is a critical problem in BCI studies [145]. We tried to remove the effect of within subject variation on our results by using 10x10 cross validation in the previous test.

6.1.2 Results of BCI Competition II Dataset III

In order to evaluate our methods on another dataset, we used the same networks described before to classify data from BCI Competition II dataset III. The input

images were generated as explained in part 4.1 with window size equal to 32 and time lapses equal to 7. Networks were trained with 140 trials in the training set and tested on 140 trials in the test set. These training and test sets were fixed and provided by the competition organizers.

The results for BCI Competition II dataset III are shown in Table 6.4. The accuracy of the winner algorithm of the competition is 89.3% [134]. The accuracy performance of CNN-SAE algorithm was obtained as 90.0%, which is better than the winner algorithm of the competition. Since the winner algorithm was applied long time ago, we also compared our results to a recent study [10] where a deep learning network is used for feature extraction. The accuracy result of study [23] is 88.2%. The accuracy results of CNN and SAE methods are 89.3% and 60% respectively.

Table 6.4 BCI competition II dataset III. accuracy (%) results for CNN, SAE, CNN-SAE , the winner algorithm [134] and convolutional DBN [10] methods

| Method | CNN | SAE | CNN-SAE | Winner | Convolutional DBN |
|------------|-------|-------|---------|--------|-------------------|
| Accuracy % | 89.3 | 60.0 | 90.0 | 89.3 | 88.2 |
| Kappa | 0.786 | 0.200 | 0.800 | 0.783 | 0.764 |

6.1.3 Discussion of Proposed Network for Public Datasets

As described in [77, 145], certain subjects may face difficulties in performing MI task, where others perform it successfully. This causes a large difference between classification performances of subjects.

The difference of kappa value between best subject (subject 4, kappa=0.905) and worst subject (subject 2, kappa=0.324) is 0.581 when CNN-SAE method is used. This value is 0.680 for the method proposed in the winner algorithm (FBCSP) of the competition. Furthermore, inter subject standard deviation value for CNN-SAE is

0.161 which is lower than FBCSP and Twin SVM. This is showing that CNN-SAE overcomes difficulties related to subject dependent disturbances by providing subject specific training, which is an important issue in BCI applications.

The average of input images of right and left hand MI classes are shown in Figure 6.1 for subjects 2 and 4. The difference between these two classes is quite clear on these average images for subject 4. While there is a decrease of activation in C4 area and increase in C3 area for left hand MI and it is just reverse for the right hand MI. However, average images of these classes are not that different for subject 2. Input images are designed to represent time, frequency and location information from EEG signals. By using 1D convolution (in the horizontal axis) in CNN method, filters are trained to learn the location of the activation in the vertical axis.

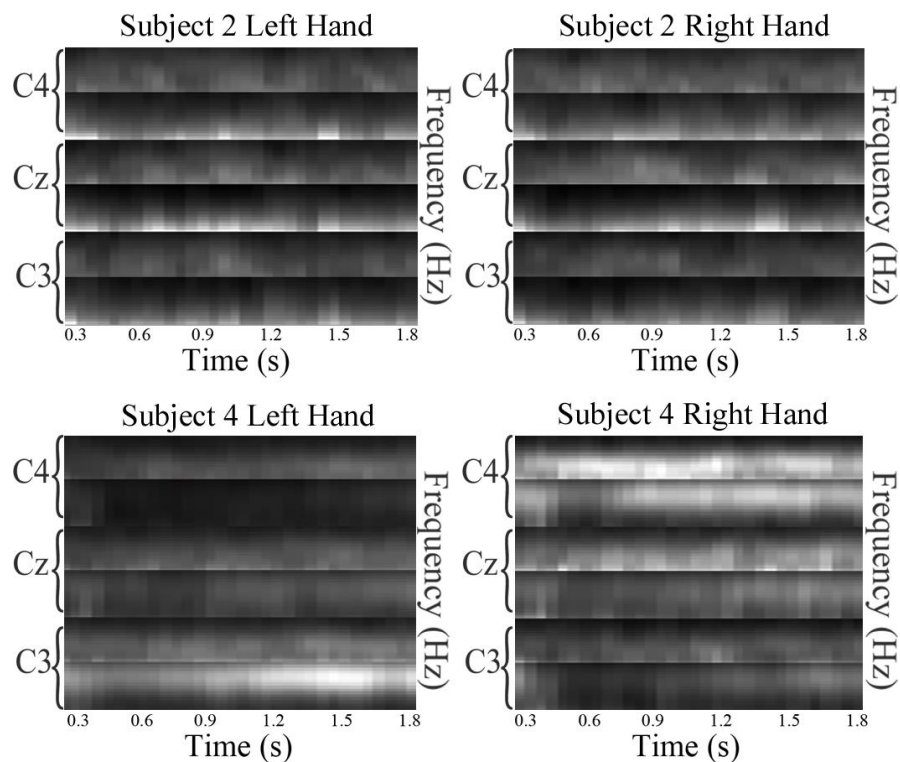


Figure 6.1. Average of input images for right and left hand classes and subjects 2 and 4.

The set of filters of size $N_h \times 3$ learned in the convolution layer of CNN is presented in Figure 6.2. For each filter, there are $N_h=93$ components along vertical axis while there are 3 components along horizontal axis. These filters are computed in a training session for subject 4. Although, these filter weights do not necessarily have any semantic meaning by themselves, multiple filters may be thought as the basis vectors of some space that represents image patches. As it can be seen in Figure 6.2, some filters such as 7, 9, 12 and 14 are learned to detect activation in specific regions along the vertical axis. This corresponds to difference in activation of C3 and C4 electrodes related to the left and right parts of the motor cortex of the brain. Some other filters such as 3, 8 and 10 are learned to detect more detailed information.

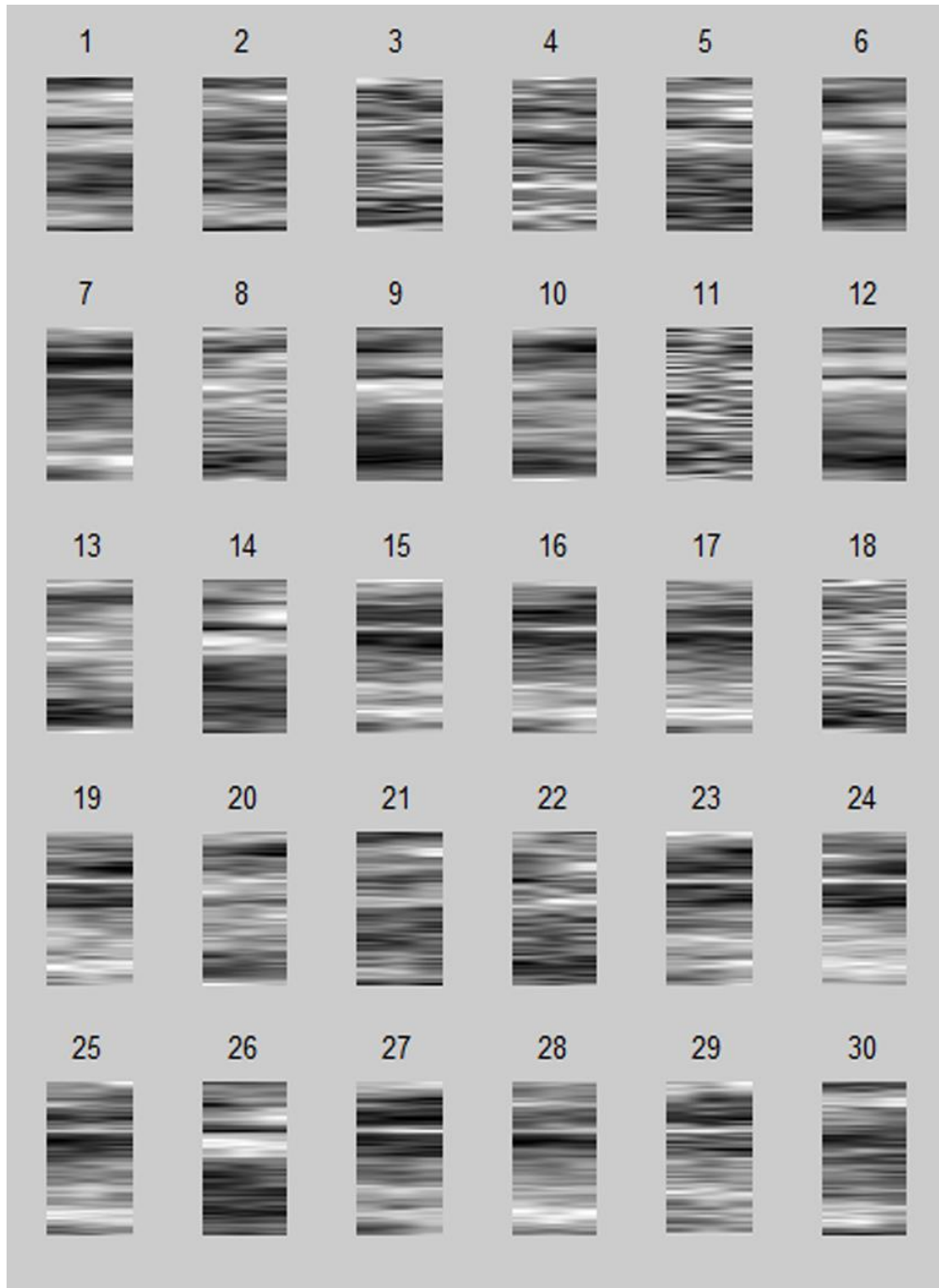


Figure 6.2. Weight values W^k $k=1, 2, \dots, N_F=30$, of filters of size $N_h \times 3$ learned by CNN for subject 4. For each filter there are $N_h=93$ components along vertical axis while there are 3 components along horizontal axis.

In the pooling layer, max-pooling is resulted in a considerable performance improvement compared to average pooling. In our application, activation of any location in image (higher intensity value) is an important factor for classification. Averaging the outputs of convolutional layer may decrease the effect of these activations.

The effect of epoch size on performance (kappa) is shown in Figure 6.3 together with the average training time (for one training set with 360 trials). As you can see in the figure, the performance is higher than others for 300 epochs with an appropriate computation time (1157 seconds). Number of epochs is selected as 300 in this study.

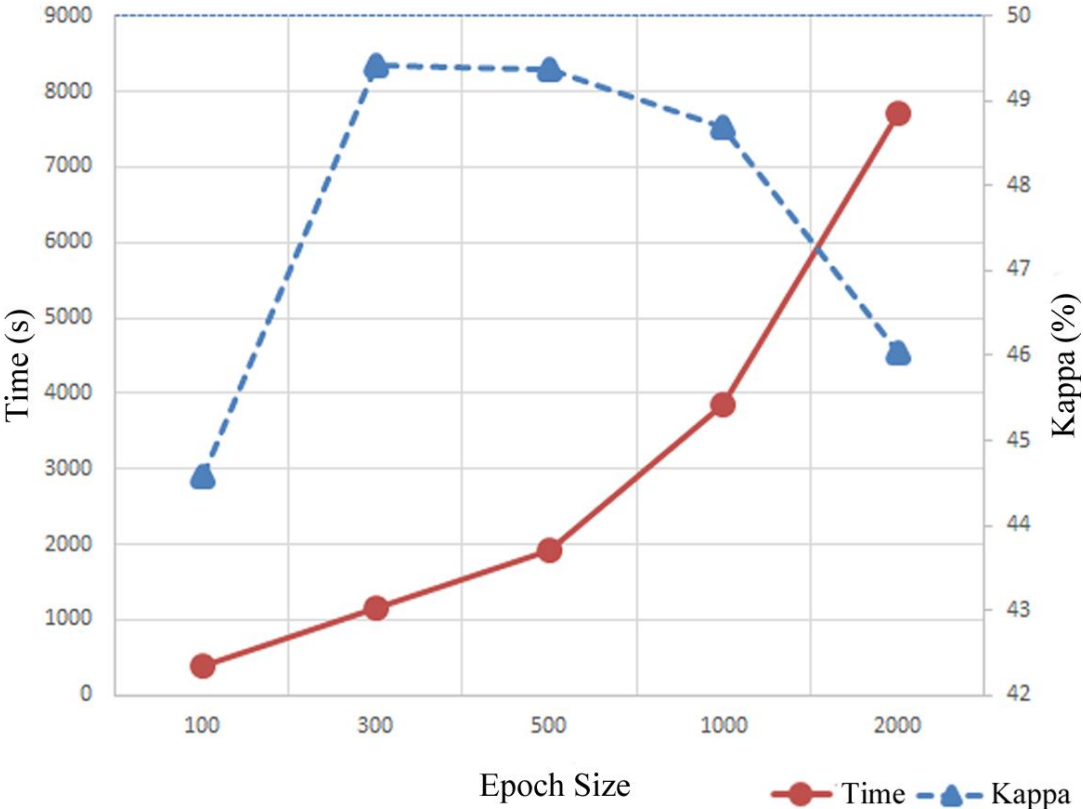


Figure 6.3. Effect of number of epoch on kappa value and training time

The size of filters in the convolutional layer of CNN also change the performance of classification. A comparison between performances of different filter sizes is presented in Table 6.5. Since the performance decreases considerably by increasing the filter size, the results of larger filters are not investigated. Notice that N_h is fixed due to 1D filtering and it has the value which is the height of the input images. As it is shown in Table 6.5, a convolutional layer with filter size equal to $N_h \times 3$ obtains best classification performance. The performance of $N_h \times 2$ filter is very close to $N_h \times 3$ filter. However, in our experiments, the performance of CNN-SAE network was higher with $N_h \times 3$ filter. This means that the features are presented better by using this filter size.

Table 6.5. Effect of filter size on CNN performance. $N_h=93$

| Filter size | Accuracy (%) | Kappa (%) | Time (s) |
|----------------------------------|--------------|-------------|----------|
| $N_h \times 1$ | 73.4 | 46.5 | 785 |
| $N_h \times 2$ | 74.8 | 49.2 | 972 |
| $N_h \times 3$ | 74.8 | 49.4 | 1157 |
| $N_h \times 4$ | 70.9 | 41.1 | 1401 |
| $N_h \times 5$ | 70.4 | 40.4 | 1653 |

The proposed CNN_SAE framework takes advantage of multi domain (time, frequency and electrode location) feature extraction characteristic of CNN model as well as deep learning benefit of SAE method. In SAE part, the size of hidden layers are selected to be less than the size of the previous layer but not less than 25%. In our experiments, the performance was not changing considerably after 200 epochs for pre-training and fine-tuning.

One training session with 360 trials takes about 1157 seconds for CNN-SAE method. However, testing is almost immediate with about 400 ms duration. The computational time for training the same amount of trials using FBCSP method was 246 seconds in our application. Also the time needed for testing the same amount of trials was 508 ms. Our system performs faster than FBCSP in testing state where the training time of our method is higher. Since BCI systems are usually being trained prior to

operation and perform testing in real time, testing time is much more critical than the training time for these systems.

6.2 Results on Data Collection Experiments

In this part, the results of performed motor imagery experiments are discussed. In experiment I, recorded data was classified using our proposed CNN and combined CNN_SAE methods and also FBCSP method. The classification performance of these methods are compared and discussed in part 6.2.1. We also performed an eye artifact rejection method for the recorded data in this experiment. The results of classification after artifact rejection are also included in part 6.2.1.

The results of experiment II are presented in part 6.2.2. 10 different MI tasks in this experiment were classified using 2, 3 and 4 class classifications. The experiment conditions were also improved in this experiment comparing to experiment I. CNN-SAE and FBCSP methods were used for the classification of the recorded signals in this experiment. At the end of this experiment one successful subject and the most distinguishable MI tasks were determined.

In experiment III, real time MI experiments were performed where CSP-LDA and CNN methods were used separately for online classification. The CSP-LDA method is a well-known method used in Graz experiment [25]. The timing of experiment III was similar to Graz experiment and was performed on the selected successful subject from experiment II. The results of this experiment are presented in part 6.2.3. The performance of MI was observed to be improved by subject training in this experiment.

Finally experiment IV was performed in order to investigate the effect of subject training during several subject training sessions. This experiment was performed in 15 sessions for 1 subject. The proposed CNN-SAE method was used for classification and the performance changes through sessions were investigated. The results of this experiment are discussed in part 6.2.4.

It is important to mention that, only the value of C3, Cz and C4 electrodes were used while performing the classification with the proposed method during all performed experiments. However, data from all recording electrodes were used while using FBCSP and CSP-LDA methods.

6.2.1 Experiment I

In this experiment four class (right hand, left hand, feet and both hands) MI tasks were performed by 9 subjects. The total number of trials for each subject was 320 where the number of trials for each MI task was 80. Recorded EEG data included 28 channels sampled at 500 Hz. 4 seconds period of signal during motor imagery period was extracted for each trial and used for classification. Our proposed signal processing methods CNN and CNN-SAE were used to classify motor imagery tasks. The network parameters of these methods were identical to part 6.1.1. In order to evaluate the results of our proposed method, we also applied FBCSP method. This method is a well-known method in MI classification which is used in many studies in this field.

The train and test processes were applied for each subject's data separately. 10 fold cross validation method was used for classification. . In this way, 90% of the trails were selected randomly as the training set and the remaining 10% were selected as the test set. This process was repeated for 10 times. CNN was trained with batch size equal to 50 and epoch number as 300 as proposed in part 6.1.1. Training parameters for Autoencoder and SAE were also similar to part 6.1.1.

Unlike used public datasets, the data in this experiment included four classes. Therefore, classification was performed for 2 class, 3 class (right hand, left hand and feet), 3 class (right hand, left hand and both hands) and 4 class problems separately. The performance results of our proposed method are presented in Tables 6.6 and 6.7 for accuracy and kappa metrics. The performance results of FBCSP method are presented in the same manner in Tables 6.8 and 6.9. Average classification

performances of the proposed method and FBCSP are shown in Table 6.10 so they can be compared easily.

Table 6.6. Accuracy results for experiment I dataset using proposed method

| Subjects | 2 class | | 3 class | | 3 class | | 4 class | |
|----------|---------|--------|----------|--------|----------|--------|-------------|--------|
| | RH LH | | RH LH FE | | RH LH BH | | RH LH FE BH | |
| | CNN | CNNSAE | CNN | CNNSAE | CNN | CNNSAE | CNN | CNNSAE |
| 1 | 64,4 | 66,3 | 42,9 | 40,4 | 42,5 | 39,6 | 28,1 | 31,9 |
| 2 | 53,1 | 55,0 | 41,3 | 37,1 | 34,2 | 35,0 | 26,3 | 26,6 |
| 3 | 55,0 | 49,4 | 34,6 | 34,2 | 28,3 | 25,4 | 20,9 | 24,4 |
| 4 | 48,1 | 46,9 | 31,7 | 34,2 | 37,9 | 40,8 | 24,1 | 24,4 |
| 5 | 53,8 | 56,3 | 37,5 | 34,2 | 30,8 | 35,8 | 27,2 | 29,4 |
| 6 | 75,0 | 77,5 | 50,8 | 54,2 | 56,3 | 55,4 | 36,3 | 36,9 |
| 7 | 71,9 | 69,4 | 51,3 | 52,1 | 53,3 | 53,3 | 44,4 | 37,5 |
| 8 | 57,5 | 61,9 | 41,3 | 43,3 | 36,7 | 40,0 | 29,1 | 29,4 |
| 9 | 51,9 | 48,1 | 34,2 | 34,6 | 34,2 | 37,1 | 28,4 | 30,3 |
| Average | 59,0 | 59,0 | 40,6 | 40,5 | 39,3 | 40,3 | 24,4 | 30,1 |

Table 6.7. Kappa results for experiment I dataset using proposed method

| Subjects | 2 class | | 3 class | | 3 class | | 4 class | |
|----------|---------|--------|----------|--------|----------|--------|-------------|--------|
| | RH LH | | RH LH FE | | RH LH BH | | RH LH FE BH | |
| | CNN | CNNSAE | CNN | CNNSAE | CNN | CNNSAE | CNN | CNNSAE |
| 1 | 0,29 | 0,32 | 0,14 | 0,11 | 0,13 | 0,09 | 0,04 | 0,09 |
| 2 | 0,06 | 0,12 | 0,13 | 0,05 | 0,02 | 0,00 | 0,01 | 0,02 |
| 3 | 0,10 | 0,02 | 0,03 | 0,01 | -0,04 | -0,12 | -0,04 | -0,01 |
| 4 | -0,04 | -0,09 | -0,02 | 0,01 | 0,08 | 0,13 | -0,01 | 0,01 |
| 5 | 0,08 | 0,14 | 0,05 | 0,02 | -0,01 | 0,03 | 0,04 | 0,06 |
| 6 | 0,51 | 0,54 | 0,25 | 0,30 | 0,33 | 0,31 | 0,15 | 0,16 |
| 7 | 0,43 | 0,38 | 0,26 | 0,27 | 0,28 | 0,30 | 0,25 | 0,16 |
| 8 | 0,16 | 0,25 | 0,11 | 0,15 | 0,08 | 0,12 | 0,06 | 0,07 |
| 9 | 0,02 | -0,06 | 0,00 | 0,03 | 0,00 | 0,04 | 0,05 | 0,08 |
| Average | 0,18 | 0,18 | 0,10 | 0,10 | 0,09 | 0,10 | 0,06 | 0,07 |

Table 6.8. Accuracy results for experiment I dataset using FBCSP method

| Subjects | 2 class | 3 class | 3 class | 4 class |
|----------|---------|----------|----------|-------------|
| | RH LH | RH LH FE | RH LH BH | RH LH FE BH |
| 1 | 60,8 | 41,7 | 45,2 | 32,4 |
| 2 | 48,1 | 35,0 | 36,7 | 27,2 |
| 3 | 45,0 | 38,1 | 29,7 | 23,1 |
| 4 | 45,0 | 35,9 | 35,6 | 24,7 |
| 5 | 53,3 | 42,8 | 34,7 | 31,2 |
| 6 | 69,4 | 44,1 | 40,3 | 32,0 |
| 7 | 74,4 | 51,9 | 44,4 | 37,1 |
| 8 | 55,0 | 43,8 | 41,3 | 28,8 |
| 9 | 53,8 | 40,6 | 33,8 | 31,3 |
| Average | 56,0 | 41,5 | 38,0 | 29,8 |

Table 6.9. Kappa results for experiment I dataset using FBCSP method

| Subjects | 2 class | 3 class | 3 class | 4 class |
|----------|---------|----------|----------|-------------|
| | RH LH | RH LH FE | RH LH BH | RH LH FE BH |
| 1 | 0,21 | 0,13 | 0,17 | 0,09 |
| 2 | -0,03 | 0,05 | 0,06 | 0,05 |
| 3 | -0,12 | 0,05 | -0,06 | -0,03 |
| 4 | -0,10 | 0,05 | 0,07 | 0,00 |
| 5 | 0,09 | 0,15 | 0,02 | 0,07 |
| 6 | 0,34 | 0,13 | 0,12 | 0,09 |
| 7 | 0,42 | 0,27 | 0,14 | 0,17 |
| 8 | 0,14 | 0,17 | 0,10 | 0,04 |
| 9 | 0,09 | 0,10 | 0,01 | 0,09 |
| Average | 0,11 | 0,12 | 0,07 | 0,06 |

Table 6.10. Comparison between accuracy results of methods for experiment I

| Methods | 2 class | 3 class | 3 class | 4 class |
|---------|---------|----------------|----------------|--------------------|
| | RHM LHM | RHM LHM FEM | RHM LHM BHM | RHM LHM FEM BHM |
| CNN | 59,0 | 40,6 | 39,3 | 24,4 |
| CNN-SAE | 59,0 | 40,5 | 40,3 | 30,1 |
| FBCSP | 56,0 | 41,5 | 38,0 | 29,8 |

As you can see in Table 6.6, the motor imagery performances of subjects 6 and 7 are similar to average value of BCI Competition IV dataset 2b. However the performance of other subjects is so poor for this experiment. The results of FBCSP method are also not very successful for this experiment.

The results of our proposed method is compared to the results of FBCSP method in Table 6.10. As you can see in this table, our proposed method outperforms the FBCSP method for three of four classification. The results of CNN-SAE method is 3% higher for 2 class, 2.3% higher for 3 class (RHM, LHM, BHM) and less than 1% higher for 4 class classification. It is important to mention that 29 data channels were used in FBCSP method while only 3 channels were used in CNN and CNN-SAE methods. This provides much simpler set up with higher classification rate in BCI applications. The networks used in this experiment were not optimized for this dataset and were identical to what we used in part 6.1.1. The classification performance can be improved by changing network parameters. However the networks were not changed in order to keep generality of the method.

We used two electrodes (VEOG and HEOG) placed near the subjects eye in order to measure eye movement and blinking. The values measured in these electrodes can be used to detect eye artifact. It is proposed in [148] to reject any trial with VEOG value larger than 50 μ V. By using this criteria, about 60% of our trials were detected as artifacts and rejected. Since the amount of remaining trials were not enough for training a deep network, 70 μ V criteria was used for artifact detection. This way only 30% of data was rejected. CNN, CNN-SAE and FBCSP methods were applied on the

remaining trials. The classification accuracy results after artifact removal are presented in Tables 6.11 and 6.12 for CNN, CNN-SAE and FBCSP methods.

Table 6.11. Accuracy results of CNN and CNN-SAE methods for experiment I after artifact removal

| Subjects | 2 class | | 3 class | | 3 class | | 4 class | |
|----------|---------|--------|----------|--------|----------|--------|-------------|--------|
| | RH LH | | RH LH FE | | RH LH BH | | RH LH FE BH | |
| | CNN | CNNSAE | CNN | CNNSAE | CNN | CNNSAE | CNN | CNNSAE |
| 1 | 61,7 | 60,8 | 39,4 | 44,4 | 37,8 | 39,4 | 30,4 | 34,6 |
| 2 | 47,3 | 43,6 | 28,2 | 28,2 | 32,4 | 28,2 | 22,8 | 24,4 |
| 3 | 50,0 | 43,8 | 35,0 | 24,2 | 37,0 | 37,0 | 14,1 | 19,4 |
| 4 | 50,8 | 55,4 | 38,5 | 35,0 | 33,2 | 37,4 | 25,6 | 28,9 |
| 5 | 48,6 | 48,6 | 25,6 | 23,3 | 28,0 | 32,0 | 19,3 | 27,9 |
| 6 | 70,9 | 71,8 | 51,9 | 50,6 | 51,9 | 47,5 | 41,3 | 33,5 |
| 7 | 67,3 | 68,2 | 41,2 | 40,0 | 44,7 | 40,0 | 38,8 | 42,5 |
| 8 | 53,3 | 61,7 | 46,7 | 38,9 | 38,9 | 44,4 | 33,3 | 37,2 |
| 9 | 50,0 | 50,0 | 38,3 | 43,9 | 35,0 | 38,3 | 27,0 | 29,6 |
| Average | 55,5 | 56,0 | 38,3 | 36,5 | 37,6 | 38,3 | 28,1 | 30,2 |

Table 6.12. Accuracy results of FBCSP method for experiment I after artifact removal

| Subjects | 2 class | | 3 class | | 3 class | | 4 class | |
|----------|---------|--|----------|--|----------|--|-------------|--|
| | RH LH | | RH LH FE | | RH LH BH | | RH LH FE BH | |
| 1 | 57,6 | | 40,2 | | 37,9 | | 29,5 | |
| 2 | 49,8 | | 32,3 | | 33,5 | | 24,1 | |
| 3 | 42,0 | | 31,1 | | 33,8 | | 19,1 | |
| 4 | 49,4 | | 35,3 | | 33,4 | | 27,9 | |
| 5 | 53,0 | | 39,5 | | 35,0 | | 25,7 | |
| 6 | 62,3 | | 43,4 | | 41,6 | | 35,9 | |
| 7 | 67,0 | | 46,0 | | 44,0 | | 41,9 | |
| 8 | 60,4 | | 35,7 | | 34,6 | | 29,8 | |
| 9 | 49,1 | | 39,0 | | 34,4 | | 31,2 | |
| Average | 54,5 | | 38,0 | | 36,5 | | 29,5 | |

As you can see in Tables 6.11 and 6.12, the classification performance is reduced after rejection of data with eye artifacts. This may be because of loss of training data for classification methods. Deep learning methods are known to perform better with larger datasets and loss of data may cause the performance to drop. The differences between CNN, CNN-SAE and FBCSP methods are very low (about 1%) for all classifications.

Independent component analysis (ICA) method was also used to remove the components related to the eye artifacts without reducing the dataset size. ICA was applied by using EEGLAB toolbox. However no improvement in performance was observed by using this method. Another issue with ICA is the manual interaction that is needed to remove the artifact components that reduces our systems automaticity.

The average of input images of right and left hand MI classes are shown in Figure 6.4 for unsuccessful subject 4 and successful subject 6. As you can see in this picture, the average of input images are different for two classes in subject 6 while the average input images look similar for subject 4.

The decrease of activation in C3 area and increase in C4 area for right hand MI is clear for subject 6. However the reverse effects are not that clear for left hand MI. The difference between classes were more clear for the most successful subject of public dataset BCI Competition IV 2b.

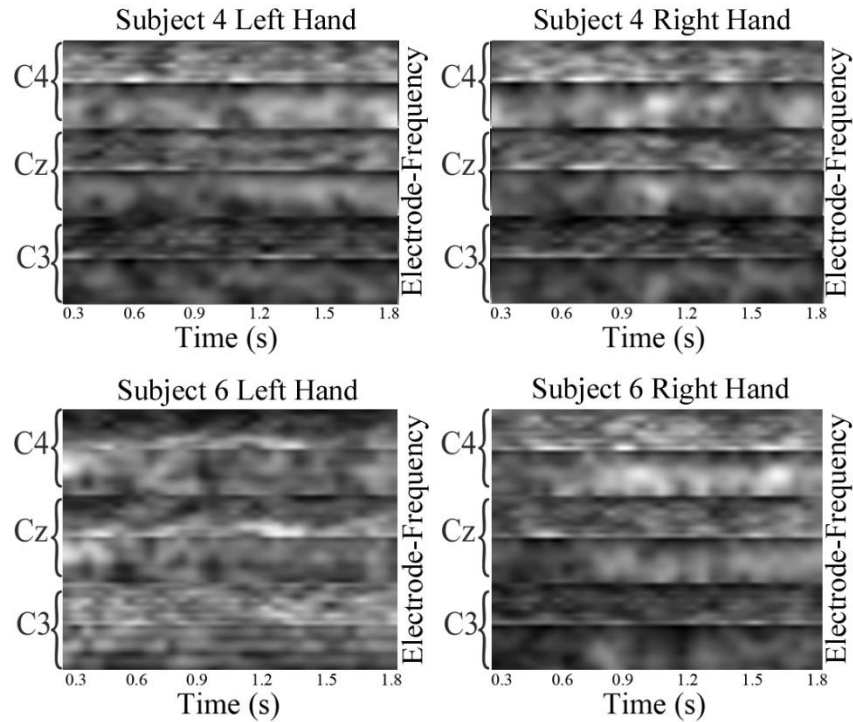


Figure 6.4. Average of input images for right and left hand classes and subjects 4 and 6

The classification results of this experiment show that most of the subjects were not able to perform successful motor imagery tasks. Eye artifact was presented on about 60% of the trials which decreases the quality of the signal. Only 2 subjects were able to perform successful motor imagery tasks. The classification results were high for these subjects using both proposed method and FBCSP.

At the end of this experiment we observed that the time of the recording sessions were too long. This caused the subjects to loose concentration and increased their body movements. We also saw that the MI tasks were not evident. So subjects were performing different type of acts for the same task. For example for the same right hand MI task, subjects were performing right hand movement in one trail while performing right hand finger squeezing in the other trial. By using these experiences, experiment II was designed with shorter recording times and evident MI tasks.

6.2.2 Experiment II

In this experiment 10 different motor imagery tasks were performed in 3 sessions. Right hand movement (RHM), left hand movement (LHM), right foot movement (FEM) and tongue movement (TOM) MI tasks were included in session one. Squeeze ball with right hand fingers (RHS), squeeze ball with left hand fingers (LHS), squeeze right foot fingers (FES) and squeeze ball with both hands fingers (BHS) was performed in Session two. Finally push (PSH) and pull (PLL) complex MI tasks were included in session 3.

CNN-SAE and FBCSP methods were applied similar to experiment I for classification of different tasks. The classification results of these tasks were investigated in this experiment in order to find out most distinguishable tasks for each subject.

The number of trials for 2, 3 and 4 class classification was 80, 120 and 160 respectively. 10 fold cross validation method was used to evaluate classification performance similar to previous experiment. The classification results of our proposed method are presented in Tables 6.13 and 6.14 for accuracy and kappa metrics. The classification results of FBCSP method are also provided in Tables 6.15 and 6.16.

Table 6.13. Accuracy results of CNN-SAE method for experiment II

| Subject | 2 class | | | 3 class | | 3 class | | 4 class | |
|---------|------------|------------|------------|-------------------|-------------------|-------------------|-------------------|--------------------------|--------------------------|
| | RHM LHM | RHS LHS | PSH PLL | RHM LHM FEM | RHS LHS FES | RHM LHM TOM | RHS LHS BHS | RHM LHM TOM FEM | RHS LHS BHS FES |
| S1 | 53,8 | 57,5 | 50,0 | 41,7 | 50,0 | 52,5 | 45,0 | 38,1 | 35,0 |
| S2 | 71,3 | 71,3 | 44,4 | 64,2 | 52,5 | 67,5 | 40,8 | 48,1 | 36,3 |
| S3 | 67,5 | 75,0 | 43,8 | 45,0 | 48,3 | 50,0 | 45,0 | 35,6 | 29,4 |
| S4 | 61,3 | 55,0 | 47,5 | 41,7 | 38,3 | 40,0 | 36,7 | 31,3 | 28,1 |
| S5 | 62,5 | 75,0 | 46,3 | 40,0 | 55,0 | 43,3 | 60,0 | 38,8 | 43,8 |
| S6 | 53,8 | 67,5 | 50,0 | 43,3 | 45,8 | 44,2 | 49,2 | 33,1 | 35,0 |
| S7 | 67,4 | 53,2 | 50,1 | 52,1 | 44,7 | 49,3 | 39,3 | 46,1 | 38,6 |
| Average | 62,5 | 64,9 | 47,4 | 46,8 | 47,8 | 49,54 | 45,1 | 38,7 | 35,2 |

Table 6.14. Kappa results CNN-SAE method for experiment II

| Subject | 2 class | | | 3 class | | 3 class | | 4 class | |
|---------|------------|------------|------------|-------------------|-------------------|-------------------|-------------------|--------------------------|--------------------------|
| | RHM LHM | RHS LHS | PSH PLL | RHM LHM FEM | RHS LHS FES | RHM LHM TOM | RHS LHS BHS | RHM LHM TOM FEM | RHS LHS BHS FES |
| S1 | 7,7 | 17,5 | 4,2 | 12,0 | 24,1 | 24,9 | 18,5 | 17,7 | 13,4 |
| S2 | 37,8 | 33,0 | -11,1 | 44,4 | 28,8 | 45,0 | 14,6 | 30,9 | 14,3 |
| S3 | 34,2 | 48,2 | -11,0 | 16,3 | 22,0 | 22,9 | 15,2 | 14,2 | 5,2 |
| S4 | 20,8 | 13,5 | -2,1 | 11,7 | 9,1 | 5,9 | 6,7 | 9,2 | 5,7 |
| S5 | 24,2 | 43,4 | -2,7 | 11,5 | 31,4 | 15,7 | 38,8 | 17,3 | 25,7 |
| S6 | 11,4 | 24,5 | 4,0 | 16,0 | 22,3 | 17,6 | 25,0 | 10,0 | 14,5 |
| S7 | 36,7 | 6,1 | 0,0 | 31,5 | 16,4 | 23,2 | 12,4 | 29,9 | 18,6 |
| Average | 24,7 | 26,6 | -2,7 | 20,5 | 22,0 | 22,2 | 18,7 | 18,5 | 13,9 |

Table 6.15. Accuracy results of FBCSP method for experiment II

| Subject | 2 class | | | 3 class | | 3 class | | 4 class | | |
|---------|---------|------|------|---------|------|---------|------|---------|------|-----|
| | RHM | RHS | PSH | RHM | RHS | RHM | RHS | RHM | RHS | |
| | LHM | LHS | PLL | LHM | LHS | LHM | LHS | LHM | LHS | BHS |
| | | | | FEM | FES | TOM | BHS | TOM | | FES |
| | | | | | | | | FEM | | |
| S1 | 55,0 | 75,0 | 42,5 | 44,2 | 62,5 | 55,0 | 51,7 | 44,4 | 56,3 | |
| S2 | 52,5 | 63,1 | 55,2 | 47,5 | 48,0 | 50,8 | 34,6 | 36,9 | 38,4 | |
| S3 | 56,3 | 61,3 | 42,5 | 39,2 | 50,8 | 35,0 | 40,8 | 28,8 | 26,3 | |
| S4 | 65,0 | 48,8 | 42,5 | 40,0 | 50,0 | 51,7 | 41,7 | 27,5 | 41,3 | |
| S5 | 56,3 | 60,0 | 36,3 | 39,2 | 35,8 | 35,8 | 40,0 | 30,6 | 28,8 | |
| S6 | 46,3 | 57,5 | 40,0 | 36,7 | 50,8 | 40,8 | 45,0 | 26,9 | 33,1 | |
| S7 | 56,3 | 53,8 | 46,3 | 46,7 | 40,8 | 37,5 | 40,8 | 34,4 | 35,0 | |
| Average | 55,3 | 59,9 | 43,6 | 41,9 | 48,3 | 43,8 | 42,0 | 32,7 | 37,0 | |

Table 6.16. Kappa results of FBCSP method for experiment II

| Subject | 2 class | | | 3 class | | 3 class | | 4 class | | |
|---------|---------|------|------|---------|------|---------|------|---------|------|-----|
| | RHM | RHS | PSH | RHM | RHS | RHM | RHS | RHM | RHS | |
| | LHM | LHS | PLL | LHM | LHS | LHM | LHS | LHM | LHS | BHS |
| | | | | FEM | FES | TOM | BHS | TOM | | FES |
| | | | | | | | | FEM | | |
| S1 | 0,11 | 0,50 | - | 0,17 | 0,42 | 0,31 | 0,23 | 0,27 | 0,41 | |
| S2 | 0,05 | 0,27 | 0,14 | 0,22 | 0,23 | 0,25 | 0,03 | 0,14 | 0,20 | |
| S3 | 0,13 | 0,22 | - | 0,09 | 0,26 | 0,03 | 0,11 | 0,06 | 0,02 | |
| S4 | 0,29 | - | 0,15 | 0,11 | 0,24 | 0,29 | 0,15 | 0,04 | 0,21 | |
| S5 | 0,14 | 0,02 | 0,16 | 0,07 | 0,05 | 0,04 | 0,11 | 0,09 | 0,05 | |
| S6 | -0,07 | 0,14 | 0,26 | 0,05 | 0,26 | 0,12 | 0,14 | 0,03 | 0,12 | |
| S7 | 0,13 | 0,08 | 0,21 | 0,22 | 0,13 | 0,07 | 0,12 | 0,11 | 0,12 | |
| | | | 0,08 | | | | | | | |
| Average | 0,11 | 0,20 | - | 0,13 | 0,22 | 0,15 | 0,12 | 0,10 | 0,16 | |
| | | | 0,12 | | | | | | | |

Table 6.17. Comparison between accuracy results of methods for experiment II

| Methods | 2 class | | | 3 class | | 3 class | | 4 class | | |
|---------|---------|------|------|---------|------|---------|------|---------|-----|---------|
| | RHM | RHS | PSH | RHM | RHS | RHM | RHS | RHM | RHS | LHS BHS |
| | LHM | LHS | PLL | LHM | LHS | LHM | LHS | LHM | LHS | FES |
| | | | | FEM | FES | TOM | BHS | TOM | FEM | |
| CNN-SAE | 62,5 | 64,9 | 47,4 | 46,8 | 47,8 | 49,54 | 45,1 | 38,7 | | 35,2 |
| FBCSP | 55,3 | 59,9 | 43,6 | 41,9 | 48,3 | 43,8 | 42,0 | 32,7 | | 37,0 |

The amount of trials with eye artifact (VEOG larger than 50 μ V) was about 30% for this experiment. This may be due to decreasing the time of each session so the subjects didn't get tired. However the amount of artifact is still big for BCI applications. Since no improvement in classification performance was observed in the previous experiment, no artifact removal method was used in this experiment.

According to Table 6.13 the average classification results were improved in this experiment comparing to experiment I. This improvement is observable for all 2 class, 3 class and 4 class classifications. However the results are still worse than public datasets. It's important to mention that in BCI competition 4 dataset 2b dataset, the trials with artifact were eliminated manually by expert.

The results of proposed CNN-SAE and FBCSP methods are compared in Table 6.17. As you can see in this table our proposed method outperforms FBCSP in 7 out of 9 classifications. The average LHM/RHM classification accuracy is 62.5% for our proposed method which is 7.2% higher than the result of FBCSP. FBCSP method was applied using all 29 electrodes where only 3 channels (C3, Cz, C4) were used in our proposed methods.

It is known that some subjects are more successful in performing specific motor imagery tasks [145]. This issue can be observed in our results as well. As you can see in Table 6.13, some subjects are more successful in performing squeezing related tasks while the others are more successful in performing movement related tasks.

In order to perform further experiments, subject *S7* was selected in this experiment. Motor imagery performance of this subject was good comparing to the other subjects. However she was not the most successful subject. The subject was selected due to availability of the subject for further experiments.

10 class classification was performed on subject *S7* in order to find out most distinguishable tasks. A confusion matrix was constructed by using the results of this classification. The related confusion matrix is shown in Figure 6.5. Each row in this matrix corresponds to the actual label of the trial and each column corresponds to the predicted label. The values in each cell indicate the percentage of the trials which are detected as the column label. As you can see in this figure, the correct detection rate is 30% for LHM and 28% for RHM. Therefore these two tasks were selected for online experiments on this subject.

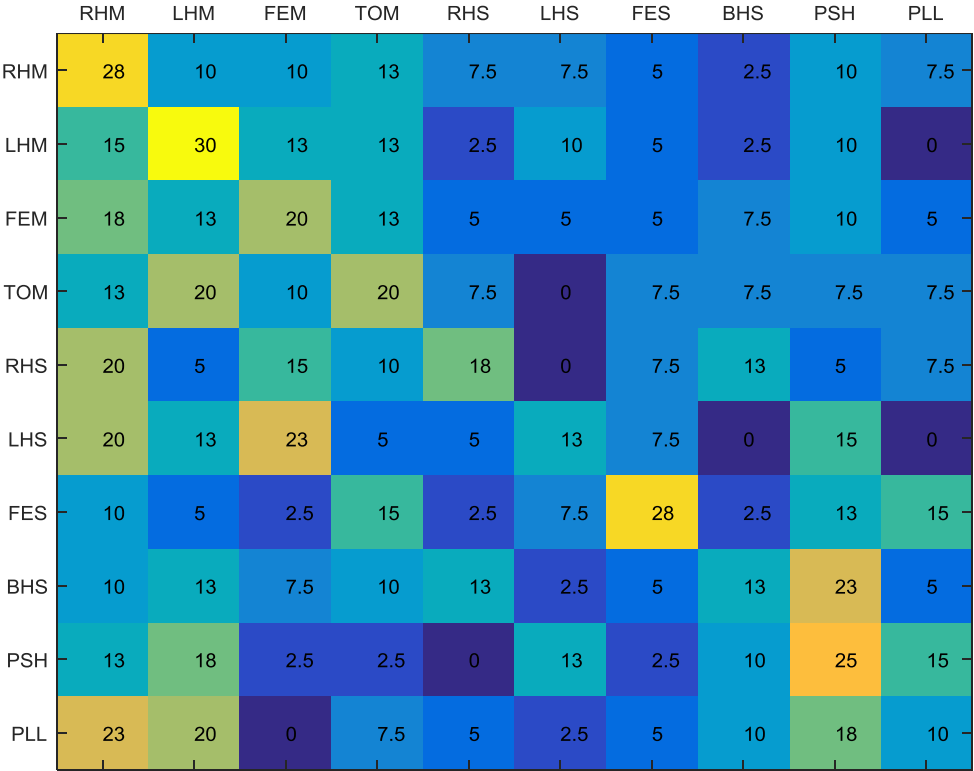


Figure 6.5 Confusion matrix for subject *S7*

6.2.3 Experiments III

In experiments III, an online motor imagery experiment with feedback was performed similar to Graz experiment [25]. Two sessions of experiment III were performed identical to Graz experiment by using CSP-LDA method for classification.

In these sessions, the classifier was trained by 40 trails (20 right and 20 left) in each session. Then an online classification step was performed as described in part 4.8. The number of trials in this step was similar to the training step. The accuracy results of two sessions of Graz experiment are provided in Table 6.18.

Our proposed CNN network was also used for signal processing in experiment III. In this part, similar amount of data was used to train CNN network and 2 sessions of online motor imagery experiments were applied afterwards. Online sessions were applied by using the same trained network. The accuracy results of these two sessions are presented in Table 6.19.

Table 6.18. Accuracy results of experiment III, Graz sessions

| Session | Number of trials | Training time (s) | Accuracy (%) |
|---------|------------------|-------------------|--------------|
| Graz 1 | 40 | 37 | 68 |
| Graz 2 | 40 | 36 | 73 |

Table 6.19. Accuracy results of experiment III, CNN sessions

| Session | Number of trials | Training time (s) | Accuracy (%) |
|---------|------------------|-------------------|--------------|
| CNN 1 | 40 | 3950 | 73 |
| CNN 2 | 40 | 3950 | 80 |

In the above experiments, the classification algorithm was called several times during online feedback period of each session. The final classification result was computed by averaging all of the results during this period. The variance between different classification results was very low in most of the cases that means the algorithm returns the same result during the 3 second feedback period. It is also important to mention that the trained network was the same for both sessions in CNN experiment. Therefore, the improvement in accuracy is only due to subject's performance.

As it is shown in Tables 6.18 and 6.19, CNN method leads to better classification results comparing to CSP-LDA. Increment from session 1 to 2 can also be observed in these tables which may be because of subject training. However the amount of results are not enough to provide statistically significant conclusion. In order to investigate the effect of subject training on MI performance, experiment IV was designed and performed in several recording sessions.

6.2.4 Experiments IV

The effect of subject training on motor imagery performance was investigated in experiment IV. In this experiment 15 sessions with online feedback were performed during 45 days. Experiment sessions are explained in part 5.8.

In each session, data from 3 last run was used to perform classification. 10 fold cross validation was used to compute average accuracy. In each step, 90% (81 trials) of the trails were selected as training set and the remaining 10% (9 trials) were used as test set. Data for 1 second period during motor imagery period was extracted and used to construct input images as described in part 4.1. Then combined CNN-SAE method was applied to the extracted input images. The network parameters were similar to part 6.1.1.

The accuracy results of experiment IV is presented in Table 6.20 for 15 sessions. Accuracy changes trough sessions can also be observed in Figure 6.6.

Table 6.20. Results of experiment IV for 15 recording sessions

| Sessions | Run 7 | Run 8 | Run 9 | Average |
|----------|-------|-------|-------|---------|
| 1 | 63,3 | 70,0 | 63,3 | 65,5 |
| 2 | 66,6 | 66,6 | 63,3 | 65,5 |
| 3 | 63,3 | 53,3 | 60,0 | 58,9 |
| 4 | 70,0 | 66,6 | 63,3 | 66,6 |
| 5 | 66,6 | 56,6 | 63,3 | 62,2 |
| 6 | 66,6 | 66,6 | 73,3 | 68,8 |
| 7 | 73,3 | 66,6 | 70,0 | 70,0 |
| 8 | 63,3 | 60,0 | 66,6 | 63,3 |
| 9 | 70,0 | 60,0 | 60,0 | 63,3 |
| 10 | 60,0 | 66,6 | 66,6 | 64,4 |
| 11 | 70,0 | 63,3 | 70,0 | 67,8 |
| 12 | 73,3 | 63,3 | 66,6 | 67,7 |
| 13 | 76,6 | 76,6 | 70,0 | 74,4 |
| 14 | 73,3 | 76,6 | 83,3 | 77,7 |
| 15 | 80,0 | 76,6 | 76,6 | 77,7 |

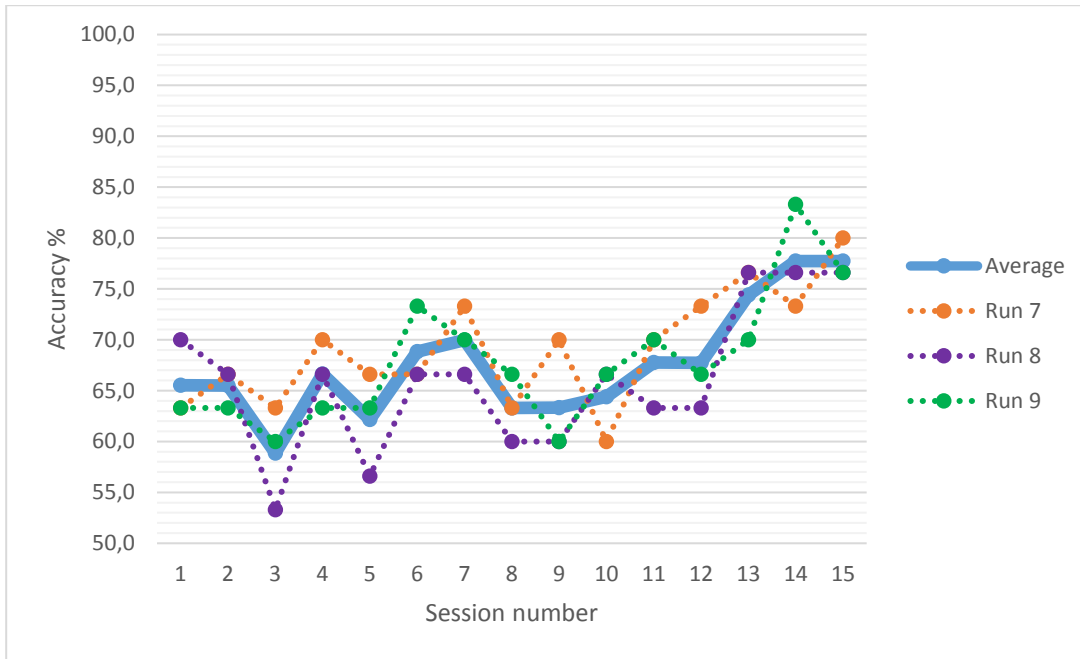


Figure 6.6 Accuracy results of experiment IV for 15 sessions

As you can see in Figure 5.5, the average of three sessions was 65.5% in the first session which was increased to 77.7% after 15 sessions. These 15 sessions were performed during 45 days period. Motor imagery performance of the subject was increased by 12.2% in this period. The value of accuracy is 77.7% in the last two sessions which can be considered as successful performance comparing to similar studies. However this accuracy is not enough for most of BCI applications.

This experiment was performed on only one subject due to limited time and resources. However the improvement in the MI performance of one subject can be observed in this experiment. It is important to mention that our proposed classification method is trained for each subject separately. Therefore the amount of subjects does not affect the classification results of each subject.

CHAPTER 7

CONCLUSION

In this thesis, the classification problem in motor imagery based Brain Computer Interface (BCI) systems is investigated. Three different neural network models, one of which is proposed in this study, were used to classify EEG Motor Imagery (MI) signals. Convolutional Neural Network (CNN), Stacked Autoencoder (SAE) and combined CNN-SAE methods were applied in this thesis.

We designed a new input form by using time, frequency and location information of EEG signals. These inputs are used in a CNN network with one 1D convolutional and one max-pooling layers. The filters in the convolutional layer of CNN are being trained to learn the location of activation patterns as well as the frequencies while they are partially invariant to placement in time axis due to max-pooling. A new combined network is proposed in this thesis by using CNN and SAE models. In this network, features of input EEG signal are first extracted by training the filters in convolutional layer of CNN. Then these features are used in a deep SAE network to perform classification.

The filters learned in CNN takes into account the activation in the neighboring regions but CNN does not provide any information on which filter contributes to classification performance more than the others. Instead, pooling is applied on the next layer. On the other hand, the neighboring information is lost in the SAE, but the weight values provide information to the network on the importance of the input elements. However, when the outputs of the filters trained by CNN are given as input to SAE, the advantages of each network are unified and the performance increases.

Proposed neural networks were evaluated on two public datasets which are Dataset III from BCI Competition II and training set of dataset 2b from BCI Competition IV. The classification results of these networks were compared to current state of art methods. We showed that the classification performance of the CNN-SAE network that we proposed is higher than other state of art methods for both datasets. The average kappa value for CNN-SAE method was 0.547 on BCI competition IV dataset. The kappa value of the winner algorithm of competition IV was 0.502, so kappa value is improved about 9% by using our approach. To our knowledge, our approach is the one that yields the best accuracy performance on BCI competition IV dataset 2b.

The accuracy result of CNN-SAE method on dataset III was 90.0% that is higher than the winner algorithm of competition III. Our proposed network also obtained better performance results than the deep network introduced in [10] for feature extraction.

CNN and SAE networks were also applied for classification separately and the results were discussed. While the performance of the CNN network is close to the CNN-SAE network, the performance of SAE method is poor. This poor performance is because of losing neighborhood information in SAE input layer. Several network parameters like filter size and training epochs were also analyzed and the effect of each parameter was discussed.

The proposed method was evaluated by using datasets with 3 electrodes. However it can be extended to use larger number of electrodes. The input image can be constructed by aligning data from any number of electrodes. In this case, the size of the filters in the convolutional layer of the network should be changed in order to fit the input image. It should be noted that, by increasing the size of filters, the number of variables in the network also increases and larger amount of data may be needed in order to train the network.

Our proposed deep learning network performs fast classification with a higher performance than other methods in literature. 2D images were used in this method as the network input by combining time frequency and location information. In future studies, multi-dimensional inputs can be used in order to cover more detailed information about the data. These inputs can be employed in deeper networks so that

all of the features would be extracted from the data. CNN can be used in these networks with 3 or higher convolution dimension.

Our study was one of the premier applications of deep learning methods in BCI. The amount of studies employing deep learning methods for BCI applications is increasing afterwards. We believe that further investigations of deep learning methods in BCI studies can make these methods a proper choice for BCI applications.

In order to investigate the performance of the proposed method on BCI systems, several motor imagery experiments were performed during this thesis. In experiments I, EEG signals related to 4 different motor imagery tasks were recorded for 9 subjects. Afterwards, the recorded data was classified using our proposed CNN-SAE method. The results were compared to FBCSP method and it was shown that our method provides better classification performance in most cases. However, the average performance was lower than the results of public datasets.

By using the experiences from experiment I, the experiment conditions were improved and 10 evident MI tasks were selected for experiment II. In this experiment, movement and squeezing of hand and foot were investigated separately. This way we were able to determine most distinguishable motor imagery tasks for each subjects. Total 7 subjects were attended this experiment. CNN-SAE and FBCSP methods were used to classify the recorded data. The classification performance of our proposed method was higher comparing to FBCSP like the previous experiment. The MI performance was observed to be improved in this experiment comparing to experiment I.

After performing two data recording and offline classification experiments, a simple BCI system was designed in experiment III. In this experiment, the subject was guided to perform right or left hand motor imagery task and a feedback showing the detected task was presented to the subject in real time. This experiment was applied to one successful subject, selected from experiment II. The CSP-LDA and CNN methods were used to perform online classification in separate sessions. The best accuracy results in this experiment were 73% for CSP-LDA and 80% for CNN. In this experiment the MI performance was observed to improve by subject training.

However, the number of experiment sessions were not enough to statistically prove this.

In order to investigate the effect of subject training on MI performance, experiment IV was designed such that activity patterns of the brain was presented to the subject after performing each motor imagery task. This way, the subject was able to improve his motor imagery performance by observing the visual feedback. This experiment was performed on one subject and repeated for 15 sessions in a 45 days period. A wireless EEG recording device was used in this experiment and the recording environment was more likely to daily life environment. The Right and left hand motor imagery tasks used in this experiment were classified using the CNN-SAE method. The experiment results revealed that the classification accuracy was improved from 65.5% to 77.77% during this period.

Our experiments showed that there are many factors that affect the performance of motor imagery. Signal quality is an important issue that affects the motor imagery performance directly. Besides, the impedance of recording electrodes should be low and in the same level in order to achieve similar activity patterns. However currently there is no metric to measure motor imagery signal quality and practical methods were used in this thesis.

The artifacts caused by eye movement are another source of problem that changes the recorded activity patterns of the brain in large scale. In this thesis, subjects were asked to not move their eyes during recording period. However there was eye artifact detected in nearly half of trials. Eye artifact is inevitable in a daily life BCI system and should be overcome by automatic methods. Currently there isn't any fully successful method for automatic eye artifact removal in motor imagery studies. We believe that improvements in recording devices will make it possible to improve the signal quality and eliminate the artifacts. These improvements will lead to more successful BCI systems usable in daily life.

The motor imagery performance was observed to change in large scale between subjects and also between sessions for the same subject in our experiments. These issues are also been reported in other studies and being considered as problems of

motor imagery based BCIs [145]. It is known that significant amount of people are BCI-illiterate which means they cannot control BCI systems. We also observed that some subjects are more successful in performing a specific motor imagery task than other tasks. This issue should be considered in designing a subject specific motor imagery based BCI system.

Difficulties in arranging subjects for long term experiments made us to perform each real time MI experiment only on one subject. However, we were able to successfully design and perform real time MI experiments in this study and show the effect of subject training in the MI performance. In the future, the experiments should be applied to more subjects in order to generalize the results.

Motor imagery based BCI systems are currently far from commercial applications. Although our proposed algorithm was successful in classification of different motor imagery tasks, the performance values in our experiments were not enough for a successful BCI system to be used in practice. In order to be able to design such a system, close interdisciplinary cooperation between neuroscientists, engineers and psychologists is needed. Meanwhile, further developments in recording sensors and also classification algorithms would be essential.

APPENDIX A

IMPEDANCE MEASUREMENT FOR BRAINAMP DEVICE

The impedance measurement was performed by using a constant AC current of less than 1 microampere. The current flows from data electrodes or reference electrode to the ground electrode and the impedances are measured by using the electrode voltages. The measured impedances are not precise and include about 10-20% error.

Three different group of impedances are measured by BrainAmp. These groups are Data electrodes, reference electrode and ground electrode. Block diagrams for impedance measurement of data, reference and ground electrodes are presented in Figures A.1-3.

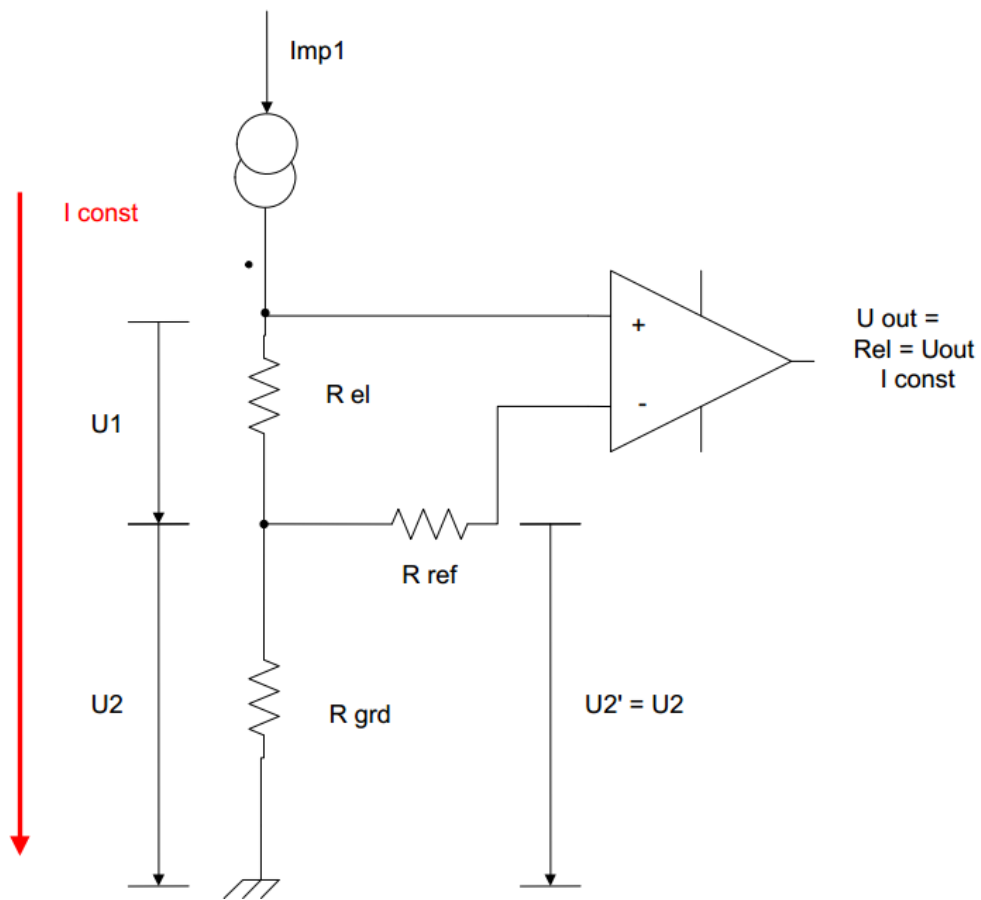


Figure A.1. Impedance measurement of data electrodes

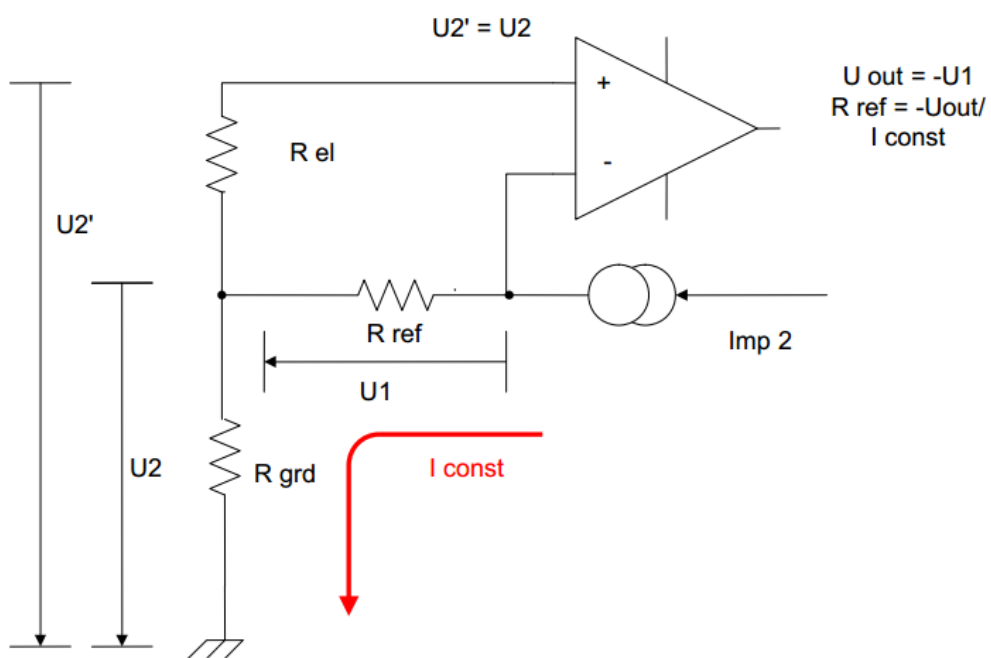


Figure A.2. Impedance measurement of reference electrodes

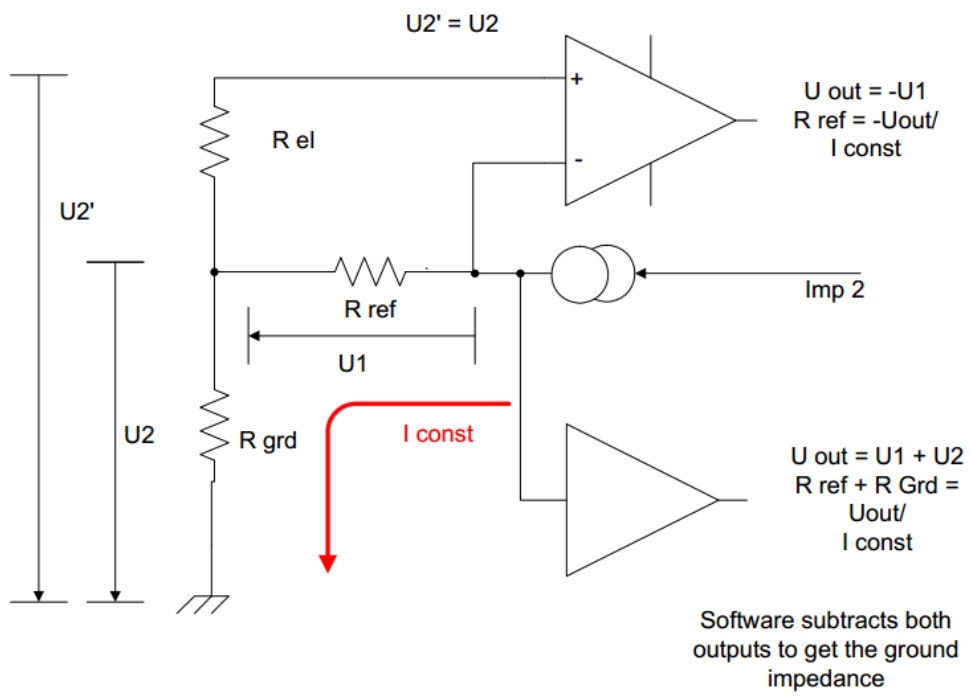


Figure A.3. Impedance measurement of ground electrodes

REFERENCES

- [1] Tabar Y R and Halici U 2016 A novel deep learning approach for classification of EEG motor imagery signals *Journal of neural engineering* **14** 016003
- [2] Mirowski P, Madhavan D, LeCun Y and Kuzniecky R 2009 Classification of patterns of EEG synchronization for seizure prediction *Clinical neurophysiology* **120** 1927-40
- [3] Wulsin D, Gupta J, Mani R, Blanco J and Litt B 2011 Modeling electroencephalography waveforms with semi-supervised deep belief nets: fast classification and anomaly measurement *Journal of neural engineering* **8** 036015
- [4] Cecotti H 2011 Spelling with non-invasive Brain-Computer Interfaces-Current and future trends *Journal of Physiology-Paris* **105** 106-14
- [5] Långkvist M, Karlsson L and Loutfi A 2012 Sleep stage classification using unsupervised feature learning *Advances in Artificial Neural Systems* **2012** 5
- [6] Ahmed S, Merino L M, Mao Z, Meng J, Robbins K and Huang Y 2013 A deep learning method for classification of images rsvp events with eeg data. In: *Global Conference on Signal and Information Processing (GlobalSIP), 2013 IEEE: IEEE* pp 33-6
- [7] Stober S, Cameron D J and Grahn J A 2014 Using Convolutional Neural Networks to Recognize Rhythm^[OB] Stimuli from Electroencephalography Recordings. In: *Advances in neural information processing systems*, pp 1449-57
- [8] Cecotti H, Eckstein M P and Giesbrecht B 2014 Single-trial classification of event-related potentials in rapid serial visual presentation tasks using supervised spatial filtering *IEEE transactions on neural networks and learning systems* **25** 2030-42
- [9] An X, Kuang D, Guo X, Zhao Y and He L 2014 *Intelligent Computing in Bioinformatics: Springer* pp 203-10
- [10] Ren Y and Wu Y 2014 Convolutional deep belief networks for feature extraction of EEG signal. In: *Neural Networks (IJCNN), 2014 International Joint Conference on: IEEE* pp 2850-3
- [11] Bashivan P, Rish I, Yeasin M and Codella N 2015 Learning Representations from EEG with Deep Recurrent-Convolutional Neural Networks *arXiv preprint arXiv:1511.06448*
- [12] Stober S, Sternin A, Owen A M and Grahn J A 2015 Deep feature learning for EEG recordings *arXiv preprint arXiv:1511.04306*

- [13] Manor R and Geva A B 2015 Convolutional neural network for multi-category rapid serial visual presentation bci *Frontiers in computational neuroscience* **9**
- [14] Sakhavi S, Guan C and Yan S 2015 Parallel convolutional-linear neural network for motor imagery classification. In: *Signal Processing Conference (EUSIPCO), 2015 23rd European: IEEE* pp 2736-40
- [15] Yang H, Sakhavi S, Ang K K and Guan C 2015 On the use of convolutional neural networks and augmented CSP features for multi-class motor imagery of EEG signals classification. In: *2015 37th Annual International Conference of the IEEE Engineering in Medicine and Biology Society (EMBC): IEEE* pp 2620-3
- [16] Antoniadou A, Spyrou L, Took C C and Sanei S 2016 Deep learning for epileptic intracranial EEG data. In: *Machine Learning for Signal Processing (MLSP), 2016 IEEE 26th International Workshop on: IEEE* pp 1-6
- [17] Liang J, Lu R, Zhang C and Wang F 2016 Predicting Seizures from Electroencephalography Recordings: A Knowledge Transfer Strategy. In: *Healthcare Informatics (ICHI), 2016 IEEE International Conference on: IEEE* pp 184-91
- [18] Page A, Shea C and Mohsenin T 2016 Wearable seizure detection using convolutional neural networks with transfer learning. In: *Circuits and Systems (ISCAS), 2016 IEEE International Symposium on: IEEE* pp 1086-9
- [19] Thodoroff P, Pineau J and Lim A 2016 Learning Robust Features using Deep Learning for Automatic Seizure Detection. In: *Machine Learning for Healthcare Conference*, pp 178-90
- [20] Shamwell J, Lee H, Kwon H, Marathe A R, Lawhern V and Nothwang W 2016 Single-trial EEG RSVP classification using convolutional neural networks. In: *Proc. SPIE*, p 983622
- [21] Lawhern V J, Solon A J, Waytowich N R, Gordon S M, Hung C P and Lance B J 2016 EEGNet: A Compact Convolutional Network for EEG-based Brain-Computer Interfaces *arXiv preprint arXiv:1611.08024*
- [22] Kwak N-S, Müller K-R and Lee S-W 2017 A convolutional neural network for steady state visual evoked potential classification under ambulatory environment *PloS one* **12** e0172578
- [23] Tang Z, Li C and Sun S 2017 Single-trial EEG classification of motor imagery using deep convolutional neural networks *Optik-International Journal for Light and Electron Optics* **130** 11-8
- [24] Cecotti H and Graser A 2011 Convolutional neural networks for P300 detection with application to brain-computer interfaces *IEEE transactions on pattern analysis and machine intelligence* **33** 433-45
- [25] Pfurtscheller G and Neuper C 2001 Motor imagery and direct brain-computer communication *Proceedings of the IEEE* **89** 1123-34
- [26] Graimann B, Allison B and Pfurtscheller G 2010 *Brain-Computer Interfaces*: Springer) pp 1-27
- [27] Sellers E W, Vaughan T M and Wolpaw J R 2010 A brain-computer interface for long-term independent home use *Amyotrophic lateral sclerosis* **11** 449-55
- [28] Rebsamen B, Guan C, Zhang H, Wang C, Teo C, Ang M H and Burdet E 2010 A brain controlled wheelchair to navigate in familiar environments

- [29] Krepki R, Blankertz B, Curio G and Müller K-R 2007 The Berlin Brain-Computer Interface (BBCI)-towards a new communication channel for online control in gaming applications *Multimedia Tools and Applications* **33** 73-90
- [30] Holz E M, Höhne J, Staiger-Sälzer P, Tangermann M and Kübler A 2013 Brain-computer interface controlled gaming: Evaluation of usability by severely motor restricted end-users *Artificial intelligence in medicine* **59** 111-20
- [31] Farwell L A and Donchin E 1988 Talking off the top of your head: toward a mental prosthesis utilizing event-related brain potentials *Electroencephalography and clinical Neurophysiology* **70** 510-23
- [32] Townsend G, LaPallo B, Boulay C, Krusienski D, Frye G, Hauser C, Schwartz N, Vaughan T, Wolpaw J R and Sellers E 2010 A novel P300-based brain-computer interface stimulus presentation paradigm: moving beyond rows and columns *Clinical Neurophysiology* **121** 1109-20
- [33] Takano K, Komatsu T, Hata N, Nakajima Y and Kansaku K 2009 Visual stimuli for the P300 brain-computer interface: a comparison of white/gray and green/blue flicker matrices *Clinical neurophysiology* **120** 1562-6
- [34] Li Y, Nam C S, Shadden B B and Johnson S L 2010 A P300-based brain-computer interface: Effects of interface type and screen size *Intl. Journal of Human-Computer Interaction* **27** 52-68
- [35] Ahi S T, Kambara H and Koike Y 2011 A dictionary-driven P300 speller with a modified interface *IEEE Transactions on Neural Systems and Rehabilitation Engineering* **19** 6-14
- [36] Cheng M, Gao X, Gao S and Xu D 2002 Design and implementation of a brain-computer interface with high transfer rates *IEEE transactions on biomedical engineering* **49** 1181-6
- [37] Trejo L J, Rosipal R and Matthews B 2006 Brain-computer interfaces for 1-D and 2-D cursor control: designs using volitional control of the EEG spectrum or steady-state visual evoked potentials *IEEE transactions on neural systems and rehabilitation engineering* **14** 225-9
- [38] Allison B Z, McFarland D J, Schalk G, Zheng S D, Jackson M M and Wolpaw J R 2008 Towards an independent brain-computer interface using steady state visual evoked potentials *Clinical neurophysiology* **119** 399-408
- [39] Segers H, Combaz A, Manyakov N V, Chumerin N, Vanderperren K, Van Huffel S and Van Hulle M 2011 Steady state visual evoked potential (SSVEP)-based brain spelling system with synchronous and asynchronous typing modes. In: *15th Nordi.-Balt. Conf. Biomed. Eng. Med. Phys*: Springer) pp 164-7
- [40] Yin E, Zhou Z, Jiang J, Yu Y and Hu D 2015 A dynamically optimized SSVEP brain-computer interface (BCI) speller *IEEE Transactions on Biomedical Engineering* **62** 1447-56
- [41] Obermaier B, Muller G R and Pfurtscheller G 2003 " Virtual keyboard" controlled by spontaneous EEG activity *IEEE Transactions on Neural Systems and Rehabilitation Engineering* **11** 422-6

- [42] Scherer R, Muller G, Neuper C, Graimann B and Pfurtscheller G 2004 An asynchronously controlled EEG-based virtual keyboard: improvement of the spelling rate *IEEE Transactions on Biomedical Engineering* **51** 979-84
- [43] Brumberg J S, Burnison J D and Pitt K M 2016 Using Motor Imagery to Control Brain-Computer Interfaces for Communication. In: *International Conference on Augmented Cognition*: Springer) pp 14-25
- [44] Nicolas-Alonso L F and Gomez-Gil J 2012 Brain computer interfaces, a review *Sensors* **12** 1211-79
- [45] Suner S, Fellows M R, Vargas-Irwin C, Nakata G K and Donoghue J P 2005 Reliability of signals from a chronically implanted, silicon-based electrode array in non-human primate primary motor cortex *IEEE transactions on neural systems and rehabilitation engineering* **13** 524-41
- [46] Freeman W J, Holmes M D, Burke B C and Vanhatalo S 2003 Spatial spectra of scalp EEG and EMG from awake humans *Clinical Neurophysiology* **114** 1053-68
- [47] Levine S P, Huggins J E, BeMent S L, Kushwaha R K, Schuh L A, Passaro E A, Rohde M M and Ross D A 1999 Identification of electrocorticogram patterns as the basis for a direct brain interface *Journal of clinical neurophysiology* **16** 439
- [48] Kennedy P R, Kirby M T, Moore M M, King B and Mallory A 2004 Computer control using human intracortical local field potentials *IEEE Transactions on Neural Systems and Rehabilitation Engineering* **12** 339-44
- [49] Wolpaw J R, Loeb G E, Allison B Z, Donchin E, do Nascimento O F, Heetderks W J, Nijboer F, Shain W G and Turner J N 2006 BCI meeting 2005-workshop on signals and recording methods *IEEE Transactions on neural systems and rehabilitation engineering* **14** 138-41
- [50] Bauernfeind G, Leeb R, Wriessnegger S C and Pfurtscheller G 2008 Development, set-up and first results for a one-channel near-infrared spectroscopy system/Entwicklung, Aufbau und vorläufige Ergebnisse eines Einkanal-Nahinfrarot-Spektroskopie-Systems *Biomedizinische Technik* **53** 36-43
- [51] Ward B D and Mazaheri Y 2008 Information transfer rate in fMRI experiments measured using mutual information theory *Journal of neuroscience methods* **167** 22-30
- [52] Ruiz S, Buyukturkoglu K, Rana M, Birbaumer N and Sitaram R 2014 Real-time fMRI brain computer interfaces: self-regulation of single brain regions to networks *Biological psychology* **95** 4-20
- [53] Coyle S M, Ward T E and Markham C M 2007 Brain-computer interface using a simplified functional near-infrared spectroscopy system *Journal of neural engineering* **4** 219
- [54] Power S D, Kushki A and Chau T 2011 Towards a system-paced near-infrared spectroscopy brain-computer interface: differentiating prefrontal activity due to mental arithmetic and mental singing from the no-control state *Journal of neural engineering* **8** 066004
- [55] Aranyi G, Pecune F, Charles F, Pelachaud C and Cavazza M 2016 Affective interaction with a virtual character through an fNIRS brain-computer interface *Frontiers in computational neuroscience* **10**

- [56] Lal T N, Schröder M, Hill N J, Preissl H, Hinterberger T, Mellinger J, Bogdan M, Rosenstiel W, Hofmann T and Birbaumer N 2005 A brain computer interface with online feedback based on magnetoencephalography. In: *Proceedings of the 22nd international conference on Machine learning: ACM* pp 465-72
- [57] Mellinger J, Schalk G, Braun C, Preissl H, Rosenstiel W, Birbaumer N and Kübler A 2007 An MEG-based brain–computer interface (BCI) *Neuroimage* **36** 581-93
- [58] Zhang J, Sudre G, Li X, Wang W, Weber D J and Bagic A 2011 Clustering linear discriminant analysis for MEG-based brain computer interfaces *IEEE Transactions on Neural Systems and Rehabilitation Engineering* **19** 221-31
- [59] Furdea A, Halder S, Krusienski D, Bross D, Nijboer F, Birbaumer N and Kübler A 2009 An auditory oddball (P300) spelling system for brain-computer interfaces *Psychophysiology* **46** 617-25
- [60] Blankertz B and Competition II B 2003 P300 Speller Dataset (webpage).
- [61] Citi L, Poli R, Cinel C and Sepulveda F 2008 P300-based BCI mouse with genetically-optimized analogue control *IEEE transactions on neural systems and rehabilitation engineering* **16** 51-61
- [62] Bell C J, Shenoy P, Chalodhorn R and Rao R P 2008 Control of a humanoid robot by a noninvasive brain–computer interface in humans *Journal of neural engineering* **5** 214
- [63] Herrmann C S 2001 Human EEG responses to 1–100 Hz flicker: resonance phenomena in visual cortex and their potential correlation to cognitive phenomena *Experimental brain research* **137** 346-53
- [64] Mora-Cortes A, Manyakov N V, Chumerin N and Van Hulle M M 2014 Language model applications to spelling with brain-computer interfaces *Sensors* **14** 5967-93
- [65] Jia C, Gao X, Hong B and Gao S 2011 Frequency and phase mixed coding in SSVEP-based brain–computer interface *IEEE Transactions on Biomedical Engineering* **58** 200-6
- [66] Hinterberger T, Schmidt S, Neumann N, Mellinger J, Blankertz B, Curio G and Birbaumer N 2004 Brain-computer communication and slow cortical potentials *IEEE Transactions on Biomedical Engineering* **51** 1011-8
- [67] Iversen I, Ghanayim N, Kübler A, Neumann N, Birbaumer N and Kaiser J 2008 A brain–computer interface tool to assess cognitive functions in completely paralyzed patients with amyotrophic lateral sclerosis *Clinical neurophysiology* **119** 2214-23
- [68] Pfurtscheller G and Da Silva F L 1999 Event-related EEG/MEG synchronization and desynchronization: basic principles *Clinical neurophysiology* **110** 1842-57
- [69] Schlögl A, Lee F, Bischof H and Pfurtscheller G 2005 Characterization of four-class motor imagery EEG data for the BCI-competition 2005 *Journal of neural engineering* **2** L14
- [70] Pfurtscheller G, Brunner C, Schlögl A and Da Silva F L 2006 Mu rhythm (de) synchronization and EEG single-trial classification of different motor imagery tasks *NeuroImage* **31** 153-9

- [71] Fabiani G E, McFarland D J, Wolpaw J R and Pfurtscheller G 2004 Conversion of EEG activity into cursor movement by a brain-computer interface (BCI) *IEEE transactions on neural systems and rehabilitation engineering* **12** 331-8
- [72] Long J, Li Y, Wang H, Yu T, Pan J and Li F 2012 A hybrid brain computer interface to control the direction and speed of a simulated or real wheelchair *IEEE Transactions on Neural Systems and Rehabilitation Engineering* **20** 720-9
- [73] Horki P, Solis-Escalante T, Neuper C and Müller-Putz G 2011 Combined motor imagery and SSVEP based BCI control of a 2 DoF artificial upper limb *Medical & biological engineering & computing* **49** 567-77
- [74] Blankertz B, Müller K-R, Krusienski D J, Schalk G, Wolpaw J R, Schlogl A, Pfurtscheller G, Millan J R, Schroder M and Birbaumer N 2006 The BCI competition III: Validating alternative approaches to actual BCI problems *IEEE transactions on neural systems and rehabilitation engineering* **14** 153-9
- [75] Blankertz B, Dornhege G, Krauledat M, Schröder M, Williamson J, Murray-Smith R and Müller K-R 2006 The Berlin Brain-Computer Interface presents the novel mental typewriter Hex-o-Spell
- [76] D'albis T, Blatt R, Tedesco R, Sbattella L and Matteucci M 2012 A predictive speller controlled by a brain-computer interface based on motor imagery *ACM Transactions on Computer-Human Interaction (TOCHI)* **19** 20
- [77] García-Laencina P J, Rodríguez-Bermudez G and Roca-Dorda J 2014 Exploring dimensionality reduction of EEG features in motor imagery task classification *Expert Systems with Applications* **41** 5285-95
- [78] Al-ani T and Trad D 2010 *Intelligent and Biosensors: InTech*
- [79] Jolliffe I 2002 *Principal component analysis: Wiley Online Library*
- [80] Comon P 1994 Independent component analysis, a new concept? *Signal processing* **36** 287-314
- [81] Lee T-W, Lewicki M S, Girolami M and Sejnowski T J 1999 Blind source separation of more sources than mixtures using overcomplete representations *IEEE signal processing letters* **6** 87-90
- [82] Jo H 1975 *Holland: "Adaption in Natural and Artificial Systems. The University of Michigan Press, Ann Arbor*
- [83] Freund Y and Schapire R E 1995 A decision-theoretic generalization of on-line learning and an application to boosting. In: *European conference on computational learning theory: Springer* pp 23-37
- [84] Ince N F, Arica S and Tewfik A 2006 Classification of single trial motor imagery EEG recordings with subject adapted non-dyadic arbitrary time-frequency tilings *Journal of neural engineering* **3** 235
- [85] Lin C-J and Hsieh M-H 2009 Classification of mental task from EEG data using neural networks based on particle swarm optimization *Neurocomputing* **72** 1121-30
- [86] Yildirim A and Halici U 2013 Analysis of dimension reduction by PCA and AdaBoost on spelling paradigm EEG data. In: *Biomedical Engineering and Informatics (BMEI), 2013 6th International Conference on: IEEE* pp 192-6

- [87] Talukdar M T F, Sakib S K, Pathan N S and Fattah S A 2014 Motor imagery EEG signal classification scheme based on autoregressive reflection coefficients. In: *Informatics, Electronics & Vision (ICIEV), 2014 International Conference on: IEEE*) pp 1-4
- [88] Boye A T, Kristiansen U Q, Billinger M, do Nascimento O F and Farina D 2008 Identification of movement-related cortical potentials with optimized spatial filtering and principal component analysis *Biomedical Signal Processing and Control* **3** 300-4
- [89] Gao J F, Yang Y, Lin P, Wang P and Zheng C X 2010 Automatic removal of eye-movement and blink artifacts from EEG signals *Brain topography* **23** 105-14
- [90] Erfanian A and Erfani A 2004 ICA-based classification scheme for EEG-based brain-computer interface: the role of mental practice and concentration skills. In: *Engineering in Medicine and Biology Society, 2004. IEMBS'04. 26th Annual International Conference of the IEEE: IEEE*) pp 235-8
- [91] Corralejo R, Hornero R and Alvarez D 2011 Feature selection using a genetic algorithm in a motor imagery-based Brain Computer Interface. In: *Engineering in Medicine and Biology Society, EMBC, 2011 Annual International Conference of the IEEE: IEEE*) pp 7703-6
- [92] Dal Seno B, Matteucci M and Mainardi L 2008 A genetic algorithm for automatic feature extraction in P300 detection. In: *Neural Networks, 2008. IJCNN 2008.(IEEE World Congress on Computational Intelligence). IEEE International Joint Conference on: IEEE*) pp 3145-52
- [93] Boostani R and Moradi M H 2004 A new approach in the BCI research based on fractal dimension as feature and Adaboost as classifier *Journal of Neural Engineering* **1** 212
- [94] Fix E and Hodges Jr J L 1951 Discriminatory analysis-nonparametric discrimination: consistency properties. California Univ Berkeley)
- [95] Jensen F V 2001 Bayesian networks and decision graphs. *Statistics for engineering and information science Springer* **32** 34
- [96] Rabiner L and Juang B 1986 An introduction to hidden Markov models *iee assp magazine* **3** 4-16
- [97] Obermaier B, Guger C, Neuper C and Pfurtscheller G 2001 Hidden Markov models for online classification of single trial EEG data *Pattern recognition letters* **22** 1299-309
- [98] Zhong S and Ghosh J 2002 HMMs and coupled HMMs for multi-channel EEG classification. In: *Neural Networks, 2002. IJCNN'02. Proceedings of the 2002 International Joint Conference on: IEEE*) pp 1154-9
- [99] Kaiser V, Bauernfeind G, Kreilinger A, Kaufmann T, Kübler A, Neuper C and Müller-Putz G R 2014 Cortical effects of user training in a motor imagery based brain-computer interface measured by fNIRS and EEG *Neuroimage* **85** 432-44
- [100] Hwang H-J, Kwon K and Im C-H 2009 Neurofeedback-based motor imagery training for brain-computer interface (BCI) *Journal of neuroscience methods* **179** 150-6

- [101] Shahid S, Sinha R K and Prasad G 2010 A bispectrum approach to feature extraction for a motor imagery based brain-computer interfacing system. In: *Proc. 18th European Signal Processing Conf. EUSIPCO*, pp 1831-5
- [102] Grosse-Wentrup M and Buss M 2008 Multiclass common spatial patterns and information theoretic feature extraction *Biomedical Engineering, IEEE Transactions on* **55** 1991-2000
- [103] Ramoser H, Muller-Gerking J and Pfurtscheller G 2000 Optimal spatial filtering of single trial EEG during imagined hand movement *Rehabilitation Engineering, IEEE Transactions on* **8** 441-6
- [104] Ang K K, Chin Z Y, Zhang H and Guan C 2008 Filter bank common spatial pattern (FBCSP) in brain-computer interface. In: *Neural Networks, 2008. IJCNN 2008.(IEEE World Congress on Computational Intelligence). IEEE International Joint Conference on: IEEE* pp 2390-7
- [105] Ang K K, Chin Z Y, Wang C, Guan C and Zhang H 2012 Filter bank common spatial pattern algorithm on BCI competition IV datasets 2a and 2b *Frontiers in Neuroscience* **6**
- [106] Fukunaga K 2013 *Introduction to statistical pattern recognition*: Academic press)
- [107] Fisher R A 1936 The use of multiple measurements in taxonomic problems *Annals of human genetics* **7** 179-88
- [108] Hoffmann U, Vesin J-M, Ebrahimi T and Diserens K 2008 An efficient P300-based brain-computer interface for disabled subjects *Journal of Neuroscience methods* **167** 115-25
- [109] Garrett D, Peterson D A, Anderson C W and Thaut M H 2003 Comparison of linear, nonlinear, and feature selection methods for EEG signal classification *IEEE Transactions on neural systems and rehabilitation engineering* **11** 141-4
- [110] Burges C J 1998 A tutorial on support vector machines for pattern recognition *Data mining and knowledge discovery* **2** 121-67
- [111] Blankertz B, Curio G and Müller K-R 2002 Classifying single trial EEG: Towards brain computer interfacing. In: *Advances in neural information processing systems*, pp 157-64
- [112] Rakotomamonjy A and Guigue V 2008 BCI competition III: dataset II-ensemble of SVMs for BCI P300 speller *IEEE transactions on biomedical engineering* **55** 1147-54
- [113] Suk H-I and Lee S-W 2011 Data-driven frequency bands selection in EEG-based brain-computer interface. In: *Pattern Recognition in NeuroImaging (PRNI), 2011 International Workshop on: IEEE* pp 25-8
- [114] Soman S 2015 High performance EEG signal classification using classifiability and the Twin SVM *Applied Soft Computing* **30** 305-18
- [115] Khemchandani R and Chandra S 2007 Twin support vector machines for pattern classification *IEEE transactions on pattern analysis and machine intelligence* **29** 905-10
- [116] Chin Z Y, Ang K K, Wang C and Guan C 2014 Discriminative channel addition and reduction for filter bank common spatial pattern in motor imagery BCI. In: *Engineering in Medicine and Biology Society (EMBC), 2014 36th Annual International Conference of the IEEE: IEEE* pp 1310-3

- [117] Ang K K and Guan C 2017 EEG-Based Strategies to Detect Motor Imagery for Control and Rehabilitation *IEEE Transactions on Neural Systems and Rehabilitation Engineering* **25** 392-401
- [118] Kirar J S and Agrawal R 2016 Optimal Spatio-spectral Variable Size Subbands Filter for Motor Imagery Brain Computer Interface *Procedia Computer Science* **84** 14-21
- [119] Masic N and Pfurtscheller G 1993 Neural network based classification of single-trial EEG data *Artificial Intelligence in Medicine* **5** 503-13
- [120] Anderson C W, Devulapalli S V and Stolz E A 1995 Determining mental state from EEG signals using parallel implementations of neural networks *Scientific programming* **4** 171-83
- [121] Felzer T and Freisieben B 2003 Analyzing EEG signals using the probability estimating guarded neural classifier *IEEE Transactions on Neural Systems and Rehabilitation Engineering* **11** 361-71
- [122] Cecotti H and Graser A 2008 Time Delay Neural Network with Fourier transform for multiple channel detection of Steady-State Visual Evoked Potentials for Brain-Computer Interfaces. In: *Signal Processing Conference, 2008 16th European: IEEE*) pp 1-5
- [123] Haselsteiner E and Pfurtscheller G 2000 Using time-dependent neural networks for EEG classification *IEEE transactions on rehabilitation engineering* **8** 457-63
- [124] Hamedi M, Salleh S-H, Noor A M and Mohammad-Rezazadeh I 2014 Neural network-based three-class motor imagery classification using time-domain features for BCI applications. In: *Region 10 Symposium, 2014 IEEE: IEEE*) pp 204-7
- [125] Gandhi V, Arora V, Behera L, Prasad G, Coyle D and McGinnity T M 2011 EEG denoising with a recurrent quantum neural network for a brain-computer interface. In: *Neural Networks (IJCNN), The 2011 International Joint Conference on: IEEE*) pp 1583-90
- [126] Andrew Ng J N, Chuan Yu Foo, Yifan Mai, Caroline Suen 2017 UFLDL Tutorial, *Stanford University*
- [127] Le Cun B B, Denker J S, Henderson D, Howard R E, Hubbard W and Jackel L D 1990 Handwritten digit recognition with a back-propagation network. In: *Advances in neural information processing systems: Citeseer*)
- [128] LeCun Y, Bottou L, Bengio Y and Haffner P 1998 Gradient-based learning applied to document recognition *Proceedings of the IEEE* **86** 2278-324
- [129] <http://deeplearning.net/tutorial/lenet.html>
- [130] Rumelhart D E, Hinton G E and Williams R J 1985 Learning internal representations by error propagation. California Univ San Diego La Jolla Inst for Cognitive Science)
- [131] Ng A 2011 Sparse autoencoder *CS294A Lecture notes* **72** 1-19
- [132] Hinton G E, Osindero S and Teh Y-W 2006 A fast learning algorithm for deep belief nets *Neural computation* **18** 1527-54
- [133] Hinton G E 2002 Training products of experts by minimizing contrastive divergence *Neural computation* **14** 1771-800
- [134] Lemm S, Schäfer C and Curio G 2004 BCI competition 2003-data set III: probabilistic modeling of sensorimotor μ rhythms for classification of

- imaginary hand movements *Biomedical Engineering, IEEE Transactions on* **51** 1077-80
- [135] Schlögl A 2003 Outcome of the BCI-competition 2003 on the Graz data set *Berlin, Germany: Graz University of Technology*
- [136] Leeb R, Lee F, Keinrath C, Scherer R, Bischof H and Pfurtscheller G 2007 Brain–computer communication: motivation, aim, and impact of exploring a virtual apartment *Neural Systems and Rehabilitation Engineering, IEEE Transactions on* **15** 473-82
- [137] Easycap. (Herrsching-Breitbrunn, Germany)
- [138] Melnik A, Legkov P, Izdebski K, Kärcher S M, Hairston W D, Ferris D P and König P 2017 Systems, Subjects, Sessions: To What Extent Do These Factors Influence EEG Data? *Frontiers in human neuroscience* **11**
- [139] Amaral C P, Simões M A, Mouga S, Andrade J and Castelo-Branco M 2017 A novel Brain Computer Interface for classification of social joint attention in Autism and comparison of 3 experimental setups: a feasibility study *Journal of Neuroscience Methods*
- [140] Stan A, Irimia D C, Botezatu N A and Lupu R G 2015 Controlling a hand orthosis by means of P300-based brain computer interface. In: *E-Health and Bioengineering Conference (EHB), 2015: IEEE* pp 1-4
- [141] Coyle D, Stow J, McCreddie K, Sciacca N, McElligott J and Carroll Á 2017 *Brain-Computer Interface Research: Springer* pp 51-69
- [142] Nunez P L and Srinivasan R 2006 *Electric fields of the brain: the neurophysics of EEG: Oxford University Press, USA*
- [143] Brainard D H and Vision S 1997 The psychophysics toolbox *Spatial vision* **10** 433-6
- [144] Renard Y, Lotte F, Gibert G, Congedo M, Maby E, Delannoy V, Bertrand O and Lécuyer A 2010 OpenViBE: an open-source software platform to design, test, and use brain–computer interfaces in real and virtual environments *Presence: teleoperators and virtual environments* **19** 35-53
- [145] Ahn M and Jun S C 2015 Performance variation in motor imagery brain–computer interface: A brief review *Journal of neuroscience methods* **243** 103-10
- [146] Palm R B 2012 Prediction as a candidate for learning deep hierarchical models of data *Technical University of Denmark*
- [147] Sim J and Wright C C 2005 The kappa statistic in reliability studies: use, interpretation, and sample size requirements *Physical therapy* **85** 257-68
- [148] Croft R J and Barry R J 2000 Removal of ocular artifact from the EEG: a review *Neurophysiologie Clinique/Clinical Neurophysiology* **30** 5-19

CURRICULUM VITAE

PERSONAL INFORMATION

Surname, Name: Rezaei Tabar, Yousef

Nationality: Iran

Date and Place of Birth: 03.04.1982, Urmia

Marital Status: Married

Email: rezaeetabar@gmail.com

EDUCATION

| Degree | Institution | Year of Graduation |
|---------------|--|---------------------------|
| M.S. | Middle East Technical University, Biomedical Engineering | 2011 |
| B.S. | Urmia University, Electrical and Electronics Engineering | 2006 |

WORK EXPERIENCE

| Year | Place | Enrollment |
|-----------|--|-------------------|
| 2006-2008 | Iran water and waste water organization | Software Engineer |
| 2011 | Middle East Technical University North Cyprus Campus | T.A. |

PUBLICATIONS

- Tabar, Yousef Rezaei, and Ugur Halici. "A novel deep learning approach for classification of EEG motor imagery signals." *Journal of neural engineering* 14.1 (2016): 016003.
- Tabar, Yousef Rezaei, and Ugur Halici. "Brain Computer Interfaces for Silent Speech." *European Review* 25.2 (2017): 208-230.
- Yousef Rezaei Tabar And Ilkay Ulusoy, "The Effect Of Labeled/Unlabeled Prior Information For Masseter Segmentation," *Mathematical Problems In Engineering*, Vol. 2013
- Rezaeitabar Y, Ulusoy I. Automatic 3d Segmentation Of Individual Facial Muscles Using Unlabeled Prior Information. *Int J Comput Assist Radiol Surg*. 2012 Jan;7(1):35-41.
- Aytakin, C.; Rezaeitabar, Y.; Dogru, S.; Ulusoy, I., "Railway Fastener Inspection By Real-Time Machine Vision," *Systems, Man, And Cybernetics: Systems, Ieee Transactions On* , Vol.Pp, No.99, Pp.1,1
- Ilkay Ulusoy, Yousef Rezaitabar, Ulya Bayram And Nihan Çiçekli, "A Tracking System For The Recognition Of Long Term Events" , *Advances In Intelligent Systems And Computing*. Volume 311, 2015, Pp 85-92
- Yousef Rezaeitabar, Ilkay Ulusoy, "AUTOMATIC 3D SEGMENTATION OF FACIAL SOFT TISSUES USING UNLABELLED PRIOR INFORMATION", *IEEE 19th Conference on Signal Processing and Communications Applications (SIU)*, Oral presentation on National Conference, 20-22 April 2011, Antalya
- Orsan Aytakin, Yousef Rezaeitabar, Ilkay Ulusoy, "VHR IMAGE SEGMENTATION USING MORPHOLOGICAL PRIMITIVE OBJECTS", *IEEE Geoscience and Remote Sensing Society (IGARSS)2011*

- Itir Önal, Karani Kardas, Yousef Rezaeitabar, Ulya Bayram, Murat Bal, Ilkay Ulusoy, Nihan Kesim Çiçekli, A FRAMEWORK FOR DETECTING COMPLEX EVENTS IN SURVEILLANCE VIDEOS, 3rd IEEE International Workshop on Advances in Automated Multimedia Surveillance for Public Safety, ICME 2013